Studying optical micro-resonators coupling for future insertion in an opto-electronic oscillator

Vu Hai Nam Luong

N° ENSC-2012/…

THÈSE DE DOCTORAT
DE L'ÉCOLE NORMALE SUPÉRIEURE DE CACHAN

présentée par

Mme LUONG Vu Hai Nam

pour obtenir le grade de

DOCTEUR en SCIENCES
de l'ÉCOLE NORMALE SUPÉRIEURE de CACHAN

domaine

Physique

Sujet de la thèse

Studying optical micro-resonators coupling for future insertion in an opto-electronic oscillator

Soutenue à Cachan le 14 novembre 2012 devant le jury composé de

Daniel BOUCHIER	Université Paris XI - IEF	Président
Bruno BÊCHE	Université de Rennes	Rapporteur
Emmanuel BIGLER	ENSMM Besançon	Rapporteur
Laurent VIVIEN	Université Paris XI – IEF	Examinateur
Isabelle LEDOUX-RAK	ENS Cachan	Directrice
Bernard JOURNET	ENS Cachan	Co-directeur

Laboratoire Systèmes et Applications des Technologies de l'Information et de l'Énergie

CNRS UMR 8029, Institut d'Alembert, ENS Cachan

Acknowledgements

The work described in this thesis was performed in the "Traitement de l'Information et Multicapteurs" team at Laboratoire Systèmes et Applications des Technologies de l'Information et de l'Energie (SATIE) of Ecole Normale Supérieure de Cachan under supervision of Professor Isabelle Ledoux-Rak and Dr Bernard Journet.

First of all, I would like to thank Prof. Joseph Zyss, director of "Institut d'Alembert" for the support of its institute and Prof. Pascal Larzabal, director of SATIE, for accepting me in its laboratory.

I would like to send my sincere thanks to both my supervisors, Prof. Isabelle Ledoux-Rak and Bernard Journet, who accepted me and provided me this project. Especially I would like to express my deep gratitude to Bernard Journet, for his guidance, kind suggestions and encouragements during the length of this doctoral program. With numerous open and enthusiasm discussions between us, he gave me a great knowledge in physics domain and also gave me vast amounts of ideas on theory and application.

I would like to send my special thanks to Eric Cassan and his colleagues L. Vivien, S. Lardenois, D. Pascal, and who work in "Institut d'Electronique Fondamentale", IEF, "Silicon-based micro and nanophotonic devices" group, for supplying the micro-racetrack optical micro-resonator devices.

I also thank a lot Dr Nguyen Chi Thanh ("Laboratoire de Photonique Quantique et Moléculaire", LPQM) for his kind help on carrying out the first experimental measurement of the racetrack resonator device and also for his suggestions.

I would like specifically to thank Jean-Pierre Madrange, Patrice Vallade (from "SATIE laboratory) and Du Kim Pha David (from "Département EEA" at ENS Cachan) for their enthusiasm and indispensable help in fabricating and providing many mechanical supports.

I would like also to acknowledge all my colleagues in laboratory of semiconductor laser, IMS, Viêt Nam, Prof. Vu Van Luc, Prof. Vu Doan Miên, Tran Quôc Tiên, Pham Van Truong , Vu Thi Nghiêm and Tông Quang Công for their kind help and useful suggestion in my research.

Finally I would like to express my thanks to the family of Bac Ngân Hà, Bac Ky. In their house, I always receive a warm welcome.

I am greatly indebted to ministry of education and training, Government of Vietnam for provided me a scholarship that is an important condition to pursue my studies in France.

And finally, I would like to thank my family for their patience and unconditional support over the years.

Contents

List of tables

List of figures

Introduction

Because it can generate high-purity RF signals with very low phase noise, optoelectronic oscillator (OEO) is an important device in many applications such as: Radars, communications, and metrology of time and frequency. OEO is a fundamentally distinct approach for generating signal, both with RF and optical outputs. A conventional OEO system which brings together component such as electrooptic modulator, laser source, photodetector and an optical fiber loop can have an equivalent RF quality factor greater than 10^6 to reduce the phase noise of the generated microwave signal. With this OEO system, a 10 GHz signal with a performance of -163dBc/Hz at 10 kHz offset from the carrier was achieved. The variant of configuration of the OEO is called the coupled OEO (COEO), also generates pico-second optical pulses at its optical output. The generated pulses exhibit the same low phase noise as the actual OEO at its RF output. In particular, a long fiber loop in OEO results in micro-second storage times, corresponding to a quality factor (noted *Q*) about a million at a 10 GHz oscillation frequency. This is a high value compared to conventional type dielectric microwave cavities used in oscillators. In a general OEO system [2], the long fiber loop keeps many microwave modes on an optical wave, so a narrowband electrical filter has to be inserted into the OEO feedback loop to reach single mode operation, and the center frequency of this filter is considered as operation frequency of the OEO. This configuration achieves the spectrally pure high-frequency signals, but it cannot be considered as an OEO system which has small size due to the length kilometers of optical fiber line. Moreover, the long fiber line is sensitive to the surrounding environment as for example variations of operating temperature. Therefore, in recent decades, a new OEO configuration is developed to reduce the size of oscillator and produce an output with high long–term frequency stability: it is based on optical micro-resonators instead of the long fiber loop.

According to the light confinement method, micro-resonators are classed into four main categories: Fabry-Perot, waveguides, photonic crystal and whispering gallery mode

cavities. Among these optical resonators, **w**hispering **g**allery **m**ode (WGM) micro-cavities lead to the highest *Q* factor. In this thesis, the works has been focused on two kinds of micro-resonators: silica microsphere (a WGM resonator) and add/drop micro-racetrack resonator (a wave-guided resonator).

These optical resonators are significantly smaller compared to the fiber loop. In new OEO configuration, high finesse, high *Q* whispering gallery mode (WGM) optical micro-resonators are employed in place of long optical fiber. WGM resonators have axially symmetric dielectric structures with diameter ranging from tens of microns to a few mm which can trap light for long periods of time. The combination of high *Q* WGM resonators with laser gives result in narrow line width, highly stable signal in a small form factor.

A various geometry of WGM resonators are fabricated such as: elliptical, spherical, ring and toroidal. They have been produced by a wide range of material as: silica, silicon, glass, semiconductors, and crystalline material. Almost a century ago, Lord Rayleigh was the first to explain "whispering gallery" phenomenon. Analogically with sound, electromagnetic waves can also travel along a spherical or general cylindrically symmetric interface by total internal reflection. When the light comes back with the same phase after one round trip, a resonance is formed. This way gives a stationary light distribution that is called as a whispering gallery mode (WGM). The theory on WGMs was carried out on spherical particles by several physicists (Ludvig Lorenz, Gustav Mie, and Debye). In their mathematical solutions the angular momentum *l* of the field in sphere considered as an interference order, which relate to the number of wavelength in the sphere perimeter. The first WGM silica microspheres were presented by V. B. Braginsky *et al.* [20] and opened a large study on WGM resonator since this time. In this paper, the pure silica microspheres with smooth surface, good spherical geometry are fabricated and measured. The studied results on microsphere presented a silica microsphere with ultra-high Q factor of 10^{10} and long light storage time. The ability to confine light in a small volume is an advantage point for many applications such as: line delay in OEO system, high sensitivity detection of chemical or biological species, and submicrowatt threshold lasers [52]. The other kinds of microcavities which have microring form are developed in recent time because of their application field wide. The first optical ring resonator was presented in 1971 [82,83] which has 5 mm diameter glass rod with 0.8 µm thin film of polyurethane doped with Rh 6G is

coated on outside of the glass rod. In 2002, the ring resonators with smaller circumference 247.2 µm and free spectral range a little over 2 nm are presented [84]. In 2003, the micro-ring resonator with smaller radius of just 20.1µm with a FSR greater than 30 nm are demonstrated for application in filter, electro-optical tuned.

In order to use of ultra-high Q micro-resonator for all applications, the light coupling into and out from the WGM resonator need to be solved. The most technique to use in light coupling is known as the “prism coupling”, that is a technique also use to launch light in the guide modes of a planar waveguide [53, 94]. When the gap between prism and microsphere is good optimized, this technique allows reach high coupling efficiently up to 80%. However this technique requires difficult beam shaping or difficult in optimize gap coupling to achieve complete power transfer into the cavity and out optical energy coupled in a manner convenient. The others coupling technique were investigated such as: side-polished fibers and fiber half-block and planar waveguides [55-58]. These methods give an improvement in some areas but they all have significant drawback as: difficult to set coupling system, to fulfill both phase matching and evanescent field condition or the leakage of light from sphere into fiber cladding and into surrounding block. In recently research of micro resonators, the optical fiber tapered is most used to light couple into and out from resonator. In ref.[66], Birks et al. presented results on coupling between a tapered fiber and a silica microsphere, the results shown that this coupling technique allows the mode matching and phase matching of two coupled evanescent fields. This technique also allows near perfect coupling efficiency both into and out of a silica microsphere resonator, which can reach a value up to 90% [71]. When compare with other couplers, fiber taper coupler has several advantage such as: high coupling efficiency, low losses and flexibility for light excitation. However, beside the advantage points, this technique gives the difficulty in phase matching but this problem does not affect prism coupling.

For micro-ring resonator geometry (SOI-waveguide devices), prism couplers, grating coupler and end-butt coupled are actual coupling technique which used in SOI waveguide coupler. Beside some advantages, these techniques give a disadvantage point that is their ability in connect to the other optical components in actual systems. Using micro lens to light couple into and out of micro ring is other used method in recently decades; micro lens is developed to apply in semiconductor laser light coupler [99, 100, 101 and 102]. In this

work, the fiber micro lenses which were fabricated on end of single mode fiber is produced and used to light coupling into and out of add/drop racetrack resonator.

This thesis is divided into four chapters; the content of theses chapters is outlined as following.

In the chapter I, we briefly present an overview of a typical Opto-Electronic-Oscillator system which uses a long optical fiber loop acting as a delay line. We give some experimental results concerning the RF spectrum, the phase noise according to the length of the fiber loop, and the quality factor of the oscillator.

In the chapter II, we present an overview on the whispering gallery modes in spherical structure. The important parameters such as the quality factor *Q*, the mode volume, the free spectral range (FSR), the finesse and resonance position of micro cavities are briefly discussed. At the end of chapter, a summary on application field of micro-resonators is presented.

We begin the chapter III with a presentation about the losses mechanisms which relate to *Q* factor of optical microsphere resonator. After that, directly we present the experimental results about our fabricated optical micro sphere. We first describe the technique used to fabricate optical microsphere, based on single mode optic fiber and tapered fiber which used to light coupling into and out from microspheres. For a better understanding of the coupling mechanism of tapered fiber-micro microsphere system, we present a modeling of evanescent coupling. In the next section, the experimental excitations of whispering gallery mode are presented. Based on these results, the *Q* factor, FSR of optical microspheres which have diameters ranging from 60 µm to 300 µm are determined. We present in following section a mapping method which use tip fiber to excite the light on the surface of microsphere. This investigation is described on section III.5. Finally in this chapter, the simulation results on silica microsphere are presented. This results help to better understand about the gap effect on the tapered fiber- resonator coupler system.

The chapter IV presents the results on another resonator structure, called add/drop micro racetrack resonator. The operateing principle, important parameters and model

coupling of this device are presented at the beginning of the chapter. In the next part, the investigation attends to the light coupling. We used fiber micro-lenses to couple light into and out from the rib waveguide of this device, therefore, the technique to fabricate the fiber micro-lenses at the end of pigtail single mode fibers is presented. Some parameters of used fiber micro-lenses are also investigated and discussed. The section IV.5.2 presents the experimental transmission spectra of add/drop racetrack at both through-port and drop-port. The *Q* factor and FSR of the racetrack are determined. These parameters show that this device could be used for an OEO system. The coupling technique allows suitability in packaging a device “fiber-racetrack-fiber” that can be easily to connect to other optical components in actual systems. Finally, we present an attempt to use this add/drop racetrack in the OEO system of the laboratory.

In the conclusion some future works are underlined.

Chapter I.

The Opto-Electronic Oscillator

I.1 Introduction

A microwave oscillator is a device generating signals from some gigahertz up to some tens of gigahertz frequencies. For many applications, such as radio communications, radars or measurement it is especially important to get high spectral purity signals. However microwave oscillators are limited by the quality factor *Q* of its resonant element and by the sensitivity to temperature changes. High *Q* oscillator can be based on quartz resonator, but the frequency is limited to some hundreds of MHz and signals in the microwave domain have to be obtained by frequency multiplication leading to a decrease of the quality in term of phase noise. Following the first works on electro-optic oscillators in 1982 by A. Neyer and E. Voger [1], an opto-electronic-oscillator (OEO) based on a delay line has been firstly proposed by S.Yao and Maleki in 1994 [2]. It was the first system using an optical fiber loop to store microwave energy. This loop is used to replace a microwave resonator to obtain the high purity spectral and stability [2, 3]. Usual lengths of several kilometers are used in this kind of oscillators. For example a phase noise level of -143 dBc/Hz at 10kHz from a 10 GHz carrier has been obtained [4] for a thermally stabilized packaged OEO. The dependence of the optical refractive index on temperature is one of the parameters having the greatest influence on the oscillation frequency stability. As the variation of the refractive index is given by $\Delta n / \Delta T \approx 1.2 \times 10^{-5}$ /°C at 10 GHz oscillation frequency the frequency drift is about -8 ppm/°C [4]. The second element highly sensitive to the temperature is the RF filter. Taking all that into account it is necessary to stabilize the temperature of the fiber loop and of the filter. However, because of the several kilometers length of the fiber it is not very easy to implement the temperature control of optical fiber

loop. A big improvement would be to replace the fiber loop and the filter by a unique component, an optical resonator.

I.2 Principle of operation

An OEO system can be configured in a variety of ways with different optical and electrical components for optimizing its characteristics. The classical configuration of OEO as introduced in [1, 2] is shown in Figure I.1. The system associates a laser source, a light modulator (for example an electro-optic modulator EOM), a long fiber loop acting as an optical delay line, a photodiode detector, an amplifier, a filter and a RF coupler.

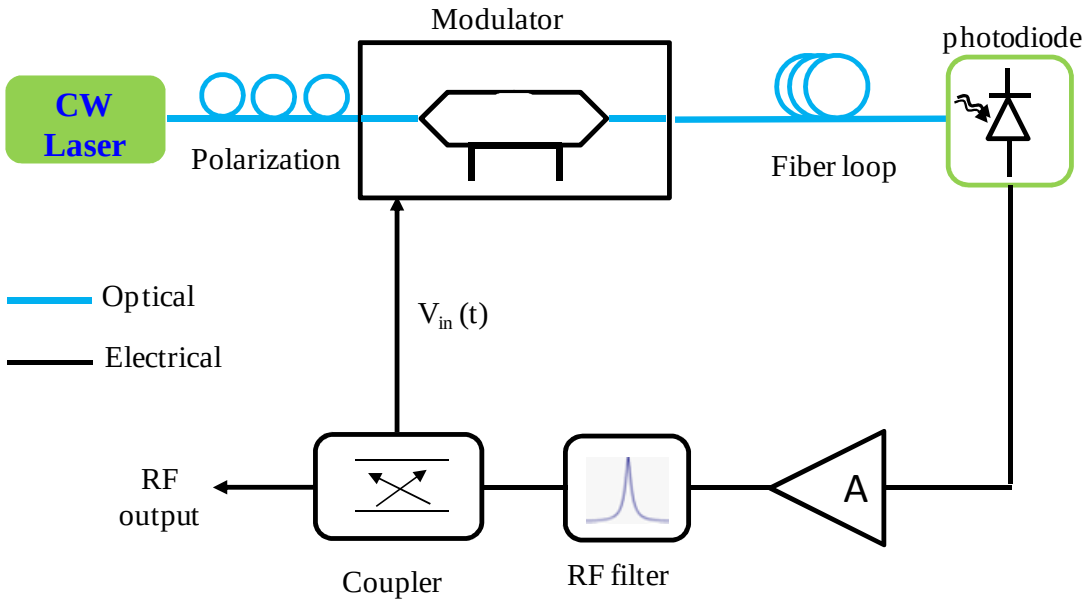

Figure I.1: Basic scheme of an Opto-Electronic Oscillator

Light coming from the laser is modulated by the electro-optic modulator and then is sent into the fiber loop; the modulated output signal is detected by a photodetector. The microwave signal at frequency ω obtained at the output detector is amplified and coupled back to the modulator for closing the loop. To obtain the desired frequency at the output of the oscillator, a filter is added in the feedback loop. By this way any frequency supported by the bandwidth of the component can be generated under the oscillation conditions. The very long optical fiber acts as a delay line providing a big delay with a rather small attenuation. During the propagation the light is stored in the fiber, as energy is stored in a

resonator; like this the fiber loop is a high quality factor component for the oscillator producing a signal that is characterized by its high spectral purity.

In case of a Mach-Zehnder intensity modulator, the signal $v_d(t)$ at the output of the photodetector dependents on the time varying input signal $v_{in}(t)$ at the EOM driving port [2], and is given by the transfer function:

$$v_d(t) = V_{ph}\left\{1-\eta\sin\left[\pi\left(\frac{v_{in}(t)}{V_\pi}+\frac{V_B}{V_\pi}\right)\right]\right\}. \tag{1.1}$$

Here V_{ph} is the maximum voltage at the output of the detector; it depends on the optical input power P_0 and on the sensitivity ρ of the photodiode. It is determined as: $V_{ph} = I_{ph}R_L$ where the photocurrent is given by $I_{ph} = \alpha P_0 \rho / 2$, R_L is the load impedance of the photo-detector, α is the fractional insertion loss of the modulator [2].

V_π is the half- wave voltage (bias voltage needed to move a point on transfer function from a maximum to a minimum of the optical power transmission),

V_B is the dc component used as biasing voltage of the EOM,

η is the extinction ratio of the modulator.

The opto-electronic-oscillator is formed by feeding the signal of Eq. (1.1) back to the RF input port of the EOM. If G_A is the total voltage amplification, including both the RF filter and coupler losses, then the signal $v_{out}(t)$ at output of the microwave loop is $v_{out}(t) = G_A v_d(t)$. Therefore the small signal gain of the loop can be obtained from (1.1):

$$G_S = \left.\frac{dv_{out}}{dv_{in}}\right|_{v_{in}=0} = -G_A\frac{\eta\pi V_{ph}}{V_\pi}.\cos\left(\frac{V_B\pi}{V_\pi}\right) \tag{1.2}$$

The modulator is positively biased if $G_S > 0$, otherwise it is negatively biased. When $V_B = 0$ the modulator is biased at negative quadrature and it is biased at positive quadrature when $V_B = V_\pi$. From the Eq. (1.2), the oscillation threshold condition of the OEO can be determined as $|G_S| = 1$ leading to:

$$V_{ph} = \frac{V_\pi}{\pi \eta G_A \cos\left(\frac{V_B \pi}{V_\pi}\right)} \tag{1.3}$$

Eq. (1.1) is nonlinear, but the output can be linearized if the feedback signal goes through a RF filter with a bandwidth which is narrow enough for blocking all harmonic components. The linearized output can be expressed as:

$$v_{out}(t) = G(V_0) v_{in}(t) \tag{1.4}$$

where V_0 is the amplitude of the input signal and $G(V_0)$ is the voltage gain coefficient and can be expressed approximately by:

$$G(V_0) = G_s \left[1 - \frac{1}{2}\left(\frac{\pi V_0}{2V_\pi}\right)^2 + \frac{1}{2}\left(\frac{\pi V_0}{2V_\pi}\right)^4 \right] \tag{1.5}$$

where G_s being defined in Eq. 1.2 [5]. Four important parameters of OEO can be introduced such as: the oscillation frequency f_{osc}, the amplitude V_{osc}, the linewidth and the power spectral density $S_{rf}(f')$ of the signal [5]. The oscillation frequency is given by $f_{osc} = \frac{(k+1/2)}{\tau_g}$ if $G(V_{osc}) < 0$ and $f_{osc} = \frac{k}{\tau_g}$ if $G(V_{osc}) > 0$. Here τ_g is the total group delay of the complete loop; it includes optical the optical delay τ_{op} and the delay caused by electronic components τ_{en} (such as the amplifier and the electronic filter). So the total group delay can be written as: $\tau_g = \tau_{op} + \tau_{en}$. It can be seen that the oscillation frequency depends not only on the loop delay but also depends on the mode number *k*. The group delay τ_g can be considered as an optical equivalent delay corresponding to a global length L_g of the loop and given: $\tau_g = N_{fib} L_g / c_0$ where N_{fib} is the effective refractive index of optical fiber and c_0 is the velocity of light in vacuum or in the air. Therefore, the oscillation frequency is given, in case of $G(V_{osc}) > 0$, by:

$$f_{osc} = \frac{k}{\tau_g} = k \frac{c_0}{N_{fib} L_g} \tag{1.6}$$

Eq. (1.6) shows that the OEO generates different oscillation frequencies or different modes. These modes are determined by the mode number k ($k = 1, 2, 3 ...$). The distance between two modes is the mode spacing, and can be called the Free Spectral Range of the oscillator and is noted FSR_{osc}; it depends on the effective refractive index of the fiber, the global length L_g of the fiber loop, and the light velocity c_0. The Figure I.2 presents the spectrum and phase noise of the OEO, developed in the laboratory of ENS Cachan, for different lengths of the optical fiber.

In Figure I.2 it appears clearly that we get many peaks, corresponding to the different modes and making a frequency comb. Nevertheless one peak gets the maximum of power; in this case the center frequency is at 8.004 GHz. The free spectral range of the OEO, $FSR_{osc} = f_{osc,k+1} - f_{osc,k}$, is given by the following formula.

$$FSR_{osc} = \frac{1}{\tau_g} = \frac{c_0}{N_{fib} L_g} \tag{1.7}$$

From equation (1.7), we can see that the mode spacing (or FSR) is the inverse of the global delay time of the fiber loop. For example, the distance between two modes can be determined from equation (1.7), considering that $N_{fib} \cong 1.45$. Some values are listed in Table I.1.

Fiber length (km)	0.5	1	1.5
Theoretical FSR_{osc} (kHz)	414	207	137
Experimental FSR_{osc} (kHz)	390	199	131

Table I.1. Free spectral range of the OEO for different values of the fiber loop.

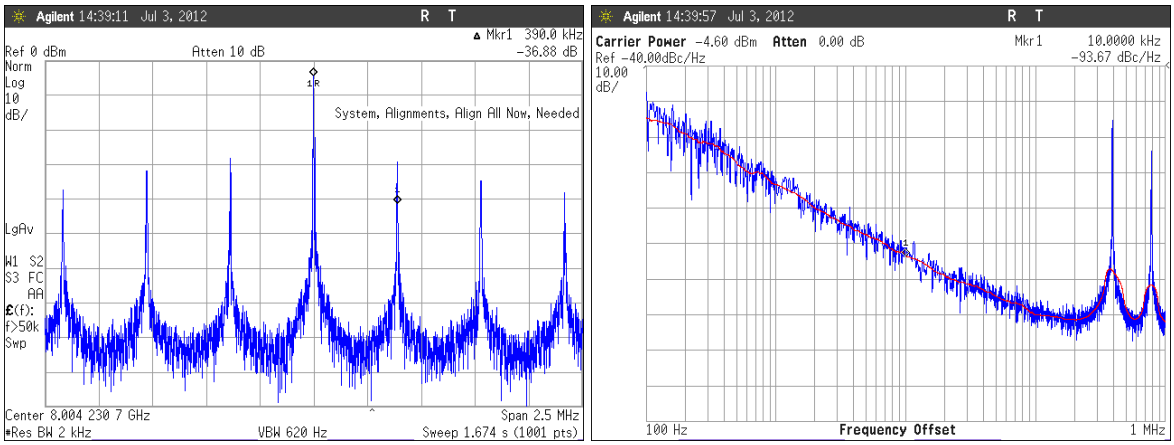

Length 500 m

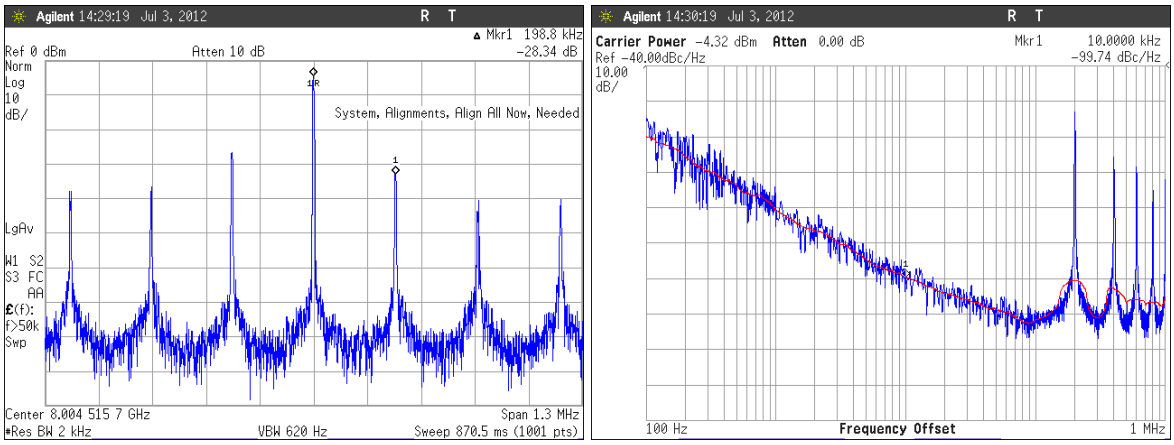

Length 1000 m

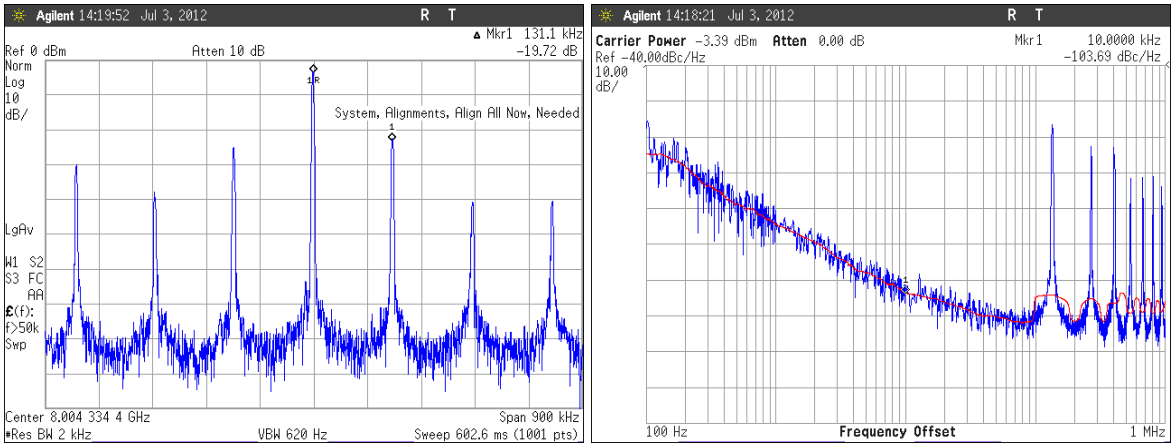

Length 1500 m

Figure I.2: Spectrum and phase noise of the OEO for three different fiber spool lengths.

The theoretical value is systematically bigger than the experimental one because the calculation has been done taking into account only the fiber loop length but neither the short fibers associated to the modulator and the detector (a 5 m section has been added for conveniences) nor the electronic delay. The difference can be explained by an additional global equivalent length of about 30 m.

Otherwise it is clearly determined in [2] that when the length of optical delay line increases, the phase noise of oscillator is reduced. The experimental phase noise at 10 kHz from the carrier at 8.004 GHz is listed in table I.2 for the three lengths of the fiber spool.

Fiber length (km)	0.5	1	1.5
Phase noise at 10 kHz from the carrier (dBc/Hz)	−93.7	−99.7	−103.7

Table I.2. Phase noise of the OEO for different values of the fiber loop.

For selecting one mode in the complete frequency comb a RF filter has to be placed in the loop. Unfortunately it is difficult to select only one mode as it can be seen in the Fig. I.2. The free spectral range of the oscillator is very small, especially if a very long fiber spool is used for improving the spectral purity. There is a tradeoff for the choice of the fiber length between the long length for low phase noise characteristics and a short length for a wider spacing of the oscillation modes.

This tradeoff can be solved by using multiloop configurations [6]. Spurious peaks can be greatly attenuated by with two loops. The first solution [ref] is to split the optical beam at the output of the modulator by an optical coupler and then to use two optical fibers, a short one and a long one, each being followed by a photodetector (see Fig. I.3). The two RF signals are then combined and finally the system is classically terminated by an amplifier, a RF filter and the RF coupler [6].

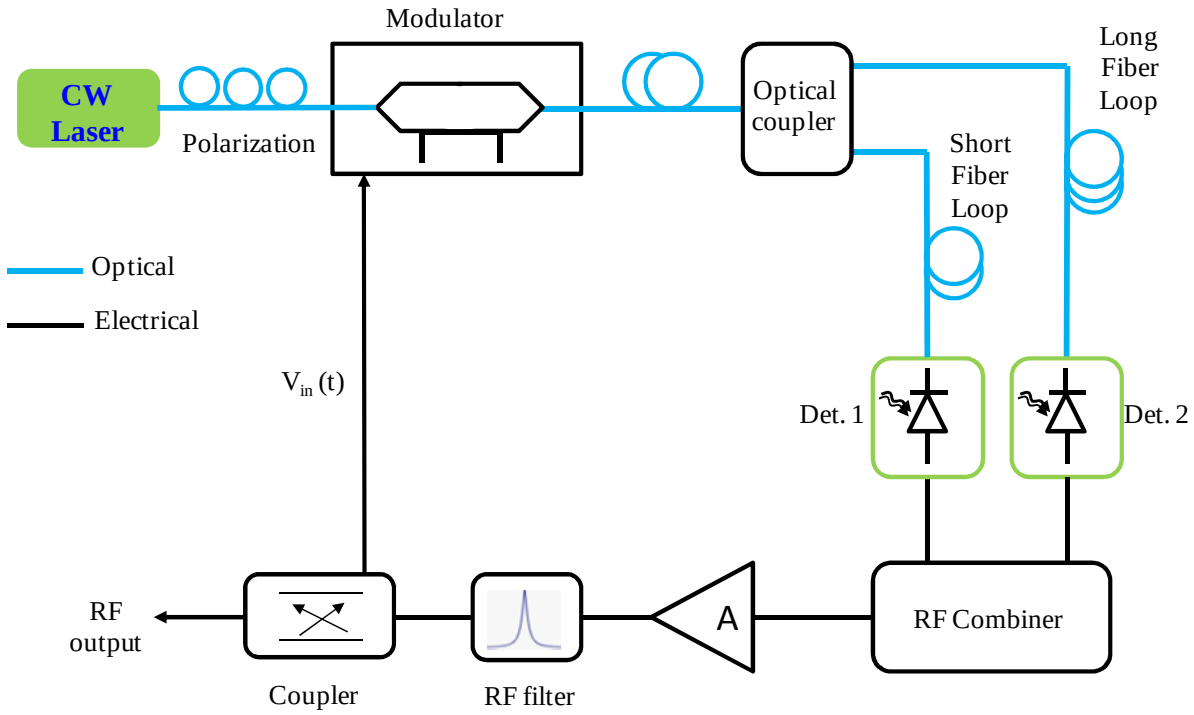

Figure I.3: Double loop opto-electronic oscillator.

The mode spacing is fixed by the short loop (attenuations of 60 dB on the spurious peaks have been registered [6]). The phase noise is mainly determined by the long loop, even if finally it is not as good as for an OEO built with only the long loop [7].

Another solution is to use a double OEO with a master/slave system [8]. The master OEO has a long fiber loop and the slave OEO has a short loop. The RF signal from the master OEO is injected into the slave one which is locked on the oscillation frequency of the master; such a system is called injection-locked dual OEO (see Fig. I.4). Because of the short loop the mode spacing is obtained from this short length. And in this case the phase noise is fixed by the long fiber loop of the master OEO.

With multiloop or dual OEO structures it is possible to solve the problem of the multimode oscillator by keeping a very low phase noise. But clearly this solution leads to more complicated system, more bulky and therefore more difficult to implement temperature control. Systems like that cannot be considered as easily transportable.

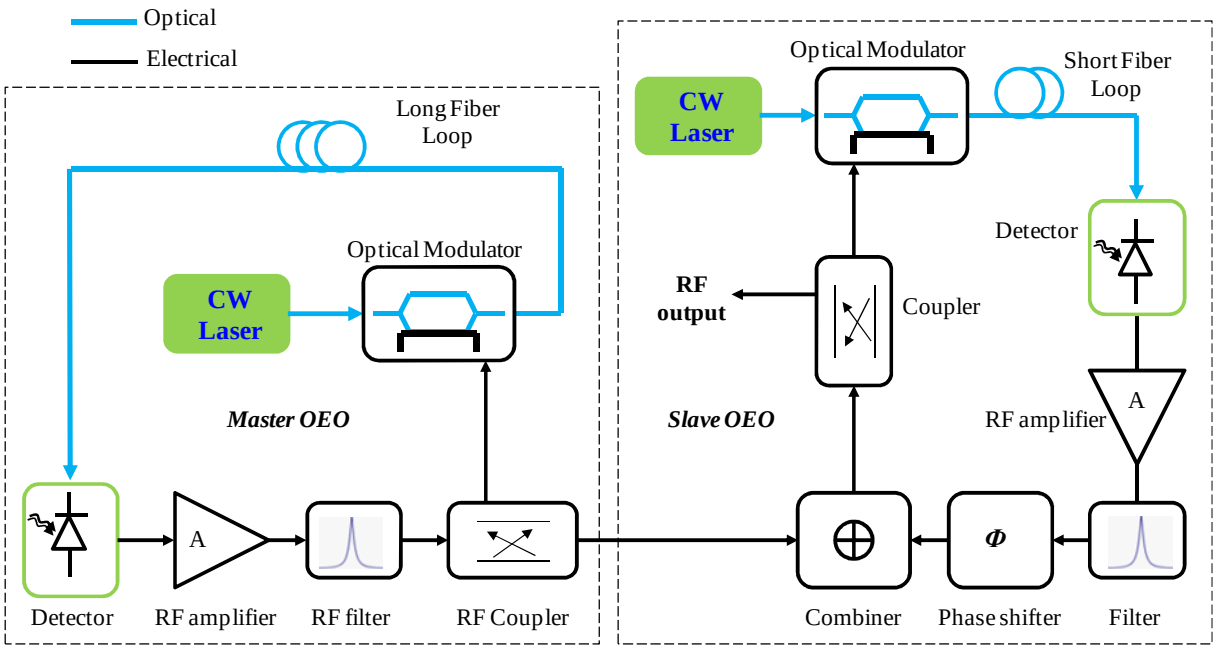

Figure I.4: Injection locked dual opto-electronic-oscillator.

Another solution is to change completely the principle of the oscillator, and to replace the fiber loop by an optical resonator. In order to keep a very low phase noise (as it is possible to obtain with the delay line technique) the characteristics of the resonator have to be determined from the properties of the delay line oscillator.

I.3 Optical resonator for OEO.

In the classical version of OEO system, the optical fiber act as a delay line, and the microwave oscillation frequency is defined by a narrow RF band-pass filter (fig.I.1). This original configuration has RF quality factor up to 10^9 at 10 GHz and excellent phase noise performance [1, 4]. The main disadvantages of such classical systems are the size, the difficulty to implement temperature control and the spurious peaks. In order to eliminate all these disadvantages, by keeping the main advantage of the OEO which is the very low phase noise an ultra-high quality factor resonator can be used instead of the optical fiber [10, 11]. A typical configuration of an OEO based on optical resonator is presented in Fig. I.5.

How to determine the quality factor of the optical resonator for the two structures being equivalent? In the classical structure (see Fig. I.1) of an OEO the optical fiber loop acts as the delay element, depending mainly on the length of the fiber. The effective index of the fiber, noted N_{fib}, can be considered as constant in the optical operating frequency range $(\nu_0 + \Delta\nu \geq \nu_{opt} \geq \nu_0 - \Delta\nu)$, so the effective delay time due to the fiber loop is equal to the propagation time and given by:

$$\tau_d = \frac{N_{fib} L_{fib}}{c_0} \tag{1.8}$$

where L_{fib} is the length of the optical fiber and c_0 is the velocity of the light. For example a 4 km optical fiber with refractive index $N_{fib} = 1.45$ generates a delay of $19.3\,\mu s$. In case of long fibers spool used for getting a high spectral quality the delay time is approximately equal to the global propagation time defined previously, $L_g \approx L_{fib}$ and $\tau_d \approx \tau_g$.

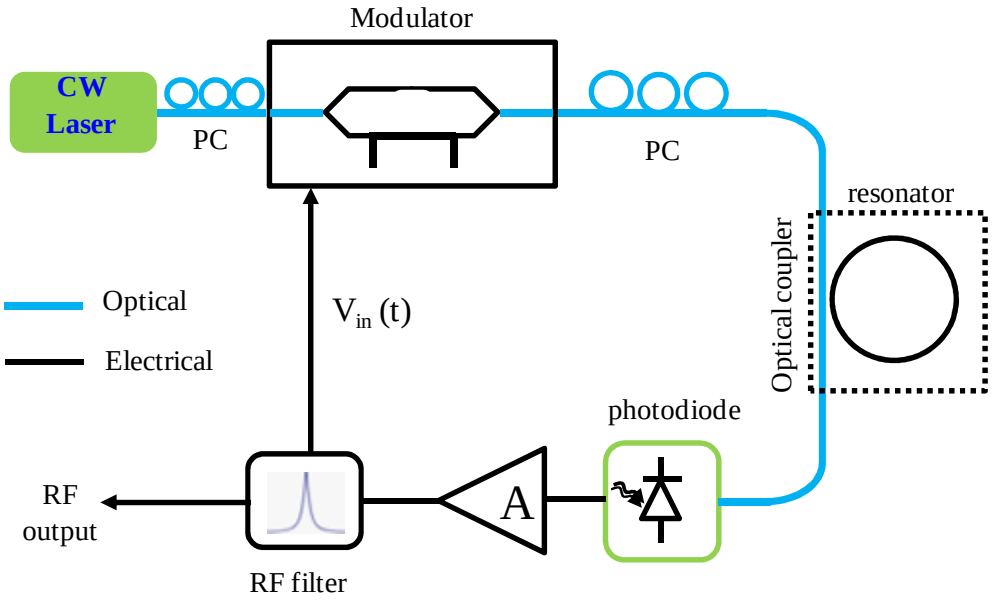

Figure I.5: Opto-electronic oscillator based on optical resonator.

As mentioned above, the function of optical fiber in an OEO is to store the energy of the signal; by this way the optical fiber can be considered as equivalent to resonator in the usual high frequency oscillator. By analogy with an electronic resonator like an LC circuit,

we can determine a relation between the storage time and the quality factor. Studying the transient response of a filter, characterized by its damping coefficient m, the variation with time of the energy stored in the filter is given by $e^{-m\omega_0 t} = e^{-\frac{\omega_0}{2Q}t}$, where Q is the quality factor of the filter. Defining the storage time as the time constant we can see that $\tau_s = \frac{Q}{\omega_0}$ or $Q = 2\pi f_0 \tau_s$.

Considering the case of the optical fiber from the point of a storage effect the propagation time can be considered as equivalent to the decay-time ($\tau_s \approx \tau_d$). In fact a pulsed send trough the optical fiber remains inside the fiber until it goes out, and the attenuation is very low. Taking into account $0.5\,\text{dB}$ losses per connector and $0.2\,\text{dB/km}$ losses in the fiber, the length leading to an attenuation of the energy inside the fiber of $1/e$ which means $4.34\,\text{dB}$ should be equal to $16.7\,\text{km}$. The quality factor of the optical delay-line (noted Q_{odl-mw}) is a function of the oscillation frequency and of the propagation time in the fiber:

$$Q_{odl-mw} = 2\pi f_{osc} \tau_d \tag{1.9}$$

For example, considering the OEO developed in the laboratory of ENS Cachan, with an oscillation frequency $f_{osc} = 8\,\text{GHz}$, a length of the optical fiber loop $L_{fib} = 1.5\,\text{km}$ and an effective refractive index $N_{fib} = 1.45$, then the corresponding delay time is $\tau_d = 7.25\mu\text{s}$ leading to a quality factor $Q_{odl-mw} = 3.64\times10^5$.

It is interesting to note that the quality factor is improved by increasing the oscillation frequency, which means by changing the RF filter which selects the desired value among the frequency comb. Otherwise we can see also that the longer the fiber, the higher the quality factor

The spectral purity of the oscillator is determined by the frequency linewidth which is related to the power RF spectral density of the OEO. This spectral power density is expressed in [3] as:

$$S_{RF}(f') = \frac{\delta}{\left(\frac{\delta}{2\tau}\right)^2 + (2\pi)^2 (f'\tau)^2} \tag{1.10}$$

where $1/\tau$ is the mode spacing of the OEO, δ is the input noise-to-signal ratio of the oscillator, f' is frequency offset from the oscillation frequency f_{osc} (the carrier). This equation shows that $S_{RF}(f')$ is a lorentzian function of frequency offset, therefore the full width at haft maximum (FWHM), which is also the -3 dB bandwidth, of the spectral line is given by:

$$\Delta f_{FWHM} = \frac{1}{2\pi}\frac{\delta}{\tau^2} \tag{1.11}$$

The quality factor Q of the oscillator is defined by:

$$Q = \frac{f_{osc}}{\Delta f_{FWHM}} = Q_{odl}\frac{\tau}{\delta} \tag{1.12}$$

According to equations 1.9 and 1.12 for a classical OEO structure the longer the fiber, the higher the quality factor.

The cavity is characterized by the free spectral range (FSR) of the resonant mode, its frequency width Δf and quality factor *Q* that defined in [18].

As shown in the scheme of the OEO system in figure I.3, the light from a laser is modulated by an electro-optical modulator (EOM) and then is sent into a fiber delay line followed by a filter and a photodiode. Here optical delay line acts as storage of the microwave energy.

Q_{opt} is determined as the quality factor of the optical fiber delay line, it is expressed as given in Eq. (1.9) by $Q_{opt} = 2\pi f_{osc}\tau_d$ where $\tau_d = \frac{N_{fib}L_{fib}}{c_0}$ (Eq. 1.8) is the energy decay time or the energy storage time of the delay line.

Assuming the resonator is used for filtering a microwave signal, the spectral width of filter is the same but the carrier frequency is reduced by the ratio of the optical and the microwave carriers. The optical resonator creates an optical frequency comb with microwave spacing. Each mode of this optical comb corresponds an optical Q factor (Q_{opt}) and an equivalent RF Q factor. Therefore, an equivalent microwave Q factor determined in [14] as:

$$Q_{RF} = Q_{opt} \frac{f_{osc}}{f_{opt}} \tag{1.15}$$

where f_{opt} is the optical resonant frequency.

For example in case of the quartz disk which has a diameter of 7.7 mm [14], the optical quality factor of 10^9 and a free spectral range of 8 GHz at 1.55 µm for this resonator are determined. This measurement allows to determine the equivalent quality factor of resonator based OEO system. For $f_{osc} = 10\,\text{GHz}$, the RF quality factors $Q = 4\times10^5$.

In case of the OEO of ENS Cachan, with $f_{osc} = 8\,\text{GHz}$, a fiber delay line of 1.5 km, corresponding to $\tau_d = 7.2\mu\text{s}$, from equation (1.12) the quality factor of $Q = 3.64\times10^5$ is calculated. If a resonator which has optical quality factor Q_{opt} of 10^8 is used, the Q_{RF} factor of 10^5 is calculated from Eq. (1.13) at operate wavelength 1.55µm (193.5 THz) for this structure. From calculated results, it can say that a disk resonator which has a diameter in range of a few millimeters could be used to replace a few kilometers optical fiber line.

Chapter II.

Optical Micro-Resonator

In this chapter we present the whispering gallery mode resonators and their general.

II.1 An approach of optical resonators

II.1.1 Fabry-Perot resonator

A set of two or more mirrors arranged to cause light to propagate in a closed path is commonly called an optical resonator, an optical cavity. The simplest resonator is the Fabry-Perot resonator which consists of two parallel plane mirrors as shown in figure II.1 [16]. Because of the easy calculation that can be conducted it is a good introduction to the world of optical micro-resonators.

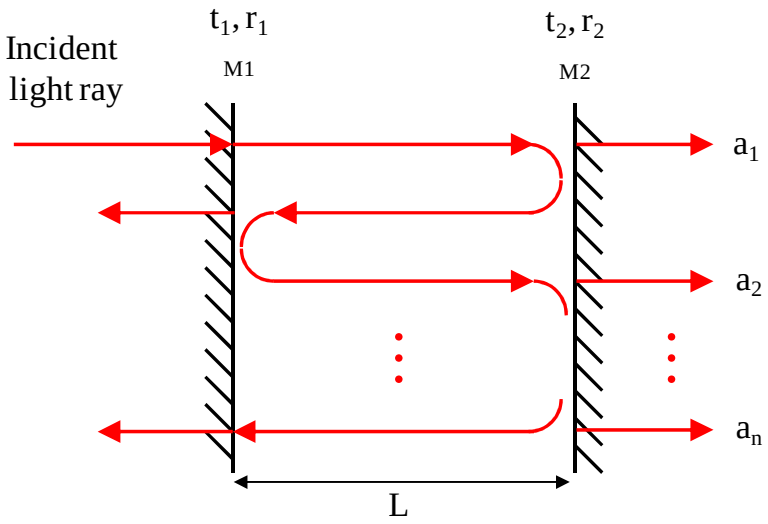

Figure II.1: Transmission of a plane wave travel in a planar- mirror resonator

Between these mirrors, the light is repeatedly reflected with little loss. Here we want to briefly present some properties of Fabry-Perot resonator to give the first approach for

resonator mode, losses or resonance spectral of optical cavity. Let us consider a plane wave travelling inside the resonator.

We note r_1 and r_2 the amplitude reflectances of the inner surface of mirrors M1 and M2; t_1 and t_2 are their amplitude transmittances. The input optical frequency is noted ν and the corresponding free-space wave number is $k = 2\pi / \lambda$. Assuming the wave with an amplitude a_0 enters the FP resonator at mirror 1 (M1), it propagates to the output mirror (M2), the amplitude a_1 coming out of M2 has the values:

$$a_1 = a_0 t_1 t_2 \exp(jkL - \alpha L) \tag{2.1}$$

A portion of this wave reflects and travels back to the input mirror where another portion of it reflects again. When it comes out of M2, it is given as:

$$a_2 = a_1 r \tag{2.2a}$$

where L is the length (distance between two plane mirror) of FP cavity $r = r_1 r_2 \exp(2jkL - 2\alpha L)$, and α is distribution losses coefficient between the mirrors. Basically the same thing happens to the wave with each round trip so that after *n* round trips, the amplitude a_n is given as:

$$a_n = a_1 r^{n-1}. \tag{2.2b}$$

Thus the total amplitude at the output of the Fabry-Perot can be written as:

$$a_{tot} = \sum_{i=1}^{n \to \infty} a_i = \frac{a_1}{1 - r} \tag{2.3}$$

And the total transmission coefficient is determined when $|r| < 1$ as:

$$T_{tot} = |T_{tot}|^2 = \left| \frac{a_1}{1 - r} \right|^2 \tag{2.4}$$

The phase shift imparted by the two mirrors reflection is 0 or 2π (π at each mirror). So the phase shift imparted by a single round trip of propagation must be a multiple of 2π:

$$\varphi = k2L = m2\pi \text{ , with } m = 1, 2,... \tag{2.5}$$

It can said that the amplitude total (equation 2.3) is represented by the sum of an infinite number of phasor as shown in figure II.2

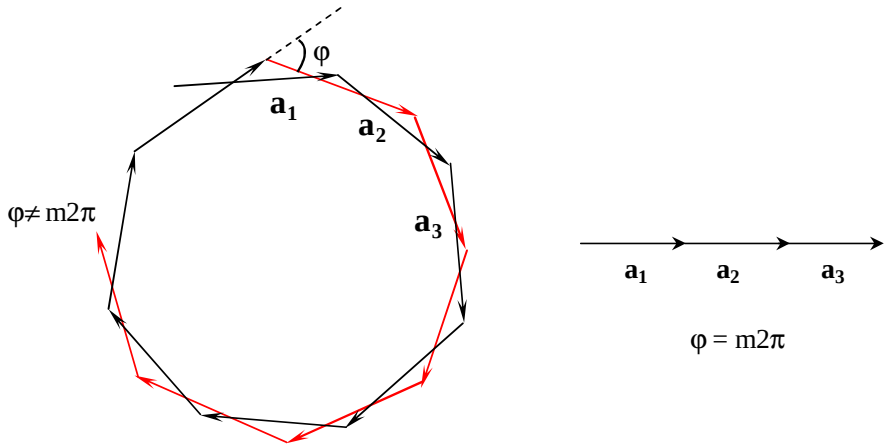

Figure II.2: Phase diagram representing the total amplitude a_n for $\varphi = m2\pi$ and $\varphi \neq m2\pi$

Thus if $\varphi = m2\pi$ an initial wave can result in buildup of finite power in the resonator.

II.1.2 Fabry-Perot main characteristics

The waves which fit into a resonator of a given length L are also called oscillating modes or just modes. Then all wave which fulfil following equation will fit into the resonator:

$$L = m\left(\frac{\lambda_m}{2}\right) \text{ where } m \text{ is an integer } (m = 1, 2, 3...) \tag{2.6}$$

So the next neighbouring mode must fulfil the condition:

$$L = (m+1)\left(\frac{\lambda_{m+1}}{2}\right) \tag{2.7}$$

Condering the resonance frequency is $\nu = \frac{c_0}{\lambda}$, from eq.(2.6) the resonance frequency determined as:

$$\nu_m = m\left(\frac{c_0}{2L}\right) \tag{2.8}$$

And the distance between two adjacent resonance modes or the free spectral range (FSR) of a Fabry-Perot is given as:

$$\Delta\nu_{FSR} = \nu_{m+1} - \nu_m = \frac{c_0}{2L} \tag{2.9}$$

The parameter which detemines the resolution capacity of Fabry-Perot is finnesse of resonator. It is defined by ratio between FSR value and the full width at half maximum Δν (linewidth) of resoannce. It given as:

$$\mathcal{F} = \frac{FSR}{\Delta\nu} \tag{2.10}$$

For a two-mirror resonator, linewidth $\Delta\nu = \frac{c_0}{2\pi L}\frac{1-r}{\sqrt{r}}$, So the cavity finesse can be rewitten as:

$$\mathcal{F} = \frac{2\pi L c_0\sqrt{r}}{2Lc_0(1-r)} = \frac{\pi\sqrt{r}}{(1-r)} \tag{2.11}$$

Because α is the loss per unit length and $c_0\alpha$ is loss per unit time, the resonator lifetime or photon lifetime can be defined as: $\tau_p = 1/c_0\alpha$ (seconds). So the quality factor of F-P resonator is related to the resonator lifetime by:

$$Q = 2\pi\nu\tau_p \tag{2.12}$$

The Fabry-Perot is the basic optical resonator. Nowadays, many kinds of optical resonators are developed with various geometrical shapes such as sphere, disk, stadium or structures based on waveguides.

II.2 General properties of whispering gallery mode resonator

II.2.1 An approach of WGMs

Whispering gallery mode resonances concern electromagnetic waves traveling in a dielectric medium characterized by a circular (cylindrical or spherical) symmetry, the light being trapped in circular orbits just within the surface of the structure [17]. Considering a sphere with the radius a and refractive index N, when the light is incident at the interface with incident angle i larger than the critical angle $i_c = \arcsin(1/N)$, total internal reflection occurs and a WGM resonance is formed when the optical path is equal to an integer number of wavelengths (fig.II.3).

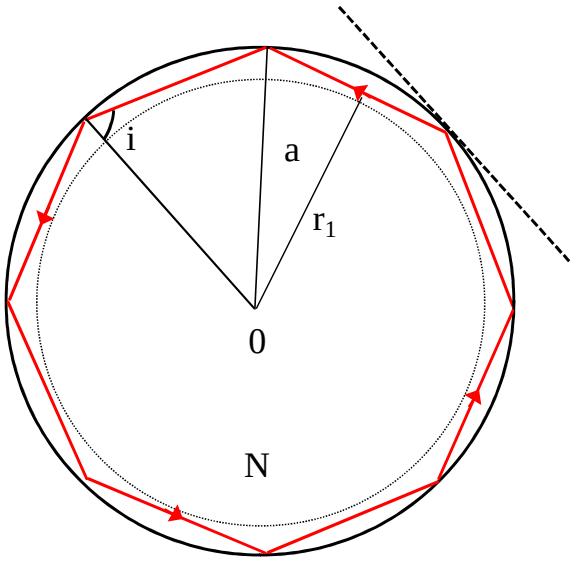

Figure II.3: Light propagation by total internal reflection (TIR) in a sphere resonator, N, a, 0 and *i* present refractive index, the radius, centre of cavity and incident angle of the light ray respectively.

Due to the spherical symmetry, the same incident angle is kept for the following reflections, therefore the light ray is confined inside the cavity by the total internal reflection effect. For large microspheres that have $a >> \lambda$ and incident angle $i \approx \pi/2$, the trapped ray propagates close to the surface with a travel distance of $2\pi a$ in one round trip. Thus an approximate condition for a WGM resonance can be written as:

$$\ell\left(\frac{\lambda_{0r}}{N}\right)=2\pi a \tag{2.13}$$

where ℓ is an integer fraction of the circumference corresponding to the number of sides of the polygon formed by the path of light ray in the resonator surface and, λ_{0r} is the resonance wavelength. From Eq. (2.6) the resonance condition for the frequency is:

$$\nu=\frac{\ell c_0}{2\pi aN} \tag{2.14}$$

Here c_0 is the speed of light in vacuum. Defining a dimensionless size parameter $x=\frac{2\pi a}{\lambda_{res}}$, the resonance condition is $x=\frac{\ell}{N}$. With $\frac{\Delta x}{\Delta l}=\frac{1}{N}$ from Eq. (2.14) the free spectral range (*FSR*) can be written in frequency and wavelength as:

$$\Delta\nu_{FSR}=\frac{\Delta\nu}{\Delta\ell}=\frac{d\nu}{d\ell}=\frac{c_0}{2\pi Na} \tag{2.15}$$

$$\Delta\lambda_{FSR}=\frac{\Delta\lambda}{\Delta\ell}=\frac{d\lambda}{d\ell}=\frac{{\lambda_0}^2}{2\pi Na} \tag{2.16}$$

For a fused silica sphere with a radius $a=50\,\mu\text{m}$, $N=1.45$ at operation wavelength $\lambda_0=1550\,\text{nm}$, its *FSR* is approximately 659 GHz in term of frequency or 5.3 nm in term of wavelength.

The angular momentum L as shown in Fig. II.4 is defined as follow:

$$L=r.k \tag{2.17}$$

In case of WGM resonance Fig.3, its angular momentum is given by:

$$L=r_1k=r_1Nk_0 \tag{2.18}$$

where k_0 is the wave number in vacuum and $r_1=a\sin(i)$.

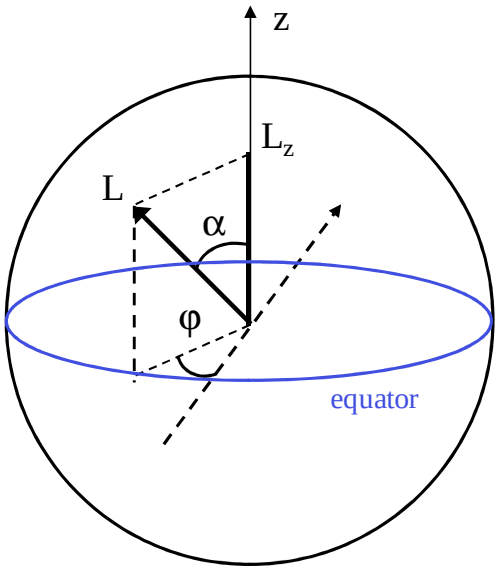

Figure II.4: Angular momentum L associated with WGM and its L_z projection on the polar axis.

Under the condition $i = \pi/2$ the angular momentum L is then:

$$L \approx aNk_0 \approx l \tag{2.19}$$

Thus, the number of wavelength ℓ in the circumference is also called the angular order. For a silica sphere with 50 µm radius at $\lambda_0 = 1550$ nm and a refractive index $N = 1.45$, we obtain $\ell = 293$. So whispering gallery modes can be viewed as high angular momentum electromagnetic modes in which light propagates by total internal reflection at grazing incidence with proper phase condition after travel along the resonator surface.

II.2.2 Electromagnetic field

A WGM can be characterized by it polarization TE-mode transversal electric (the electric field of the wave makes a 90° angle with respect of the propagation direction), or TM-mode transversal magnetic (the magnetic field of the wave makes a 90° angle with respect of the propagation direction) and three integer orders n, ℓ, m where n denotes the radial order, ℓ the angular mode number and m the azimulthal mode. The mode number n is the number of maxima in the radial distribution of the internal electric field, the mode number ℓ corresponds to the number of wavelengths around the circumference and the

mode number m gives maxima in the polar distribution of internal electric field. For a better understanding about whispering gallery mode in a micro cavity, the solution of electromagnetic field in a dielectric microsphere is presented. The work of Stratton [18] presents Hansen's method where the solution of the vector Helmholtz's equation has an angular dependence described by three vectors spherical harmonics [19] expressed as:

$$\vec{X}_\ell^m = \frac{1}{\sqrt{\ell(\ell+1)}}\vec{\nabla}Y_\ell^m \times \vec{r} \tag{2.20a}$$

$$\vec{Y}_\ell^m = \frac{1}{\sqrt{\ell(\ell+1)}} r\vec{\nabla}Y_\ell^m \tag{2.20b}$$

$$Z_\ell^m = Y_\ell^m \vec{r} \quad \vec{Z}_\ell^m = Y_\ell^m \hat{r} \tag{2.20c}$$

with $\hat{r}$ is the unit vector along the radial direction and $\vec{r}$ is the position vector.

In this equation, the mode number ℓ indicates the order of the spherical harmonic Y_ℓ^m that describes the angular field distribution, and the index m is called the azimuthal mode number. The electric and magnetic fields for both polarizations, TE and TM, can be expressed as:

$$\text{TE mode: } \begin{cases} \vec{E}_{\ell,m}^{TE}(\vec{r}) = E_0 \dfrac{f_\ell(r)}{k_0 r}\vec{X}_\ell^m(\Omega) \\ \vec{B}_{\ell,m}^{TE}(\vec{r}) = -\dfrac{iE_0}{c}\left(\dfrac{f_\ell'(r)}{k_0^2 r}\vec{Y}_\ell^m(\Omega) + \sqrt{\ell(\ell+1)}\dfrac{f\ell(r)}{k_0^2 r^2}\vec{Z}_\ell^m(\Omega)\right) \end{cases} \tag{2.21a}$$

$$\text{TM mode: } \begin{cases} \vec{E}_{\ell,m}^{TM}(\vec{r}) = \dfrac{E_0}{N^2}\left(\dfrac{f_\ell'(r)}{k_0^2 r}\vec{Y}_\ell^m(\Omega) + \sqrt{\ell(\ell+1)}\dfrac{f_\ell(r)}{k_0^2 r^2}\vec{Z}_\ell^m(\Omega)\right) \\ \vec{B}_{\ell,m}^{TM}(\vec{r}) = -\dfrac{iE_0}{c}\dfrac{f_\ell'(r)}{k_0 r}\vec{X}_\ell^m(\Omega) \end{cases} \tag{2.21b}$$

where N is the refractive index.

In equation (2.21) $f(r)$ is the radial distribution of the electric field and can be expressed as:

$$\frac{d^2 f_\ell(r)}{dr^2} + \left[N^2(r) k_0^2 - \frac{\ell(\ell+1)}{r^2} \right] f_\ell(r) = 0 \tag{2.22}$$

The solution of this equation is given by:

$$f_\ell(r) = \begin{cases} \psi_\ell(Nk_0 r) & \text{for } r < a \\ \alpha\psi_\ell(k_0 r) + \beta\chi_\ell(k_0 r) & \text{for } r > a \end{cases} \tag{2.23}$$

Here a is the radius of sphere, α and β are two constants, and ψ_ℓ, χ_ℓ are respectively the Riccati-Bessel functions of the first and second kind. They are defined as:

$$\begin{cases} \psi_\ell(\rho) = \rho j_\ell(\rho) \\ \chi_\ell(\rho) = \rho n_\ell(\rho) \end{cases} \tag{2.24}$$

with j_ℓ and n_ℓ being respectively the Bessel and Neumann functions.

II.2.3 Resonance position

Equation (2.23) indicates that inside the sphere ($r < a$), $f_\ell(r)$ defined by the Riccati function $\psi_\ell(Nk_0 r)$. In case of $r > a$, $f_\ell(r)$ function is defined by a linear combination of evanescent functions $\chi_\ell(k_0 r)$ and $\psi_\ell(k_0 r)$. Therefore the $f_\ell(r)$ function and its derivative $f_\ell'(r)$ must be continuous across the microsphere at air interface ($a = 0$). The condition of continuity of the tangential components of the fields allows to find the equations for the positions of resonances:

TE mode: $$\begin{cases} \psi_\ell(Nk_0 a) = \alpha\psi_\ell(k_0 a) + \beta\chi_\ell(k_0 a) \\ N\psi_\ell'(Nk_0 a) = \alpha\psi_\ell'(k_0 a) + \beta\chi_\ell'(k_0 a) \end{cases} \tag{2.25a}$$

TM mode: $$\begin{cases} N^{-1}\psi_\ell'(Nk_0 a) = \alpha\psi_\ell'(k_0 a) + \beta\chi_\ell'(k_0 a) \\ \psi_\ell(Nk_0 a) = \alpha\psi_\ell(k_0 a) + \beta\chi_\ell(k_0 a) \end{cases} \tag{2.25b}$$

The Wronskian function of ψ_ℓ and χ_ℓ in equation (2.25) can be written as:

$$\begin{cases} \alpha = \psi_\ell(Nx)\chi_\ell'(x) = P\psi_\ell'(Nx)\chi_\ell(x) \\ \beta = -\psi_\ell'(Nx)\psi_\ell'(x) = P\psi_\ell'(Nx)\psi_\ell(x) \end{cases} \tag{2.26}$$

where the size parameter x is defined as $x = k_0 a$, and P represent the polarization modes Because the function ψ_ℓ increases exponentially with r, given $r \to \infty$, the constant α should be equal to 0. Thus by considering $\alpha = 0$ in the continuity equation (2.26), the resonance condition expressed in size parameter $x = 2\pi a / \lambda$ can be written as:

$$P \frac{\psi'_\ell(Nx)}{\psi_\ell(Nx)} = \frac{\chi'_\ell(x)}{\chi_\ell(x)} \tag{2.27}$$

where $P = \begin{cases} N & \text{for TE mode} \\ 1/N & \text{for TM mode} \end{cases}$

The resonance position can be obtained by solving equation (2.27).

Considering a large sphere, where the angular mode number is $\ell >> 1$, the resonance position $x_{\ell,n}$ in the sphere is, as confirmed in [20], given by

$$\begin{aligned} Nx_{\ell,n} = \nu + 2^{-\frac{1}{3}} \alpha_n \nu^{\frac{1}{3}} - \frac{P}{\left(N^2 - 1\right)^{\frac{1}{2}}} + \left(\frac{3}{10} 2^{-\frac{2}{3}}\right) \alpha_n^2 \nu^{-\frac{1}{3}} \\ - \frac{2^{-\frac{1}{3}} P\left(N^2 - 2P^{2/3}\right)}{\left(N^2 - 1\right)^{3/2}} \alpha_n \nu^{-\frac{2}{3}} + 0\left(\nu^{-1}\right) \end{aligned} \tag{2.28}$$

where $\nu = \ell + 1/2$, α_n is n_{th} zero of the Airy function $A_i(-z)$ [21].

The first term of expression in Eq. (2.28) is the most used and can be rewritten

$$Nx_{\ell,n} = \left(\ell + \tfrac{1}{2}\right) + \left(\frac{\ell + \frac{1}{2}}{2}\right)^{1/2} (-\alpha_n) - \frac{P}{\sqrt{(N^2 - 1)}} + \ldots \tag{2.29}$$

From this equation, it's clear that the resonance position depends on the mode numbers n, ℓ and on the polarization condition. Another way to get the resonance position, by using eikonal approximation, has been introduced in [22] as:

$$Nx_{\ell,n} = \left(\ell + \tfrac{1}{2}\right) + \left(\frac{\ell + \frac{1}{2}}{2}\right)^{1/2} \left[\frac{3\pi}{2}\left(n - \frac{1}{4}\right)\right]^{2/3} - \frac{P}{\sqrt{(N^2 - 1)}} + \ldots \tag{2.30}$$

The difference between equation (2.29) and equation (2.30) is zero of Airy function and $\left[\frac{3\pi}{2}\left(n-\frac{1}{4}\right)\right]^{2/3}$ is presented in table II.1.

n	1	2	3	4	5	6	7	8
$-\alpha_n$	2.338	4.088	5.521	6.787	7.944	9.023	10.040	11.009
$\left[\frac{3\pi}{2}\left(n-\frac{1}{4}\right)\right]^{2/3}$	2.320	4.082	5.517	6.784	7.942	9.021	10.039	11.007

Table II.1: Zero of Airy function and with an approximation based on eikonal approach. It can see very good agreement between two coefficients.

The radial equation (2.22), defining the radial distribution, is very similar to the Schrödinger equation for a single particle [23]:

$$\left[-\frac{\hbar^2}{2M}\Delta + V_{eff}(r)\right]\psi(r) = E\psi(r).$$

Thus, defining the energy $E = \frac{\hbar^2 k^2}{2M}$, the effective potential is given by:

$$V_{eff}(r) = \frac{\hbar^2}{2M}\left[k_0^2\left(1 - N^2(r)\right) + \frac{\ell(\ell+1)}{r^2}\right] \tag{2.31}$$

where $\begin{cases} N(r) = N & \text{if } r < a \\ N(r) = 1 & \text{if } r > a \end{cases}$

The solutions r_1 and r_2 of equation Eq (2.31) are given by:

$$r_1 = \frac{\sqrt{\ell(\ell+1)}}{N} k_0 \tag{2.32a}$$

$$r_2 = N r_1 \tag{2.32b}$$

In the range of $r_1 < r < r_2$, the WGMs are well confined inside the cavity with a small fraction outside the cavity in the evanescent form. In this well region discrete bound states exists which corresponds to the whispering-gallery modes. The region $r < r_1$ as well as $r > r_2$ corresponds to a potential barrier, in which the optical modes are exponentially decaying. The most confined modes of $n = 1$ is so called fundamental modes.

II.2.4 Free spectral range

The free spectral range is defined, as for a traditional Fabry-Perot cavity, as the frequency or wavelength separation between longitudinal modes. From Eq. (2.28), considering the different ℓ modes associated to a fixed value of radial order n, the difference between an order mode ℓ and the next mode $\ell+1$ can be evaluated as:

$$\Delta\nu_{n,\ell}^{\Delta\ell} = \frac{c\left(x_{n,\ell+1} - x_{n,\ell}\right)}{2\pi} = \frac{c}{2\pi Na}\left[1 + \alpha_n\left(\frac{\ell + 1/2}{2}\right)^{1/3}\left(1 - \left(1 + \frac{1}{\ell + 1/2}\right)^{1/3}\right)\right] \tag{2.33}$$

For large ℓ, $\left(1 + \alpha_n\left(\frac{\ell + 1/2}{2}\right)^{1/3}\right) \approx 0$, we obtain equation 2.34

$$\Delta\nu_{n,\ell}^{\Delta\ell} = \frac{c}{2\pi Na} \tag{2.34}$$

which corresponds to the FSR of a FP cavity and other geometric structure in Eq. (2.15) and Eq. (2.16). Therefore, the FSR of a micro-sphere resonator can be written in term of frequency and of wavelength as:

$$\Delta\nu_{FSR} = \frac{c}{2\pi Na} \quad \text{and} \quad \Delta\lambda_{FSR} = \frac{\lambda^2}{2\pi Na} \tag{2.35}$$

For a micro sphere with a diameter of 50 µm, a refractive index of 1.45 at an operating wavelength of 1550 nm, the calculated FSR is 5.3 nm. The large mode spacing is one of the reasons that make micro resonators to be investigated for a wide range of applications, from channel-dropping in telecommunication [29] to single mode laser sources [30].

It is possible to determine the spacing between the polarization TE and TM modes, considering they have the same n, ℓ and m; it is expressed as:

$$\Delta\nu^{TE-TM} = \Delta(Nx)\frac{c}{2\pi Na} \approx \frac{c}{2\pi Na}\sqrt{\frac{N^2-1}{N}} \tag{2.36}$$

And the spacing for different radial order mode n can be obtained:

$$\nu_{n+1,\ell} - \nu_{n,\ell} = \frac{c}{2\pi Na}\frac{\partial \nu_{n,\ell}}{\partial n} \approx \frac{c}{2\pi Na}\left(\ell+\frac{1}{2}\right)^{1/3} \times \left(\frac{\pi^2}{3n}\right)^{1/3} \tag{2.37}$$

II.2.5 Finesse

The finesse $\mathcal{F}$ of a resonator is defined as the ratio of the FSR and the width at half maximum of a resonant peak in the transfer function. This factor denotes a dimensionless single parameter which characterizes the ability to resolve the cavity resonance structure and gives as:

$$\mathcal{F} = \frac{\Delta\lambda_{FSR}}{\Delta\lambda} = \frac{\lambda Q}{2\pi Na} \tag{2.38}$$

Cavity finesse in ultra-high-Q whispering gallery mode micro-resonators can exceed 10^6 [35]. This high finesse gives the micro-resonator a good condition for applications in spectroscopy, sensors, filtering and in opto-microwave oscillators.

II.2.6 Mode volume

The volume occupied by each cavity mode, depends on the cavity resonant field distribution, which in turn depends on the particular cavity geometry. The most common definition of mode volume is related to the definition of energy density of the optical mode [27, 28] and is given as:

$$V_m = \frac{\int \varepsilon(r)\left|\vec{E}(r)\right|^2 d^3r}{\max\left(\varepsilon(r)\left|\vec{E}(r)\right|^2\right)} \tag{2.39}$$

where $\left|\vec{E}\right|$ denotes the cavity electric field $\varepsilon(r) = N^2(r)$ is the dielectric constant. Considering the fundamental WGMs in a microsphere ($\ell = |m|$ and $n = 1$), the mode volume of a TE mode is defined in [22] as:

$$v = 2\pi^2\left(\frac{\lambda}{2\pi N}\right)^3 0.809 \times \ell^{11/6} \tag{2.40}$$

For a silica microsphere with a diameter of 50 μm, a refractive index of 1.45 and an operating wavelength of 1550 nm, the first approximation $l \approx 147$ and the fundamental mode volume is expressed as $V = 605(\lambda/N)^3$ corresponding fundamental mode volume is about 740μm^3.

II.2.7 Quality factor

The performance of a resonator element is usually described in term of its capacity to store energy. The storage capacities and loss effects of various resonator types are quantified in term of quality factor *Q* [28]. For optical cavity, the *Q* factor of a mode with resonant located at wavelength λ or frequency ν is characterized by the line width at half-maximum $\Delta\lambda$ of the resonance and a cavity photon lifetime τ:

$$Q = \frac{\lambda}{\Delta\lambda} = \frac{\nu}{\Delta\nu} = 2\pi\nu\tau \tag{2.41}$$

Where ν is the optical frequency. ($\nu = c_0/\lambda$) Therefore, the highest quality factor corresponds to the longest photon storage time and to the narrowest resonance linewidth. To compare with the other micro-cavities such as: Fabry-Perot, micropilar, microcavities, the most advantage of whispering gallery mode microcavities is that they have extremely high quality factor *Q* up to 10^8 in [29] or 10^{10} in [30-33]. In practice, the *Q* factor of WGM cavities based on many mechanisms, which can be defined in [31, 34] by several factors:

$$Q_{total}^{-1} = Q_{intrinsic}^{-1} + Q_{coup}^{-1} = \left(Q_{rad}^{-1} + Q_{mat}^{-1} + Q_{surf}^{-1}\right) + Q_{coup}^{-1} \quad (2.42)$$

where Q_{total} denotes the total cavity quality factor. The intrinsic quality factor $Q_{\text{intrinsic}}$ includes the resonator material losses Q_{mat}, the radiation losses or diffraction loss Q_{rad} and Q_{surf} represents the losses due to scattering from the surface imperfections. Q_{coup} represents the energy losses due to input/output light coupling. The approximate comparative performances characteristics of fabricated cavities are presented in the following table.

Parameter	Rings, Disc	Standard sphere	Sphere limit
Q factor	~ 10^3-10^5	~ 10^5-10^8	~ 10^{11}
Resonance linewidth	GHz	MHz	kHz
Decay time	ps	ns	µs
Decay length	mm	m	km

Table II.2: Comparison of Q factor value at 1550 nm between ring and sphere resonator. The high Q in the sphere translates to narrow linewidth, long decay time and high optical intensity.

II.2.8 Losses mechanisms in a microsphere

Equation (2.42) shows that, the total Q_{total} factor of resonator results from several losses contributions: material loss, radiation loss or diffraction loss, scattering from the surface imperfection and external coupling loss. In the following sections, the Q factor limits imposed by the difference mechanisms are briefly analyzed for the case of silica microspheres.

II.2.8.1 Material losses

The cavity material loss is one of effect restricting the value of intrinsic Q factor. Due to its low intrinsic absorption losses in a wide range of wavelength, the silica glass (SiO_2) has been the most widely studied. In this work, silica single mode fibers are chosen for

fabrication of microsphere resonators. Commonly, there are two types of material losses in a silica microsphere: absorption losses and Rayleigh scattering losses. The scattering losses are due to the presence of small density fluctuations or defects and the presence of missing defects in the atomic structure, which is the main cause of absorption losses [35, 36]. The material losses in a fiber are determined by measuring the attenuation α which depends on the ratio of the optical output power to the input power and on the length of fiber. It is expressed in dB/km as $\alpha = 10\log(P_{out}/P_{\text{int}})/L$. Therefore the Q factor corresponding to the material losses is given [37] by:

$$Q_{mat} = \frac{2\pi N}{\alpha\lambda} \tag{2.43}$$

At the operating wavelength of 1550 nm, the attenuation of a single mode fiber is 0.2 dB/km, the Q factor for material losses of the microsphere is $Q_{mat} \approx 2.9\times10^{10}$.

II.2.8.2 Diffraction losses

The diffraction losses are due to the curvature of the boundary, they are also known as radiation losses. By using the Wentzel-Kramers-Brillouin (WKB) approximation [30], the quality factor limited by diffraction loss is written by:

$$Q_{rad} = x\exp\left[2\left(\ell+\frac{1}{2}\right)g\left(\frac{x}{\ell+\frac{1}{2}}\right)\right] \tag{2.44}$$

where $g(u)$ is a decreasing positive function $g(u) = -\sqrt{1-u^2} + \arg\cosh\left(1/u\right)$, and $x = 2\pi a/\lambda$ depending on the size parameter (a is the sphere radius).

Because of the quantity $x/\left(\ell+\frac{1}{2}\right)$ in equation (2.37), ranging from $1/N$ for the radial fundamental mode to approximately 1 for a less bounded mode, the Q factor depends also on the radial order of the modes.

II.2.8.3 Surface losses

Surface losses result from scattering effects due to the surface roughness of the microsphere. The Q factor limited by surface scattering loss is expressed in [37] as:

$$Q_{s.s} = \frac{\lambda^2 D}{2\pi^2 \sigma^2 B} \tag{2.45}$$

Here σ is the surface roughness, B is the correlation length of surface inhomogeneities and D is the microsphere diameter. In practice, there are other important surface losses, which are the optical losses caused by dust and water deposition. The Q factor of microsphere drops down in several hours due to water absorption if it is put in a normal working condition [31].

II.3 Applications of micro-resonators

II.3.1 Optical resonator filter

Because of their small line-width and their high stability to environment conditions, the WGMs devices are very attractive for many applications. For applications such as filtering, frequency stabilization and sensing, passive resonators are used. A prism coupler is used for optical coupling at both input and output (see Figure III.3 or IV.2). The transmission of a monochromatic electromagnetic wave of frequency f through a WGM resonator is defined in [38] as:

$$T = \frac{\gamma_c - \gamma - i(f - f_0)}{\gamma_c - \gamma + i(f - f_0)} \tag{2.46}$$

Here T denotes the amplitude transmission; γ_c, γ and f are respectively the coupling line-width, the absorption and resonance frequency of a mode of resonator. The power transmission $|T|^2$ through the resonator is a Lorentzian function and condition $\gamma = \gamma_c$ corresponds to the critical coupling of the resonator.

It is important note that the filter is characterized by absorption resonance in a single coupling prism (single coupler) configuration (stopband filter), while in the two-prisms

configuration it is characterized by transmission resonance (passband filter). In this case, assuming $\gamma_c >> \gamma$ for simplification, the transmission and reflection coefficients through the resonator are:

$$T = \frac{\gamma_c}{\gamma_c + i(f - f_0)} \text{ and } R = \frac{i(f - f_0)}{\gamma_c + i(f - f_0)} \tag{2.47}$$

where T describes the amplitude transmission (light goes into one prism and exits at the second prism), and R describes the reflection (light goes into and exits at the same prism).

A filter response of single-ring resonators with integrated semiconductor optical amplifier is presented in [39]. The device has the form of a racetrack with free spectral ranges of 25 GHz and 50 GHz. By using Pt-resistors, the tuning to a specific wavelength can be achieved. As the factor for loss compensated ring resonator is only dependent on the ring architecture, it is possible to design devices with specific Q factor.

II.3.2 WGM for sensors

Biosensors designed from WGM resonators have number of qualities. WGM resonators are used to detect the present of molecules on their surface. Because of their high Q factor, these resonators allow the detection from several nano-moles up to pico-moles. Biosensors based on the shift of WGM in microsphere accompanying protein adsorption were described in [44]. The light coming from a tunable laser is coupled into the microsphere via tapered optical fiber and travels around the sphere equator. When a protein molecule diffuses from the surrounding aqueous medium to the sphere's surface and is absorbed at position r_i, it interacts with the evanescent field of the WGM resonator. There is a change of the surface properties, shifting the frequency of the mode. In addition, WGMs could also be used for measurement of strain in optical fiber and applied in high frequency electron magnetic resonance measurement [45, 46]. Resonance features depending on its morphology are observed in the elastic-scattering spectrum of 125 µm diameter cylinders. The positions of the resonance are strain sensitive and can be tuned. The measured wavelength shifts show a linear behavior with a slope of $0.14\ \text{nm} / 0.14\ \text{nm/m}$ *strain*. Thanks to this behavior a new miniature optical strain-sensor technique with a micro-strain sensitivity at a single point can be developed. Photonic

WGM sensors using the fano-resonant line shape (a type of resonant scattering phenomenon that gives rise to an asymmetric line-shape [47] is presented in [48]. In this paper, a polymer micro-ring resonator which exhibits sharp asymmetric fano-resonances is used as a biochemical sensor. The resonant wavelength of this resonator is very sensitive to the concentration of glucose, and the resonance shift has a linear relationship with the glucose concentration. For biosensor applications, polymers resonator can be allow modify surface chemical for binding of specific bio-molecules on the resonator surface.

II.3.3 Passive WGMs for fundamental physics

Cavity quantum electrodynamics (CQED): There is great activity in both theoretical and experimental investigations of cavity quantum electrodynamics effects in WGM resonator [49, 50]. Spontaneous emission processes can be enhanced in a cavity due to a modification of the density of electromagnetic states compared with the density in a free space. A measurement of cavity QED effects for the radiative coupling of atoms in a dilute vapor to the external evanescent field of a WGM in a fused silica microsphere is presented in [51]. The high Q factor and small mode volume and unusual symmetry of micro cavity evanescent field allow velocity-selective interaction between field with photons in WGM and $\tilde{N}_T \approx 1$ atoms in the surrounding vapor. The results give the evidence that interaction between atoms and photons in high Q WGMs can reach the level of a single atom and only a few photons in the mode. The coupling of a single nano-emitter and WGM has been studied in [52, 53]. The measurements show that a sharp fiber tip could be considered as a 'nano-tool' for manipulating the very-high-Q modes present in microsphere resonators. The measured Q-degradation and the frequency shift show that it is possible to adjust the coupling between the fiber tip and high-Q whispering-gallery modes with great precision. By using a tip of a diameter about 100 nm, it should be possible to couple a nano particle to the most confined modes of a microsphere without decreasing the quality factor. The tip can be acting as a tool to establish a well-controlled coupling of a single emitter to a high Q mode in CQED.

Photonic atoms: another fundamental application of WGMs is based on the ability of resonator to mimic atomic properties [44-46]. The authors show that WGMs can be thought of as classical analogy of atomic orbital; the mode numbers of WGM resonator

corresponding to angular, radial and azimuthal numbers are also the same as the quantum numbers in atomic physics.

II.3.4 WGM Filters for OEO

A presented in the previous chapter, in classical OEO [2] the long fiber delay line supports many microwave modes imposed on an optical wave and the spacing between two modes is a few hundred kilohertz for some kilometers of delay line. A narrowband electrical filter is placed into the electronic segment of the OEO feedback loop to achieved single mode operation. The center frequency of this filter determines the oscillation frequency of the OEO. But it is difficult to find an electrical filter with a bandwidth narrow enough (a few hundred kilohertz) for selecting the desired frequency. However, the long fiber delay is very sensitive to the surrounding environment, so the OEO does not produce an output signal with high long term frequency stability. In addition, the OEO system is rather bulky because of the kilometers of fiber delay.

Because of these reasons, in the recent time, optical resonators have been investigated to be used in OEO system as optical storage element or filter. Among different kind of resonators whispering gallery mode (WGM) optical resonator can be chosen to replace the optical fiber [41, 42]. The main advantage of this kind of component is their small size. By using such an optical resonator, the optoelectronic oscillator could be really compact. They are compatible with compact temperature control system since it is limited to a much smaller volume. The properties of OEO with a high Q factor WGM resonator in place of the electronic filter, as well as the fiber delay, have been presented by Strekalov et al. [43]. With a source of optical group delay inserted into an OEO loop, the performance of a stabilized OEO is improved. This method allows tuning the desired oscillation frequency by tuning the resonator. However, in OEO system, optical resonators are also employed as photonic filters [40] for stabilizing the oscillation frequency.

In the OEO system designed with micro-resonator as storage element, the microwave oscillator frequency is defined by the free spectral range (FSR) of the resonator, while energy storage is performed by trapping laser light into the ultra-low loss WGMs. This configuration can define at the same time the oscillating frequency and ensure the energy storage, therefore the high quality factor or the low phase noise and so the high spectral

purity of the oscillator. Nevertheless the FSR or a micro-resonator also depends on external parameters such as temperature. In order to stabilize the oscillator and its oscillation frequency the laser wavelength must be controlled according to the characteristic of the micro-resonator. The wavelength of the laser diode can be tuned by controlling the temperature of the laser [14].

Because of their numerous advantages, in the recent time WGM resonators have been investigated not only for replacing the long optical fiber delay in OEO but also for other applications such as micro cavity laser, optical filters, and sensors [10]. Therefore a number of optical resonator types have been fabricated [13, 14, 15] with optical quality factor up to 10^8 for mode around 1550 nm. Different materials can be used such as MgF_2, silica or quartz; different shapes have also been studied as micro-disk or micro-sphere.

The current state of the art of resonators used in OEO system is presented in Table II.3.

Ref.	Type	Diameter (mm)	Material	Q factor	f_{osc} (GHz)
13	Minidisk	5.2	MgF_2	~10^8	7.7
14	Minidisk	7.7	Quartz	~10^9	8
15	Disk	3.3	CaF_2	~10^9	9.4

Table II.3: Current state of the art of WGM resonators used in OEO.

In the next chapter we will study a special kind of WGM resonator which can be quite easily fabricated in a laboratory, the microsphere resonator.

Chapter III.

Silica Microsphere Resonator

III.1 High *Q* optical microsphere resonator fabrication

III.1.1 Introduction

To fabricate ultra-high *Q* dielectric microsphere, several techniques have been used. Suitable method must produce micro resonator displaying an extremely smooth surface and a controlled axial symmetric shape. For this purpose, melting is one of the favorite techniques Some heating methods reaching the melting temperature for glass materials (above 1000°C) have been used as gas flame, CO_2 laser and electric arc

Gas flame: a micro-torch fueled with hydrogen is still a common technique to melt glass. The earliest work on optical microsphere was based on it [28].

CO_2 laser: CO_2 laser has a working wavelength in mid-infrared region (10.6 µm), which is efficiently absorbed by glass, resulting in strong heating phenomena. To fabricate a microsphere by this technique, a single mode fiber without coating is tapered and cut-off, then a silica micro-droplet at the end of taper is melted again. At the end of this process, an optical microsphere hold on its mother fiber is achieved [57].

Electric arc: it is another way to achieve the melting process of glass. An electric discharge is coupled with fiber splicing equipment which allows exact positioning and energy transfer, resulting in reproducible sphere shapes and sizes. In our work, the optical microspheres, tapered fibers and also fiber micro-lenses which were used in micro-ring resonator coupling are fabricated via electric arc melting.

III.1.2 Experimental Set-up

In the present work, commercial single mode fibers (SMF 28) are chosen for the fabrication of optical microspheres. The choice of these fibers is motivated by their ultra-low losses and low price. This set-up, sketched in figure III.1 can produce silica microspheres of diameter down to 20 µm. To better control the fabrication process, the single mode fiber and two electrodes connected to a high voltage source, are placed and fixed upon a 3D translation stage in order to adjust the best position of the fiber between the two electrodes.

The microsphere fabrication process includes two steps. In the first step, the fiber coating is cleaved by a stripper tool and dissolved by pure alcohol (fig. III.2a). Then the fiber is mounted and fixed on a three dimensional translator. After aligning it to the focal zone of the two electrodes, it is heated by a discharge between these electrodes. During the heating process, a weight connected to the fiber tip induces a force that stretches the fiber out, leading to the formation of a tapered fiber with a reduced diameter (less than 20 micrometers). This taper is cut by melting its bottom part (fig.III.1b).

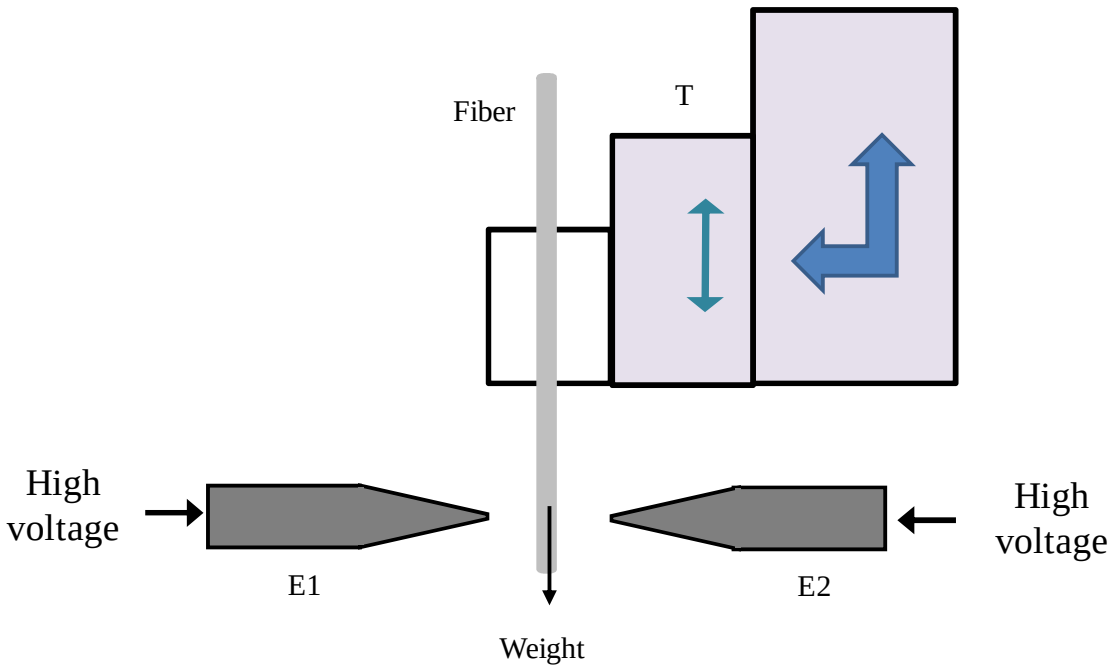

Figure III.1: Schematic of the tapering process.

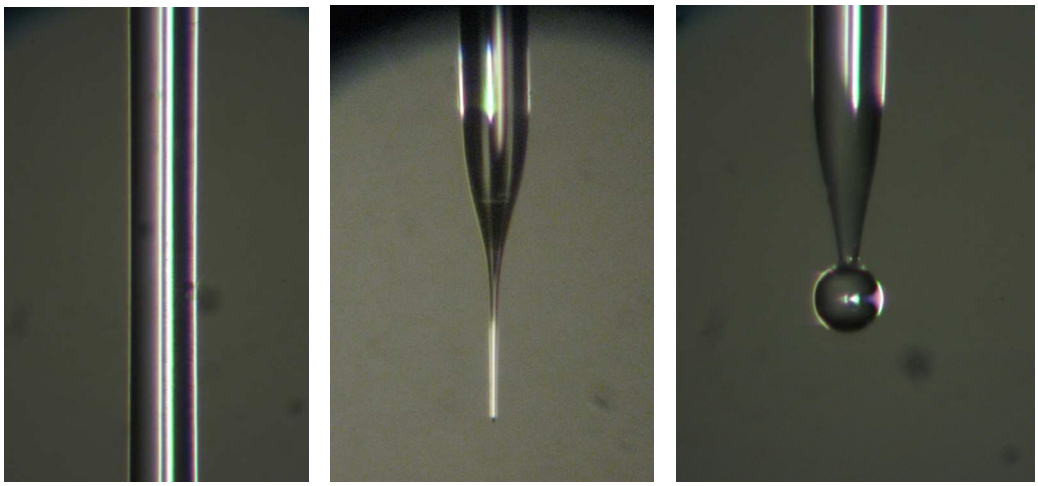

b c d

Figure III.2. Single mode fiber without coating, 125µm in diameter (a), the tapered fiber formed by cutting the taper bottom (b), and microsphere with its stem (c).

In the next step, when the temperature between two electrodes reaches the melting point of silica, surface tension immediately shapes the tapered fiber into a spherical form (fig.III.1c). At the end of the heating process, a solid optical microsphere which is attached to the fiber stem is achieved.

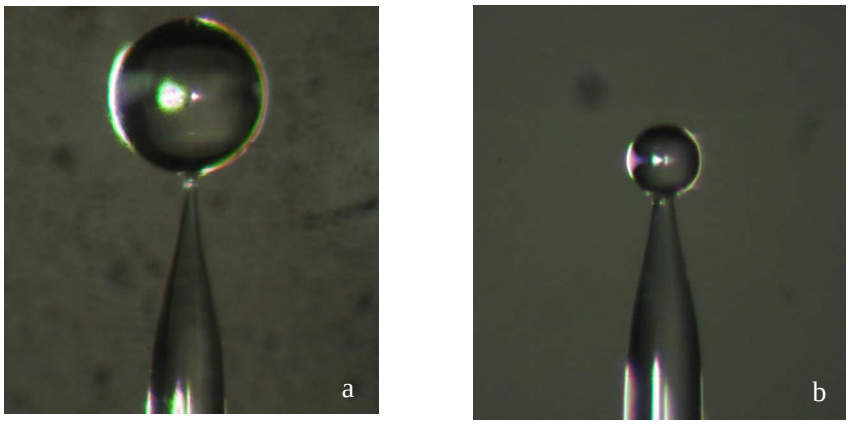

Figure III.2 : Photomicrograph of two silica microspheres with diameter approximately of 200 microns (a) and 100 microns (b) respectively. The spheres are attached to the end of a tapered optical fiber stem.

The size difference of microsphere can be produced by changing the tapered fiber size and length. This set-up is used to fabricate microspheres with diameters ranging from

20 µm to 400 µm. The optical microspheres fabricated in the lab with various diameters are presented in figure III.3.

III.2 Optical coupling of microsphere

III.2.1 Introduction

To characterize the properties of high *Q* microcavities, it is necessary to optically excite and probe the resonator. In the geometric optics point of view, the WGMs are confined by successive total internal reflections and no incoming ray can directly excite them except by using the original fiber from which the sphere has been elaborated and which remain attached to the sphere. Therefore, high *Q* WGMs excitation is performed by evanescent wave coupling, which utilizes the WGM evanescent field outside the boundaries of micro-cavity. In the last decade, several techniques have been used to couple optical microcavities such as: prism coupler, side-polished fiber block or angle polished fiber coupler.

Prism coupler: The prism coupler is one of the early coupling techniques which were used to investigate the characteristics of optical microsphere [57- 59]. An equilateral prism (refractive index N=1.72) was used. The input beam was focused onto the inner surface of the prism, at the proximity point with microsphere, the prism is placed at a small distance (0.1-1λ) from the resonator surface (figure III.3). The cross-section of the input beam was then optimized to obtain maximum response of a chosen WG mode.

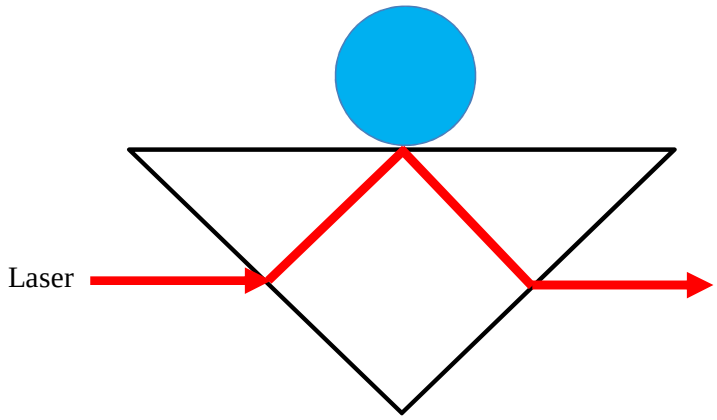

Figure III.3 : Illustration of prism coupling between a laser beam and an optical resonator.

The laser beam is focused on the “touching point” under an angle providing total internal reflection in the prism. Light tunnels through the small gap between the prism and resonator. When carefully optimized, this technique can achieve good coupling efficiency up to 80 percent [60]. However, prisms have severe drawback as a low degree of ideal coupler and spatial mode matching. Moreover, the optimal alignment of system components is challenging.

Side-polished fiber blocks is another evanescent coupling technique for optical resonators. It consists of an optical fiber buried in glass or wedged in a metal block [61, 62]. The fiber is polished to the proximity of the core with a 0.1 µm diamond suspension, a high quality surface is therefore achieved.

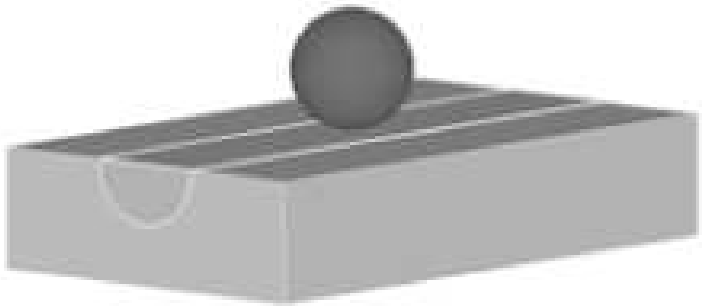

Figure III.4: Illustration of Half-block fiber couplers

The drawback of this technique is the high leakage of light from the sphere into the fiber cladding and into the surrounding block.

Angle-polished fiber coupler: in this method, the end of a single mode fiber is polished to form a plane face at an angle far from the normal to the fiber axis. This geometry favors total internal reflection of guided light from the fiber core. When the sphere is placed on this surface, it is exposed to the evanescent field from the fiber core area. The configuration provides an efficient energy exchange in resonance between the waveguide mode of the SMF and the WGMs in the sphere.

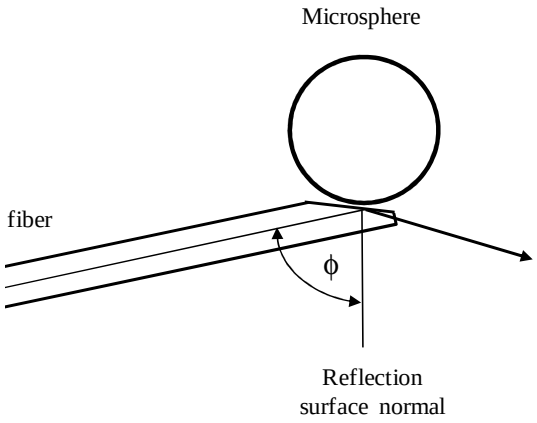

Figure III.5: Scheme of the angle-polished fiber – microsphere coupler

The polished angle is chosen to fulfill the phase-matching requirement $\phi = \arcsin\left(N_{sphere} / N_{fib}\right)$, where N_{sphere} is the effective refractive index of sphere and N_{fib} is the effective refractive index of the fiber core. This technique gives a coupling ratio of approximately 60% [63]. However, like the prism coupler, this angle-polished fiber coupler is the difficulty of coupling system settings.

Planar waveguide coupling: one of the main advantages of this waveguide coupling method is its easy integration with light wave circuitry on planar substrates. Typically, these waveguides are used in a simple rectangular or ridge waveguide configuration (fig.III.6).

Figure III.6: Illustration of Planar waveguides couplers

The planer waveguide coupling technique has been applied to low *Q* microcavities and is also used for fully integrated high-*Q* microresonator structures [64]. However, because

of its difficulty to fulfill both phase matching and evanescent field condition, the planar waveguide coupler with high refractive index cavity shows problem to realize efficient coupling to silica microsphere.

In such case, the tapered optical fiber coupler method can exhibit better properties for efficient coupling. So in this work, tapered fiber couplers are chosen to characterize WGMs in silica microspheres.

III.2.2 Tapered optical fiber coupler

Tapered single mode optical fibers have attracted attention increasingly in the last decade, due to their large evanescent field and strong light confinement. They are used as optical couplers not only to silica microspheres, but also to microdisks, microtoroids and photonic crystal cavities [65, 66]. Moreover, these tapered fibers find valuable applications for biosensors, fiber dye lasers and for nonlinear research and communication [63-70]. Tapering is an easy and efficient way to produce a coupler with low losses. In the case of an optical coupler, the fiber is typically tapered down to the micrometer scale by CO_2 laser or gas flame [71, 72]. It is known that a silica fiber is melted at 1100°C -1200°C, so an electric arc can also be used to taper the optical fiber, and it is employed in our work.

III.2.2.1 Tapered fiber fabrication

Tapering process is described as follows: the first polymer coat of a single mode optical fiber to be tapered is stripped off over 1 cm length and dissolved in pure alcohol or acetone. Then this fiber is fixed on a three axis translation stage and placed inside the gap between the two electrodes of the electric arc system. A 2-3 mm discharge between two electrodes is used to heat the taper region while the fiber is stretched apart until the diameter is reduced down to approximately 2 to 5 microns (fig. III.7). By a proper control of the heating and stretching, we may assume that the adiabatic tapering condition is satisfied. The typical final structure of a taper fiber consists in a region of approximately 0.5 to 1 cm in length. In this region the core of the initial optical fiber disappeared, and the taper become a dielectric cylinder acting as an optical waveguide guide inside the cladding.

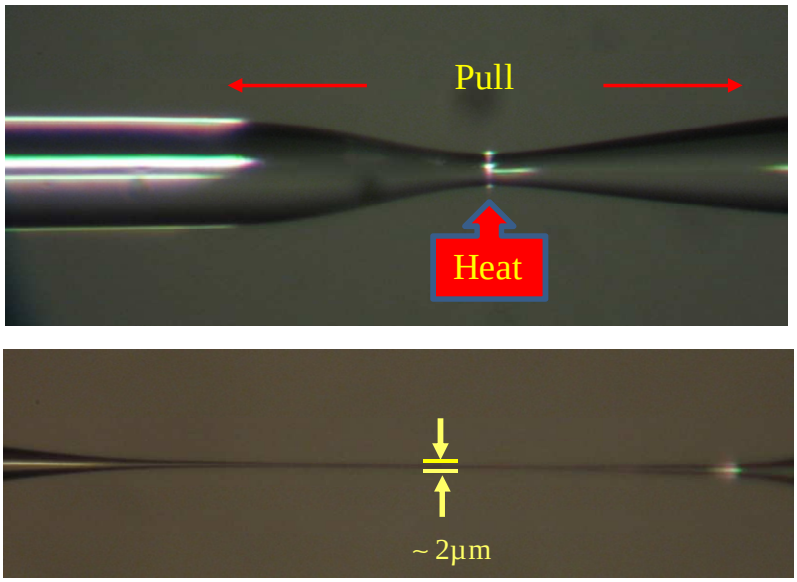

Figure III.7 : Fabrication of a tapered fiber. Photomicrograph of the waist region of a tapered optical fiber (a), which exhibits a diameter less than 2 micron shown in (b).

III.2.2.2 Result and discussion

Considering a constant taper waist zone length and an exponential shape taper, according to [73, 74], the taper shape in cylindrical coordinates with $z = 0$ at end of taper (fig III.8) is given as:

$$r(z,L) = \begin{cases} r_0 \exp\left(-z/L_w\right) & \text{for} \quad 0 < z < \dfrac{L}{2} \\ w = r_0 \exp\left(-L/2L_w\right) & \text{for} \quad 0 < z < \dfrac{L_w}{2} \end{cases} \tag{3.1}$$

In this equation r_0, is the initial fiber radius (it is equal to 9 µm for used fiber), L is the pulling length and L_w called the "hot zone", corresponds to the length of the softened part of the fiber.

As a tapered optical fiber consists of a circularly shape composed primarily of the fiber cladding of the untapered fiber, it can be considered as a simple step-index fiber with a refractive index difference of ~0.45. Therefore, even if the diameter of taper is non-uniform along the tapered fiber zone length, the interaction with a resonator occurs only in a region of 10 microns, where its diameter is constant. So at the "contact region" or the

interaction region between the taper and an optical microsphere, the tapered fiber may be considered as a dielectric rod of constant diameter with a step index profile.

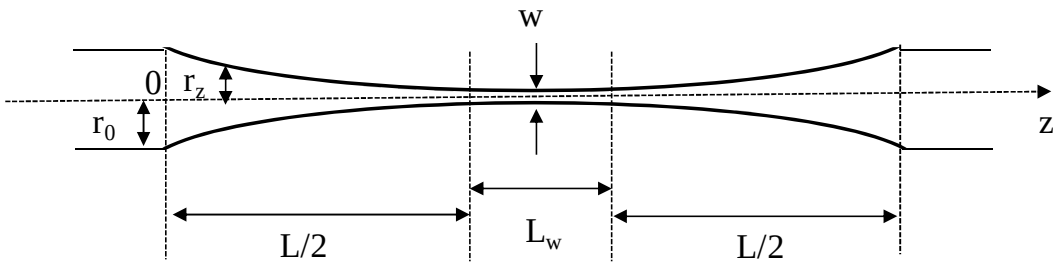

Figure III.8: Illustration of the shape of a tapered fiber: L_w is the taper waist zone length, *w* is the waits diameter, r_0 is the initial radius, $L = 2L/2 + L_w$ is the pulling length.

Fields of a tapered fiber: it is known that in a fused tapered fiber, the core and cladding have been heated and drawn to achieve a narrow waist. The core vanishes and the modes are those of an air-cladding glass rod. Here the fiber has a core index of N_{fib}, a cladding index of N_{cl} ($N_{cl} = N_{air} = 1$, refractive index of air), and r_w is the core radius of taper waist. The fields of an optical fiber have well known [75], here we assume that the fields are linearly polarized. The radial dependence of the fundamental mode F_0 is expressed as:

$$F_0 = B_f \begin{cases} J_0^{-1}(k_f r_w) J_0 k_f \rho & \text{if} \quad \rho \le r_w \\ \exp\left[-\gamma_f (\rho - r_w)\right] & \text{if} \quad \rho > r_w \end{cases} \tag{3.2}$$

$$\text{where } B_f = \frac{\alpha_f J_0(k_f r_w)}{v_f \sqrt{\pi} J_1(k_f r_w)} \tag{3.3a}$$

$$k_f = \sqrt{k^2 N_f^2 - \beta_f^2}\ ; \tag{3.3b}$$

$$\gamma_f = \alpha_f \frac{K_1(\alpha_f r_w)}{K_0(\alpha_f r_w)} \tag{3.3c}$$

$$V_f = k r_w \sqrt{N_f^2 - N_{cl}^2}\ ; \tag{3.3d}$$

$$\alpha_f = \sqrt{\beta_f^2 - k^2 N_{cl}^2} \qquad (3.3e)$$

ρ is the distance from the center of the fiber.

J_0 and J_1 are Bessel functions of zero and first order.

K_0 and K_1 are the modified Hankel functions of zero and first order.

B_f is a normalization constant and β_f is the fiber mode propagation constant. The field dependence outside of the core is typically written in term of the modified Hankel function.

Figure III.9 presents transmission data of a tapered fiber obtained simulation performed with CST software and Figure III.10 presents some experimental results. CST Microwave Studio is a well known software in the world of microwave studies, but maybe not in the world of optical studies. Nevertheless considering the principle of calculation (finite elements) and the method which is implemented there is no reason for this software not to give good results. Of course the results are presented as usually in microwave studies that means in term of S parameters, also known as Kurokawa parameters.

Let us remind that these parameters respectively present a reflection coefficient S_{ii} at a connection (or port) "*i*" and a transmission coefficient S_{ij} from port "*j*" to port "*i*".

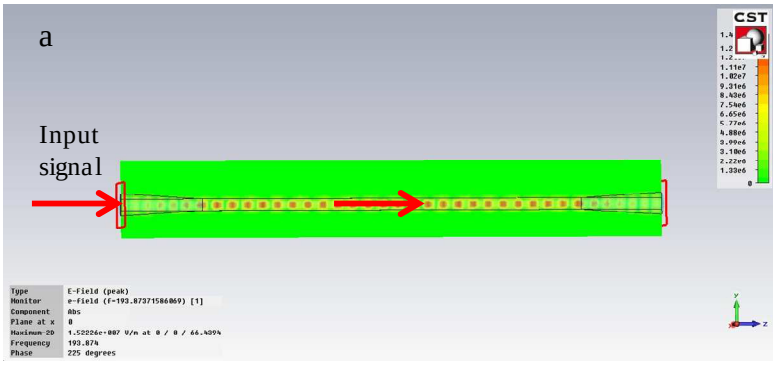

Figure III.9: Propagation modes of Gaussian beam in a tapered fiber by CST Microwave Studio simulation.

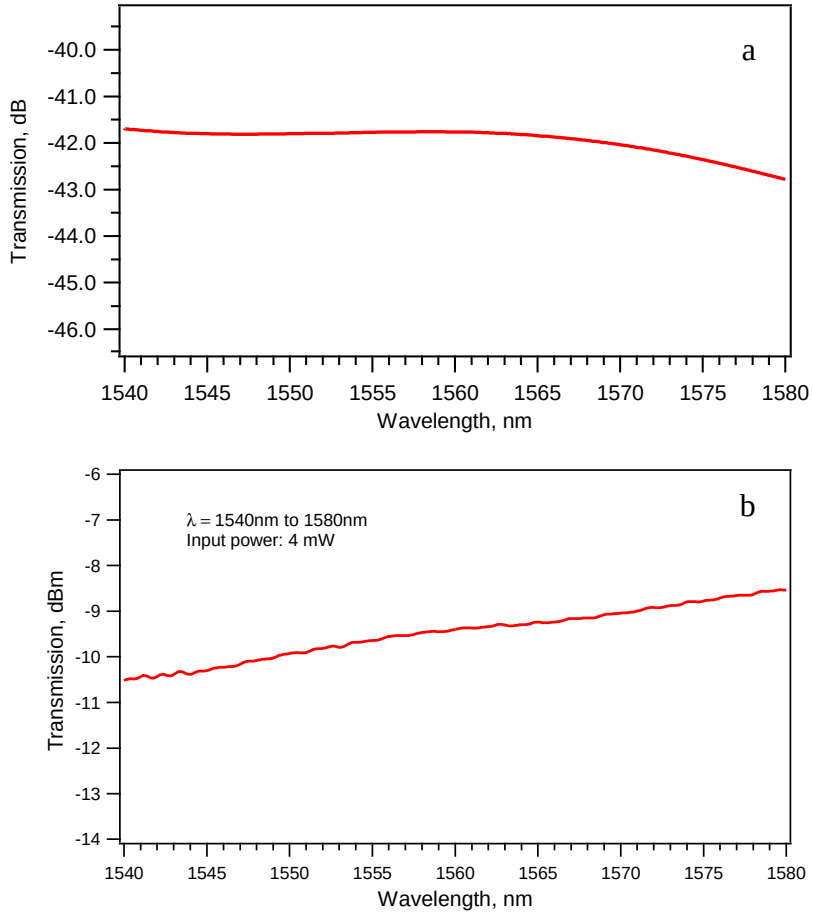

Figure III.10: Tapered fiber (a) Simulated transmission results and (b): Experimental transmission results of tapered fiber with waist taper of ~2µm, L ≈5mm, the laser power is 4 mW.

Assuming an input power of -40dB coupled into the taper fiber with L=80 µm and waist taper of 1µm, when the laser is tuned from 1540 nm to 1580 nm, the output transmission of taper fiber depends on the operating wavelength. For a wavelength range between 1540 nm and 1580 nm, the minimum transmission loss is approximately -43dB. However, at the operating wavelength range used around 1550 nm, the variations of losses in the taper is rather small, approximately 2 dB.

For an experimental fiber taper with a length L of 5 mm, a waist of 2 µm, when the laser beam with a power of 4 mW (6.02 dBm) is coupled in to fiber, at operating wavelength ranging from 1540 nm to 1580 nm, the output transmission of tapered fiber present significant losses of power when it pass the taper region. For example at 1540 nm,

the output power is $-10.5\,\text{dBm}$ at this wavelength, the power laser loss is approximately $16.5\,\text{dB}$ at the waist of the taper. This loss is decreased to $14.5\,\text{dB}$ at wavelength 1580 nm. From the experimental output transmission curve of a taper fiber, shown in fig. (III.7c), and considering the whole operating wavelength range, the average power losses are $15.5 \pm 1\,\text{dB}$. Consider that the total attenuation in a tapered fiber includes material losses (α_{mat}) and losses at the taper region (α_{tap}), we have:

$$\alpha_{total} = \alpha_{mat} + \alpha_{tap} = \left(10\log\left(\frac{P_{in}}{P_{out}} \right) / L \right) + \alpha_{tap} .$$

However, $\alpha_{mat} = 0.2\,\text{dB/km}$ for single mode optical fiber at wavelength around 1550 nm. So here, the material losses in tapered fiber is small and can be neglected. Then the loss in the fiber is defined by losses in the waist region (losses by the small waist of the taper, or by non-uniformity of taper length).

III.3 Excitation of WGMs with a tapered fiber

III.3.1 Light coupling to and from a microsphere

The optical energy transmission between a single mode waveguide and a single cavity can be described through the model proposed in ref. [76]. In this simple method, the internal cavity field is given for resonant excitation by the following equation:

$$\frac{da}{dt} = -\frac{1}{2}\left(k_0^2 + \sigma^2\right)a + ik_0 S \tag{3.4}$$

where a denotes the energy amplitude in the cavity, σ is the intrinsic resonator loss (round-trip power loss coefficient), k_0 is the external coupling coefficient and S denotes the input wave amplitude. The first term of equation (3.4) represents the total energy amplitude loss rate of the cavity due to the intrinsic resonator loss and external coupling. The last term gives the excitation of the resonator by the waveguide with the coupling coefficient k_0. The transmission through the waveguide consists of a superimposition between the amount of optical power not coupled into the resonator $t_0 \approx 1$ plus the amount coupled out of the cavity [77], which given by the expression:

$$T = \left| t_0 + ik_0 a / s \right|^2 \tag{3.5}$$

and in the steady state, the transmission can be defined as:

$$T = \left(\frac{1-K}{1+K} \right)^2 \tag{3.6}$$

The coupling parameter K is defined as the ratio of the coupling coefficient between waveguide and resonator to the intrinsic resonator loss.

In general, when coupling occurs between two waveguides (or between a waveguide and a resonator), there will be cross-coupling between all optical guides and radiation modes available (figure III.11). Therefore the coupling between a fiber taper and a microsphere resonator is more complicated than the simple single mode coupling model used above. In this case the effects of a resonator and a taper fiber (waveguide) are twofold from the input fiber mode into a resonator mode and coupling from each resonator mode into all fiber modes. By using an adiabatic taper, it is possible to establish the fundamental taper mode. However, an excitation resonance mode can transfer power back to many taper modes as fundamental and higher order modes. By adding additional loss terms (the effect of higher-order waveguide modes ($k_i > 0$) and of radiation modes $k_{rad} > 0$, the equation (3.4) can be rewritten as:

$$\frac{da}{dt} = -\frac{1}{2}\left(\sum_i k_i^2 + k_{rad}^2 + \sigma^2 \right) a + ik_0 S \tag{3.7}$$

Assuming that the power coupled into higher-order taper modes is lost, equation (3.7) can be considered as a proper description of fiber taper transmission, the coupling parameter K being now defined as:

$$K \equiv \frac{k_0^2}{\sum_{i \neq 0} \left(k_i^2 + k_{rad}^2 + \sigma^2 \right)} \tag{3.8}$$

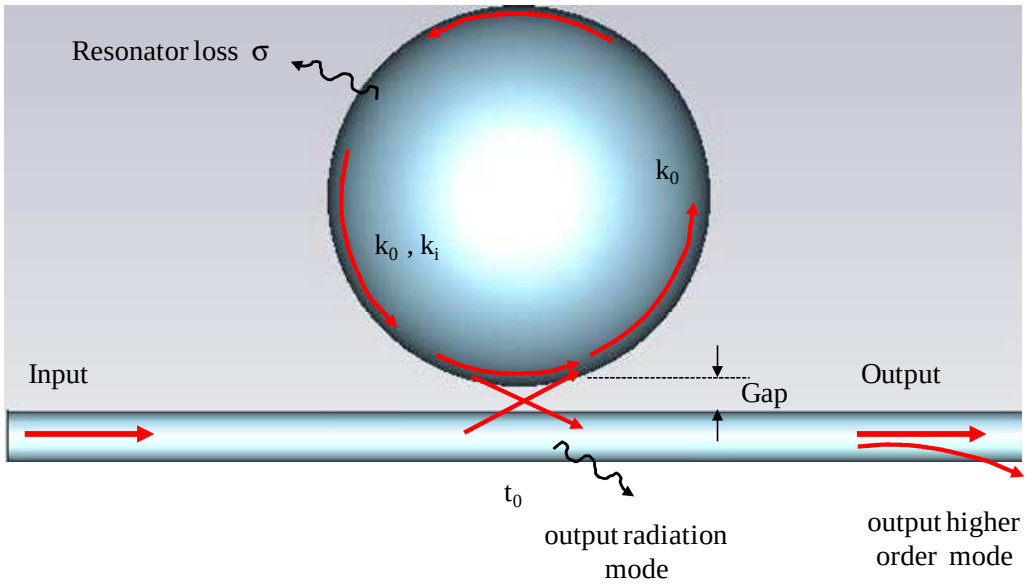

Figure III.11: Illustration of coupling and loss parameters in a taper-micro-resonator system. The input field is a fundamental taper mode which couples into the resonator with a coupling coefficient k_0 .The output field includes the fundamental taper mode and higher-order taper modes with coupling constants k_0 and k_i, respectively. The round-trip resonator intrinsic power loss is σ^2. The higher-order taper modes are radiated or coupled to cladding modes.

K is defined as the ratio of the desired taper fiber-mode power coupling to the total system power losses. The coupling factor K can be decomposed into two factors such as an intrinsic contribution expressed by:

$$K_{\text{int}} = \frac{k_0^2}{\sigma^2} \tag{3.9}$$

and a parasitic contribution expressed as:

$$K_p = \frac{k_0^2}{\sum_{i\neq 0} k_0^2 + k_{rad}^2} \tag{3.10}$$

Equation (3.8) can be rewritten as:

$$K^{-1} = K_{\text{int}}^{-1} + K_p^{-1} \tag{3.11}$$

The ratio of the power coupled into the desired mode (in this case the fundamental HE_{11} mode) to the amount of power coupled into all modes is ideality given by:

$$I \equiv \frac{k_0^2}{\sum_{i=0} k_i^2 + k_{rad,T}^2} = \frac{1}{1+K_p^{-1}} \tag{3.12}$$

K can be obtained by measuring the dependence of coupling with respect to the tapered fiber-resonator gap and inverting Eq. (3.6) to be expressed as:

$$\frac{1 \pm \sqrt{T}}{1 \mp \sqrt{T}} = K = \frac{k_0^2 \exp(-\gamma_0 g)}{k_i^2 \exp(-\gamma_i g) + \sigma^2} \tag{3.13}$$

γ_0, γ_i are spatial decay rates (versus gap g) therefore, with $g = 0$, $k_{0,i}^2 \exp(-\gamma_0 g)$ corresponds to zero separation (zero gap). The upper signs are denoted for transmission values in the overcoupled regime and the lower signs for the undercoupled regime. In the case of $k_i^2 > \sigma^2$, the relation $K^{-1} = K_{\text{int}}^{-1} + K_p^{-1}$ results in a roll-off of K for small gap distance due to parasitic coupling. In case of $k_i^2 < \sigma^2$, the higher order mode coupling is masked and a lower bound can be established.

III.3.2 Experimental observation of WGMs

III.3.2.1 Experimental setup

This section presents a brief description of our experimental setup, which has been used to characterize output optical generation of microsphere (figure III.12). An important part of this setup is a tunable laser source, in order to scan the spectral of the resonator and to evidence its resonance wavelengths. In this work, the laser source is an external cavity laser system (Agilent 81940A compact tunable laser source), which can be tuned without mode-hoping, its specifications are listed in table III.1. Another part of the coupling setup is a polarization controller used to match the polarization of the laser light with the polarization of the resonator mode. An optical signal (power 4 mW) from the laser (tuning range from 1520 nm to 1630 nm) is coupled to the microsphere via a tapered optical fiber. The transmission signal in the microsphere was coupled back to optical fiber and measured

by a power sensor module (photodiode), which provides the wavelengths and intensities in mW or dBm. Then the output signal transmission is plotted and displayed by a computer, then we can extract both the image and data of measured signal transmission. The distance between the resonator and the taper fiber can be controlled by three translation stages. By scanning continuous this distance, it is possible to identify various coupling regimes: undercoupling (intrinsic resonator losses bigger than coupling losses), critical coupling (resonator losses equal to coupling losses) and overcoupling (resonator losses smaller than coupling losses).

Parameter	value	unit
Wavelength range	1520-1630	nm
Wavelength resolution	125 (at 1550 nm)	MHz
Wavelength stability	± 2.5	pm
Linewidth	100	kHz
Maximum output power	≥ +10	dBm
Power linearity	± 0.1	dB
Power stability	± 0.0075	dB/hour

Table III.1: Specifications of the Agilent 81940A tunable laser source

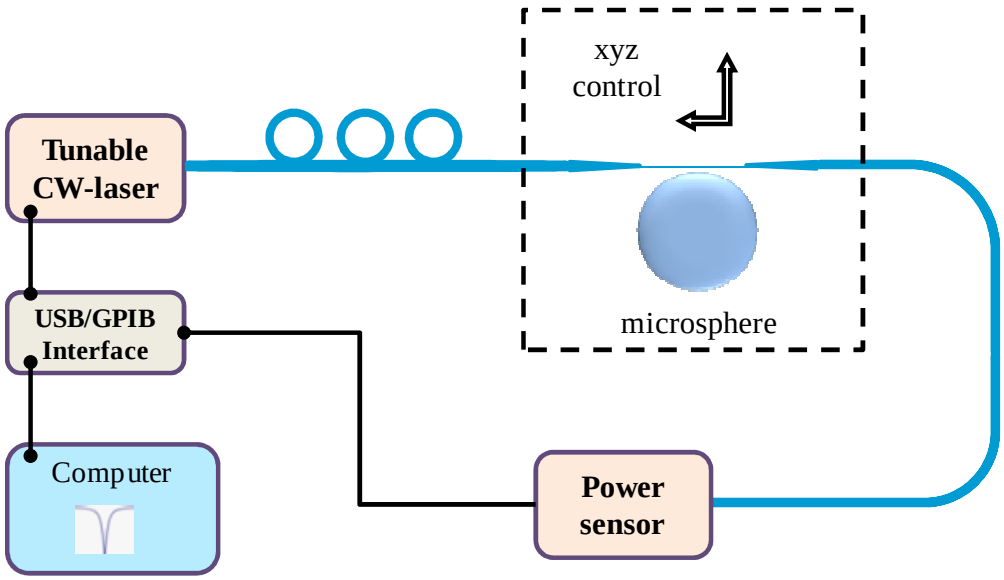

Figure III.12: Experimental setup for characterizing the spectral response of WGM resonator.

Here, we want to describe the coupling process in detail. First a tapered fiber is mounted and fixed on a three-axis translation stage, which allows a fine positioning of the fiber. Then a silica sphere is mounted on another three axis-translation stage with the finely tunable step. When the microsphere is placed into the evanescent zone of the fiber taper, by scanning the tunable laser diode, the taper output signal is monitored with a photodiode at the far end. A photograph of the coupling of tapered fiber and silica sphere is shown in figure III.13.

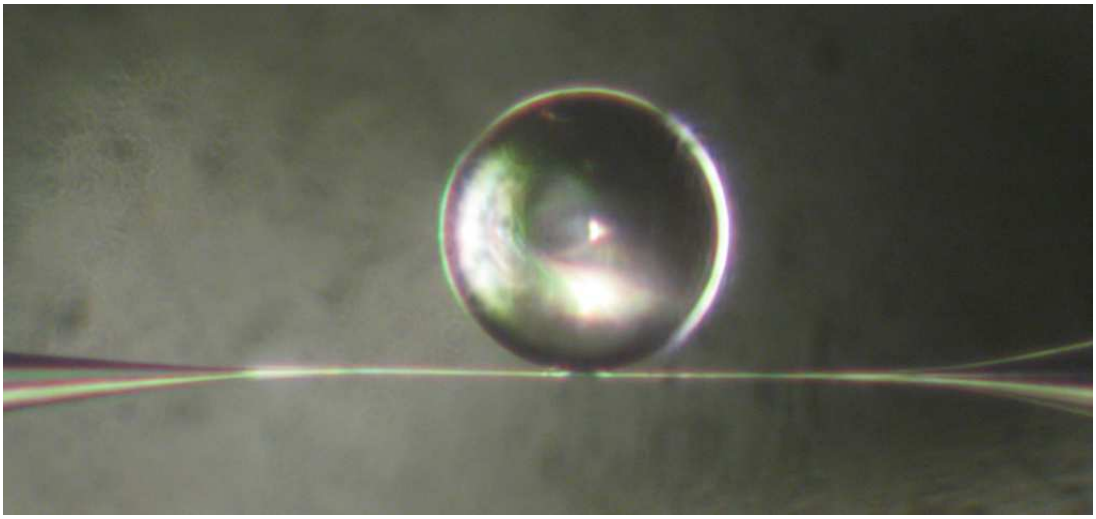

Figure III.13: A top view microphotograph of the coupling between a tapered fiber and a silica microsphere. Tapered fiber waist is ≃ 2 microns, the diameter of the sphere is ≃100µm and the gap between taper and sphere is < 1µm in this case.

III.3.2.2 Excitation of whispering gallery mode

In the waist region of the tapered fiber as described in section III.2.2, the fiber core disappeared; therefore light travels in fundamental mode along the waveguide formed by the silica waist surrounded by air. The typical size of the tapered fiber waist ranges from 1 to a few micrometers. Because the waist is small, the fundamental mode displays an evanescent tail extending significantly to the space surrounding the taper, so that the mode propagation constant is a function of waist radius. For the tapered fibers used in our experimental set-up (waist diameter ranging from 1.5 microns to 4 microns), the dependence of the propagation constant β_f of the fundamental taper mode on the taper waist radius can be expressed in [74] as:

$$\beta_f^2 = k^2 N^2 - \left(\frac{2.405}{\rho}\right)^2 \tag{3.14}$$

where N is the refractive index of fiber and k is the free-space propagation constant of the light.

A microsphere is placed in the evanescent field zone of the taper fiber at its equatorial region. The gap g between sphere and tapered fiber is approximately $g \leq 1\,\mu\text{m}$. The light beam from the tunable laser is coupled into the taper and excites only TE mode. When the tunable laser wavelength is scanned, for example from 1562 nm to 1572 nm (10 nm span), resonance dips appear in the transmitted signal (figure III.14a).

To estimate the Q factor of this microsphere, we examined a single resonance dip in the WGM spectrum (figure III.14b). At 3 dB from the dip minimum of the resonance at $\lambda_{res} = 1567.47\,\text{nm}$, the resonance line width $\Delta\lambda_{res}$ is estimated to 0.0047 nm, corresponding to a calculated quality factor of the sphere $Q = \frac{\lambda_{res}}{\Delta\lambda_{res}} = 0.3\times10^6$. In general, the free spectral range of resonator can be calculated by equation (2.34 or 2.35). In practice, the FSR value of this microsphere can be determined from experimental WGM spectrum of a 90 µm diameter sphere. Using an experimental transmission spectrum of a 90 µm diameter sphere, the laser source being tuned from 1562 nm to 1572 nm, the FSR (i.e. the spacing between two consecutive peaks) is $\Delta\lambda_{FSR} = \lambda_{1567.472} - \lambda_{1564.719} = 2.67\,\text{nm}$. Within a wavelength range of 10 nm, the $\Delta\lambda_{FSR}$ is approximately 2.8 ± 0.3 nm. From fig. III.14a, we can see that the experimental WGM spectrum is rich. This indicates that the light coupled out of sphere is not fully injected into the fundamental fiber mode ($l = |m|$). Other azimuthal modes with $l \neq |m|$ are also coupled out of the sphere. These modes are generated not only by backscattering (extracting the light out of the cavity and launching it back into the fiber) but also by the effect of the coupling gap distance between the microsphere and the tapered fiber.

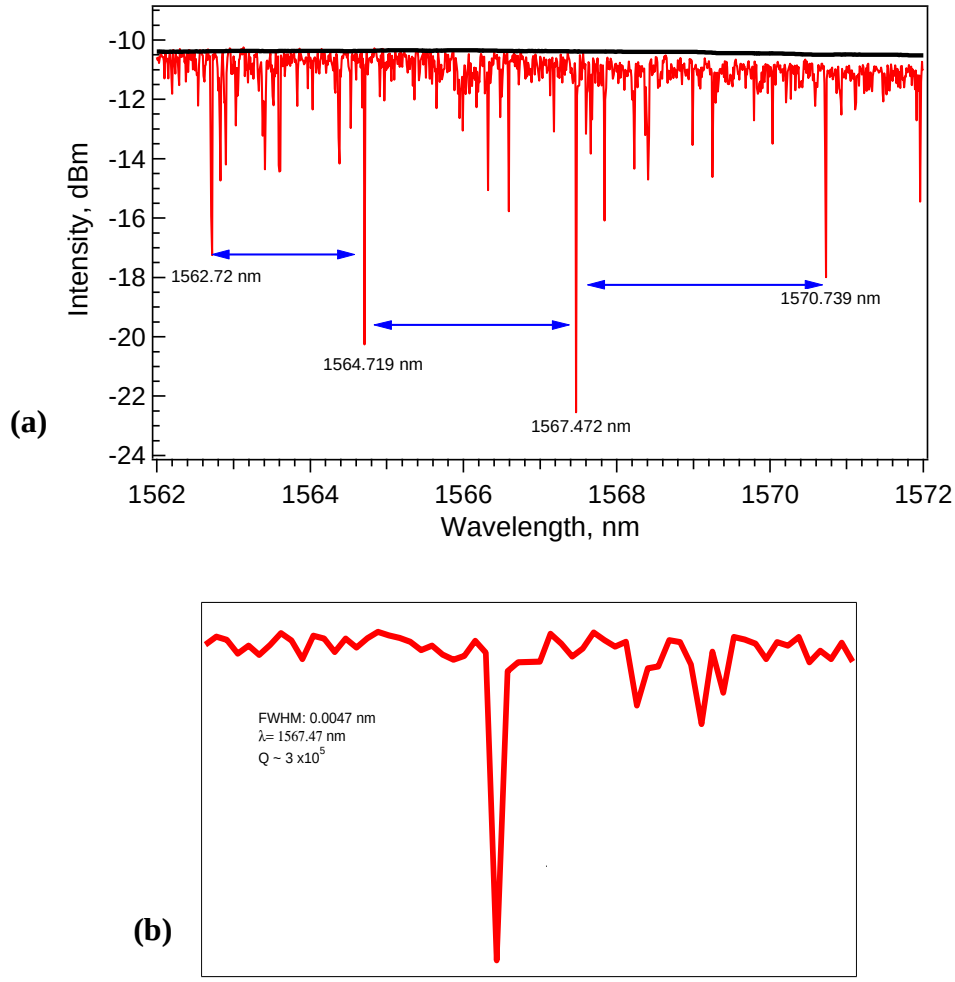

Figure III.14: The transmission spectrum for microsphere-taper fiber system. In this case, the diameter of the sphere is ≈ 90µm and the taper waist size is ρ≈ 2µm. (a): the black curve is the transmission signal of the sole tapered fiber (laser is not coupled into sphere), the red curve shows resonance dips for microsphere-fiber coupling at operating wavelength region from 1562 nm to 1570 nm ; (b) a resonance dip at 1567.47 nm with $\Delta\lambda_{FWHM} = 0.0047$ nm , corresponding to a quality factor 3×10^5.

III.3.2.3 Gap effects on output spectrum

As shown in figure III.15a, at the gap distance $1\,\mu m > g > \lambda/2\pi$ we can see the rich spectrum of WGM resonances. It is possible to say that at this distance, the 2 µm tapered fiber permits the backward propagating light within the fiber as the initial propagation direction was forward. When the gap increases ($g > 1\,\mu m$), the resulting spectrum (figure

III.14b) is much cleaner than the above one and the number of higher-order modes excitation is reduced. However, increasing the gap distance between sphere and taper induces radiation losses to low order modes.

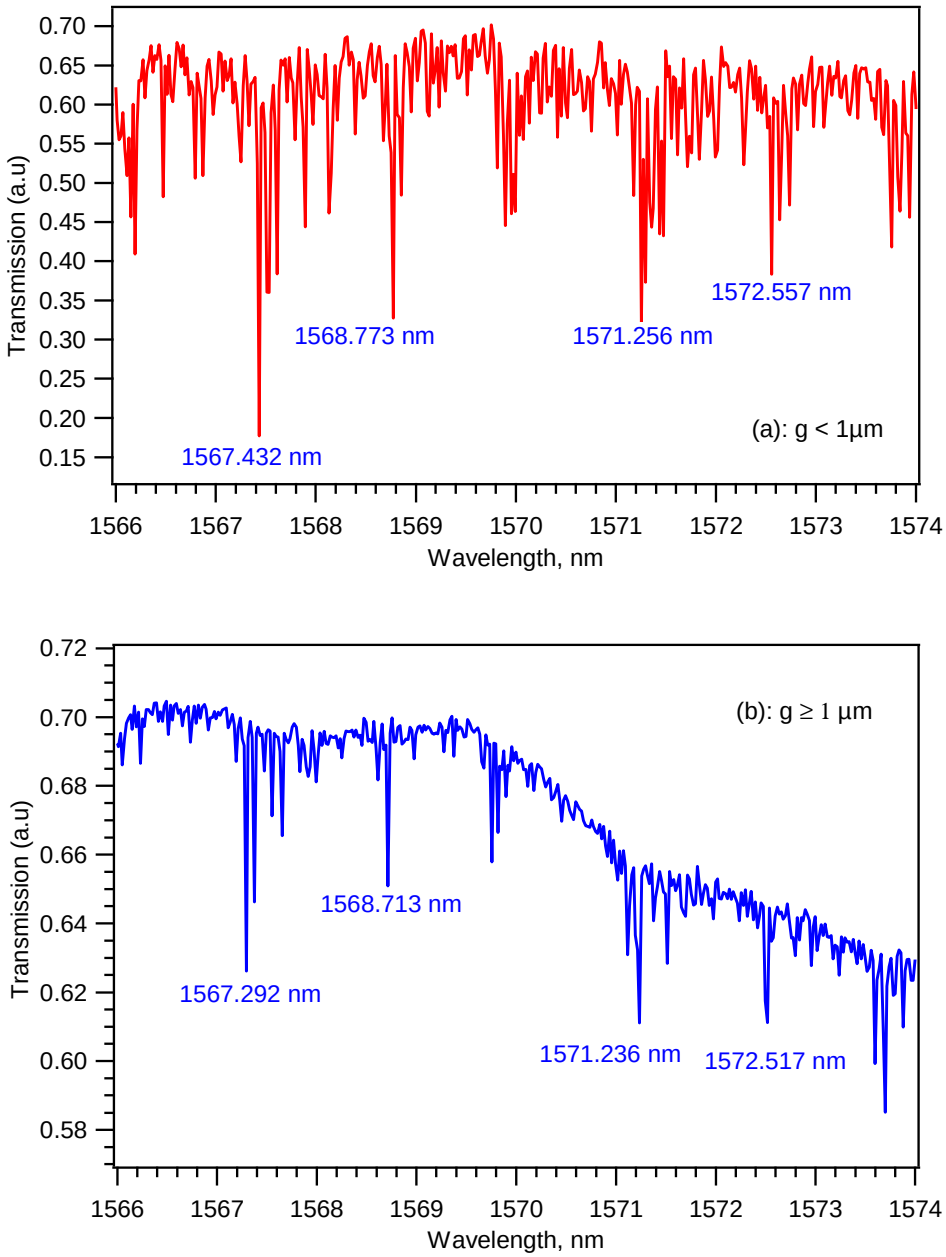

Figure III.15: Transmission spectrum of a microsphere with a 120µm diameter. Taper size is ρ≈ 2µm. Output signal at (a) g < 1µm and (b): g ≥ 1µm (g is the air gap distance between the fiber taper and sphere).

In order to gain a better understanding of the gap effect on WGM using a tapered-microsphere coupler, the gap distance between the fiber and the sphere is finely changed and the resonator is modelized using CST Microwave Studio® software. In this calculation, the diameter of microsphere and waist of taper are kept constant at 25 µm and 1 µm, respectively. The gap takes the values 1 nm, 100 nm, 200 nm, 400 nm, 600 nm, 800 nm and 1000 nm. The frequency dependence of the simulated transmission spectrum of the microsphere is presented, for different gap values, in figure III.16. This curve shows that the output intensity from the micro resonator becomes stronger and that more radiation energy is stored in the resonator when the gap distance increases. For example, at $g = 1\,\text{nm}$ the output intensity dip is -48.01 dBm at 194.28 THz in frequency (or 1544.163 nm in wavelength). When *g* increases to 100 nm, the output intensity dip is -52.30 dBm and it is -59.23 dBm when *g* increases up to 400 nm. However, the output intensity becomes weaker when the gap value continue to increase (figure III.28). For example at $g = 600\,\text{nm}$, the output intensity dip is -58.58dB and it is -49.52dB at $g = 1000\,\text{nm}$.

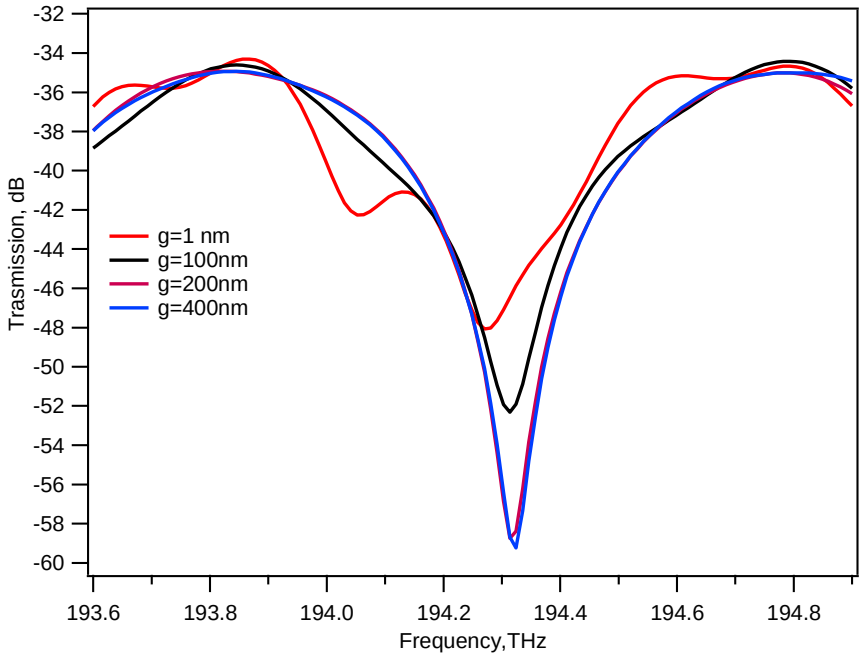

Figure III.16: Simulation results of the microsphere-tapered fiber coupler system. Transmission spectra are calculated for different gap distances (1 nm to 400 nm). In this case, the sphere diameter is D=25µm and the waist of the taper fiber is ρ=1µm.

III.3.2.4 Q factor and FSR

In order to study the excitation of the WGM resonator, microspheres with different diameters are characterized. The resonance spectra of three spheres with diameters 60 µm, 90 µm and 150 µm respectively are shown in figure Ⅲ.17. For sphere with a diameter of 60 µm, the free spectral range of the strongest resonator peaks (n=1) is determined to be 6.2 ± 0.6 nm with a wavelength range from 1560 nm to 1576 nm. A quality factor $\lambda / \Delta\lambda$ of $1.1\ 10^5$ is calculated from the resonance peak at 1561.589 nm. Assigning the major peaks to correspond to the fundamental WGM mode (n=1), the azimuthal WGM number of this sphere can be calculated by $l = Nx$, where $x = 2\pi a / \lambda$ is the size parameter and a is diameter of sphere. For resonance peak at 1561.589 nm, the WGM numbers are $l = m = 350$ and they are $l = m = 347$ for resonance at 1574 nm in figure III.17a.

Diameter of sphere	Experimental results		Calculation	
	$FSR\,(\mathrm{nm})$	λ_{res} (nm)	Sphere mode number $l = \lvert m \rvert$, $n = 1$	Q factor
60µm	6.2 ±0.06	1561.589	350	$\approx 10^6$
		1567.794	348	
		1574.054	347	
90µm	2.7 ± 0.6	1562.72	525	
		1564.719	524	
		1567.472	523	$\approx 10^6$
		1570.739	522	
150 µm	1.03 ± 0.3	1570.841	870	
		1571.723	869	
		1573.937	868	$\approx 10^6$

Table III.2: Experimental resonant wavelengths and assigned mode numbers l, n for three silica microspheres.

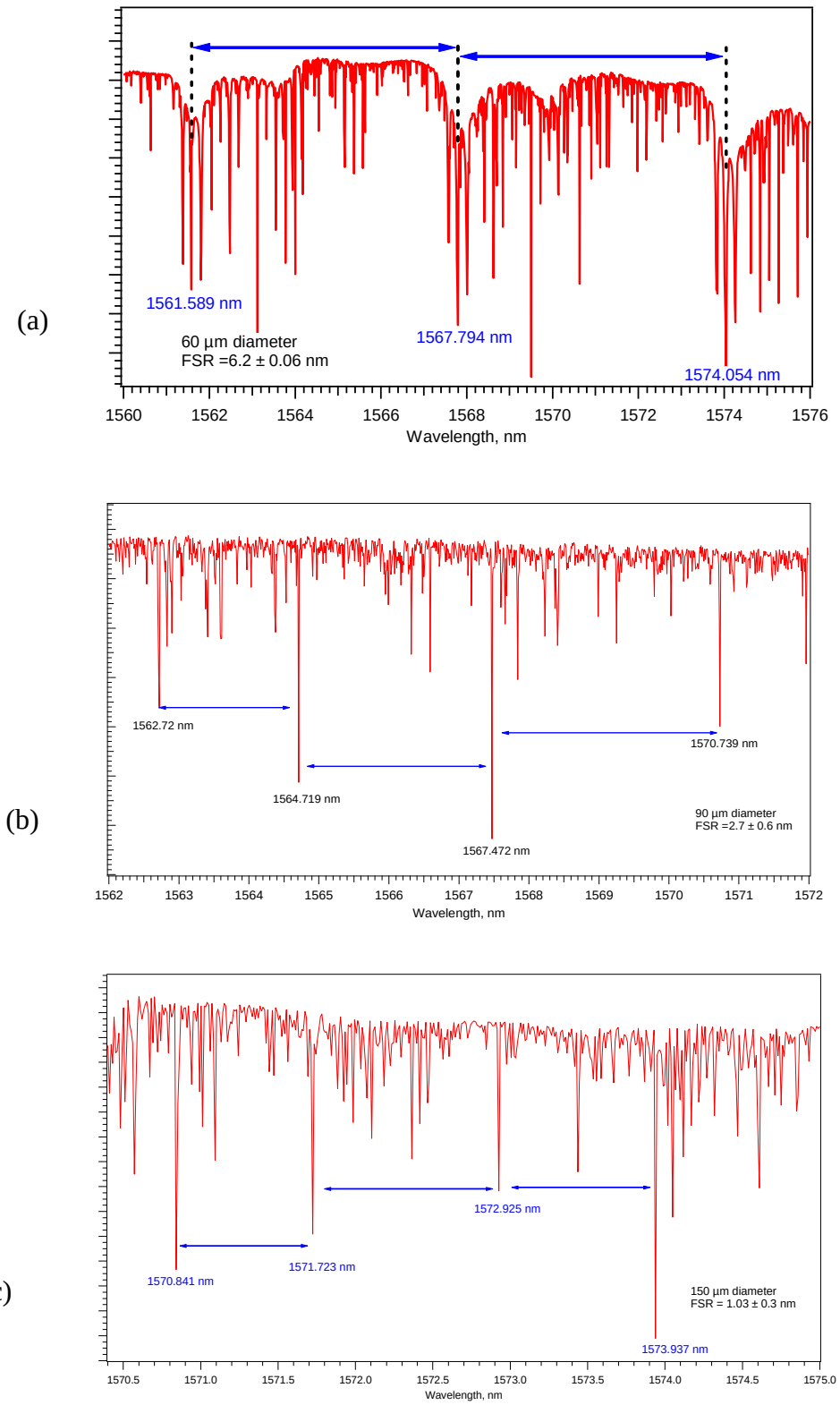

Figure III.17: Transmission spectra of three different microspheres. (a): wavelength range: 1560nm-1576 nm, FSR: 6.2 nm ± 0.06; (b): 1562 nm-1572 nm, FSR: 2.7nm ±0.6; and (c): 1570-1575 nm, FSR: 1.03nm ±0.3.

The experimentally observed resonant wavelengths and the calculated mode numbers of the fundamental radial mode ($n=1$) for three difference microsphere sizes are presented in table III.2. Sphere mode number is calculated at the refractive index $N=1.45$ of silica for all these spheres.

The taper coupling mechanism is in general mode selective; the input fundamental mode is coupled into microsphere and is outcoupled via tapered fiber. But as shown on the transmission spectra of the spheres, the taper coupling mechanism allows to excite higher azimuthal modes ($|m|<l$).

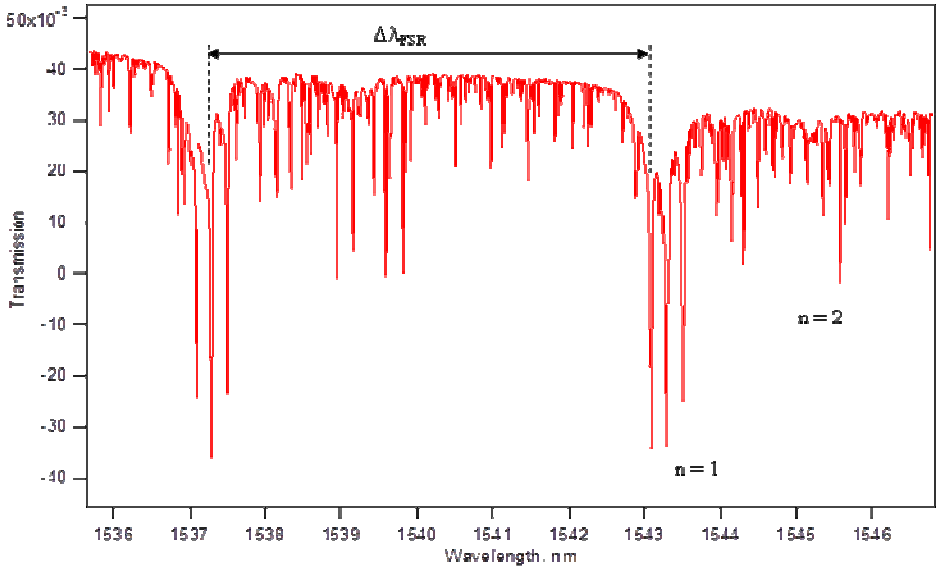

Figure III.18: Transmission spectrum of a microsphere with diameter of 60µm. The strongly coupled modes are considered as fundamental radial modes (n=1), and the weakly coupled modes are indentified as higher order coupled modes (n>1).

It can be seen in the transmission spectrum of a microsphere with 60 µm diameter (fig. III.17) that besides fundamental modes, the tapered optical fiber can efficiently excites higher order azimuthal modes.

III.4 Excitation of WGMs with fiber tip

In the above section, we presented results on coupling to the evanescent field of WGM resonator by a tapered fiber. In this experimental setup, we want to present another

technique to characterize the optical properties of microsphere. Upon laser wavelength tuning the resonances of sphere are observed as resonance dips. Additionally, when the resonance condition is fulfilled, a small fraction of the light in resonant mode is scattered out of the sphere. To collect this scattered light, a tip fiber fabricated on the top of a single mode optical fiber was employed. This tip is placed in the evanescent field of sphere at a point close to the sphere equator. The brief description about tip fabrication is presented in the following section.

III.4.1 Fiber tip fabrication

A single mode optical fiber is cleaved and cleaned, and then mounted on a three dimensions translation stage and placed into the focal zone of two electrodes. The fiber is heated by an electric arc and drawn until the desired tip is achieved. Finally we obtain a 500 µm long fiber tip with a diameter of 1 µm-1.5 µm as shown in figure III.18. After heating and drawing the fiber to reduce its diameter to 1 micron, the cladding of fiber disappears, therefore the fiber tip operates as a waveguide with a core refractive index of $N_{fib} = 1.45$ and cladding refractive index $N_{clad} = 1$ corresponding to the air

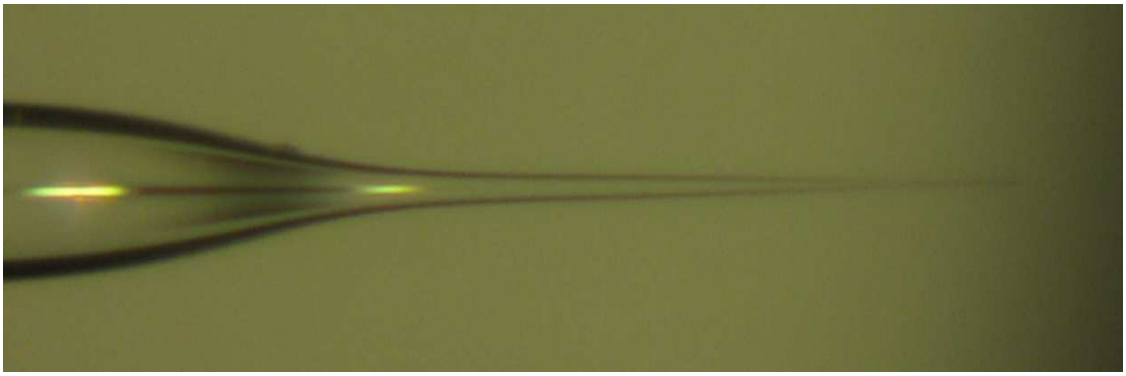

Figure III.19: Photograph of a fabricated optical fiber tip with length of tip $\approx 500\mu m$ and tip diameter $\approx 1\mu m$.

III.4.2 Excitation of whispering gallery mode by fiber tip

III.4.2.1 Experimental setup

The schematic experimental setup of a tapered fiber-microsphere-tip fiber coupling system is shown in figure III.19. In this setup the light from the tunable laser is coupled

into the sphere via a tapered fiber with a waist of approximately 2 µm. The output transmission signal is measured at the end of the tip fiber and displays resonance dips. Close to sphere equator, the fiber tip is positioned to collect the scattered light that goes out of sphere surface. The polarization controller is used to matching the polarization of the laser light with the polarization of the resonator mode. The distance between the resonator and the tapper fiber can be finely controlled by a three dimensions translation stage.

For optimizing the gap distance between the tip fiber and the equatorial zone of the sphere, this tip fiber is mounted and fixed on another three-axis translation stage, which allows for fine positioning. The scattering light is collected by the tip and monitored with a photodiode at the other end of the fiber. A photograph of the tapered fiber-optical microsphere-tip fiber coupler is shown in figure III.20a.

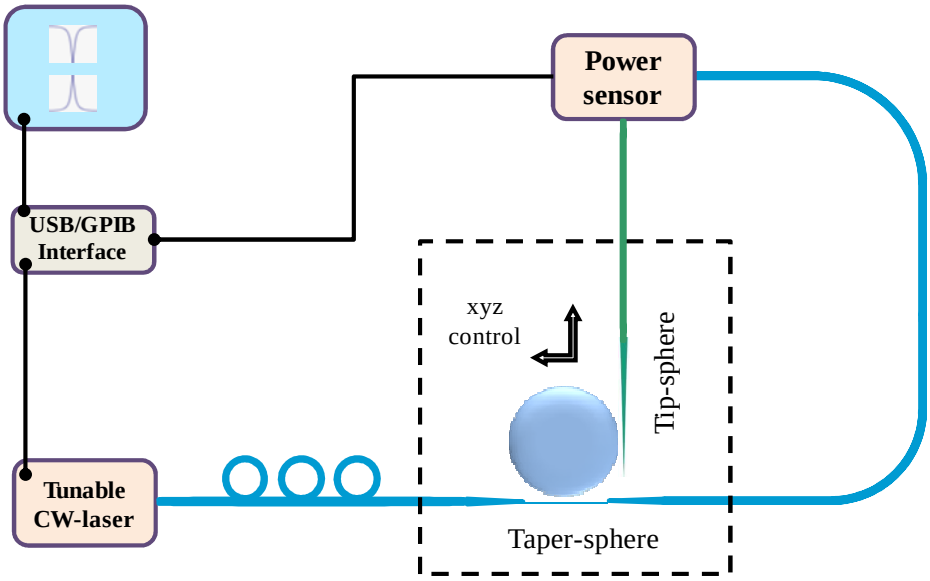

Figure III.20: Schematic of experimental setup. Light is coupled into the sphere via a taper fiber; resonance dips are detected in absorption at the other extremity of the taper fiber. Scattered light is detected via the tip fiber.

With this setup, we are able to characterize the intensity distribution of WGM and to scan the influence of a small scatter located in the evanescent field on the degradation of the optical response of the resonator in real time.

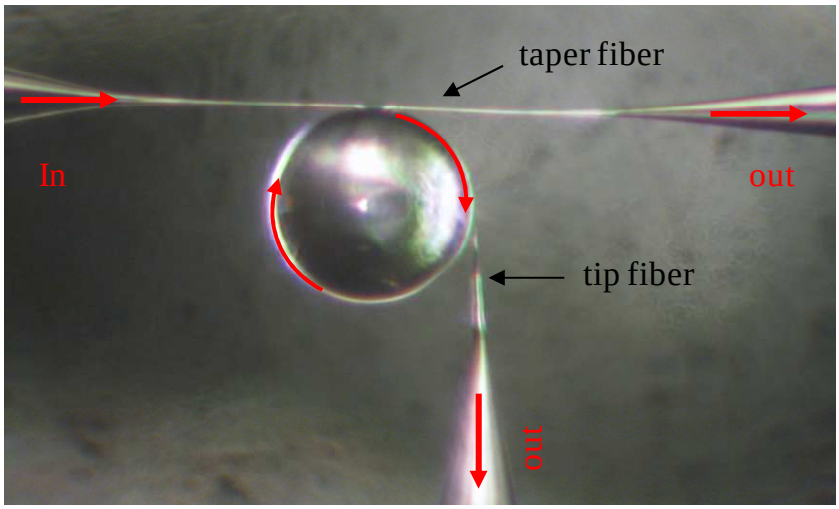

Figure III.21: A photograph of taper fiber-microsphere-fiber tip fiber coupler. In this case, the sphere used here has a diameter of 90 µm, the waist of the taper fiber is ρ ≈ 2µm; the tip diameter is ≈ 1µm.

III.4.2.2 Scattering spectra

In order to measure intensity of the scattered resonance peaks of microsphere resonator, the single mode fiber tip is placed close to the sphere surface at its equatorial zone to collect the light from the evanescent field. The distance between tip and sphere surface is kept constant at 1 µm approximately. A typical scattering spectrum of a microsphere with a diameter of 90 µm is shown in figure III.21. The inset zooms into a mode at 1562.21 nm wavelength with a full width at half maximum (FWHM) of 0.009 nm. This FWHM value corresponds to a Q factor of 1.7×10^5. The free spectral range of this microsphere is determined from this scattering spectrum. When the laser is tuned from 1562 nm to 1572 nm, the FSR value of this resonator determined from the scattering spectrum is 2.58 ± 0.57 nm. On another hand, the FSR value is found to be 2.8 ± 0.3 nm when investigating the absorption spectrum of this microsphere collected by the previously used tapered fiber (upper curve). The small difference between the two FSR values (approximately 0.2 nm) can be explained by a difference in the coupling position of tapered fiber and fiber tip with respect to the microsphere equator. It is known that the mode in a dielectric sphere is characterized by mode numbers l, m and n [17, 79], where l is approximately the number of wavelengths packed along the circumference of the resonator, m is the azimuthal order number and n is the mode number of intensity

distribution. In a perfect spherical resonator, modes having the same n and l values are degenerate, but in a real sphere, due to a finite eccentricity which is typically smaller than 10^{-2}, this degeneracy is lifted, and leads to a mode spacing of several hundreds of MHz. Moreover there a splitting of modes because of their different polarization (TE and TM polarized modes).

When a tip is close to the surface of the sphere, the evanescent field of the mode is converted into propagating waves within the fiber. Effective scattering is desirable for near-fields microscopy in order to enhance the detectable signal. With this experimental setup, it is possible to achieve coupling via a near-field probe of the microsphere. The fundamental modes are identified via the scattered resonant modes. The result shows that this technique could be used to characterize a microsphere resonator and its optical mode structure.

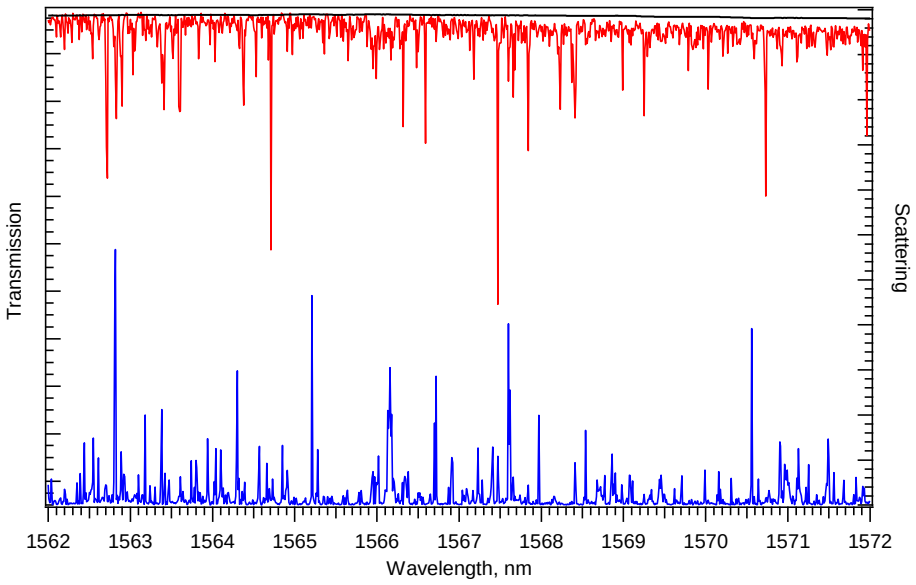

Figure III.22: Scattering spectra as collected by the tip fiber for wavelengths tuned from 1562 nm to 1572 nm. The inset shows a narrower mode at 1562.21 nm with $\Delta\lambda_{FHWM} = 0.009$ nm corresponding to $Q \approx 1.7\times10^{5}$.

In order to investigate the excitation of WGM via both coupling methods: tapered fiber and tip fiber. The experimental FSR values of microspheres are determined and plotted as function of the sphere diameter (figure III.22).

From equation (2.35) FSR depends on the sphere diameter. However, on the basis of the experimental results from microspheres with different diameters, the calculated FSR can be inferred from a fit with experimental FSR values (fig.III.23, red curve). From the red curve, it can be clearly seen that FSR will decrease when the microsphere diameter increases. For example, a 60 µm microsphere diameter displays an experimental FSR value of ≈ 6.2 nm (or 774 GHz), but this value decreased to 0.2 nm (25GHz) for a 300 µm diameter sphere.

As presented in section III.4.2.1, a polarization controller is used to matching the polarization of the laser light with the polarization of the resonator mode. The transmission spectra of the microsphere for two different polarization are shown in figure III.24.

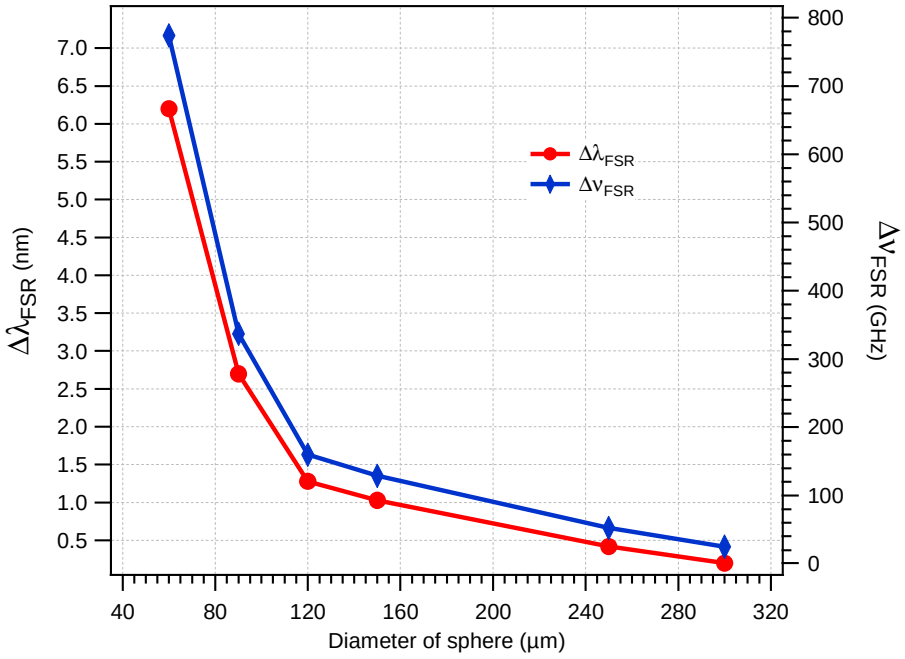

Figure III.23: The free spectral range for the resonance peaks, corresponding to a fundamental microsphere mode ($n=1$, $m=l$), depends on the sphere diameter at operation wavelengths within 1550 nm region.

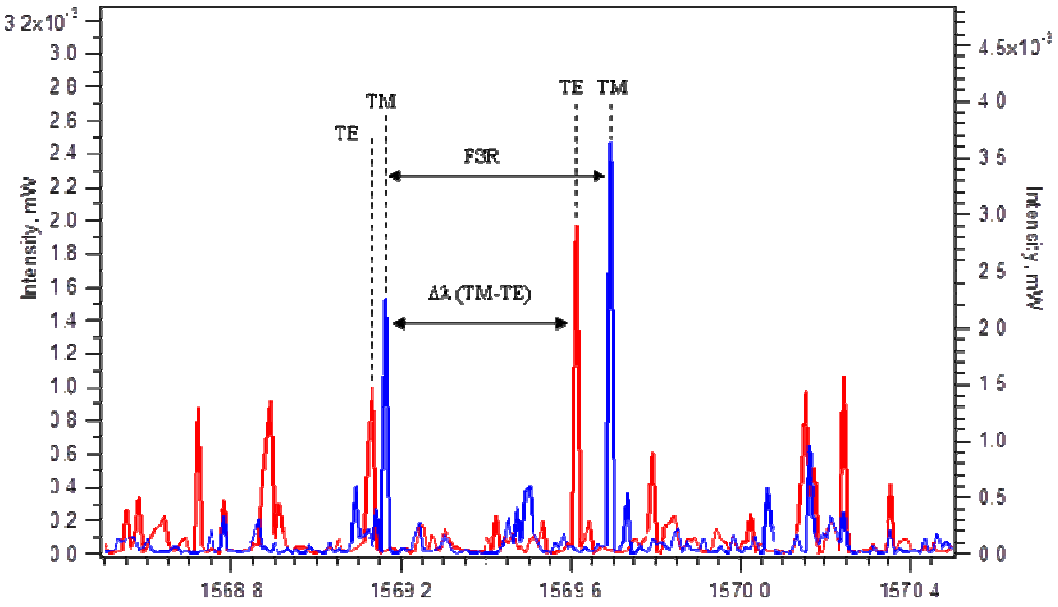

Figure III.24: Transmission spectral of microsphere when laser scans from 1569 nm to 1570nm. The sphere with diameter of ≈ 100 µm, waist of taper fiber ρ ≈ 2µm, the tip diameter is ≈ 1µm.

Figure III.24 shows that the TE mode shifts to shorter wavelengths while the TM mode weakly shifts to longer wavelengths. From equations (2.35), the radius of sphere can be expressed as:

$$a = \frac{c}{2\pi N \Delta \nu_{FSR}} \tag{3.15}$$

with the index refractive N of sphere being determined as:

$$N = \frac{\Delta\lambda_{FSR}}{\sqrt{\Delta\lambda_{FSR}^2 - \Delta\lambda_{TM-TE}^2}} \tag{3.16}$$

As we have previously explained that in an opto-electronic oscillator system (OEO), the long fiber loop acts as a delay line providing a spectrally pure high-frequency signal. Such an OEO configuration, for a small size system, is challenging because of a long fiber delay is obtained for some kilometers of fiber. Moreover, the fiber delay is sensitive to the surrounding environment. Here we will examine whether we can replace the long fiber loop by an optical micro-resonator in an OEO system. With the assumption that the OEO

system operates at the frequency of $f = 8\,\mathrm{GHz}$, we can infer the radius of microsphere, which is needed for obtaining this frequency, from equation (3.15). For example, for an OEO system operating at 8 GHz and a wavelength of 1550 nm, a silica sphere with a radius of ≈ 4 mm is required. However, with electric-arc system, we can only fabricate small microspheres (from 20 µm to 400 µm) as compared to the radius of the desired sphere (≈4 mm).

Therefore, in order to investigate a resonator that can be employed in an Opto-Electronic-Oscillator system working at the above mentioned GHz range, another type of resonator must be designed and fabricated. Its characteristics are presented and discussed in the next chapter.

III.5 Optical taper-microsphere coupling simulation

CST Microwave Studio® is a fully featured software package for electromagnetic analysis and design in the high frequency range. Under this software, we present a theoretical study of the taper fiber- silica microsphere resonator coupler. The light propagating within the microsphere is coupled to a tapered fiber with a fixed diameter, and we investigate the simulation results of the output resonance mode when changing the coupling distance. Resonators with different diameters are studied. The first part present simulation results on tapered fiber and the second part is developed to couple the taper fiber and sphere resonator. The study focuses on the design and realization of silica sphere resonator with small diameters (smaller than one millimeter).

III.5.1 Simulation of tapered fiber

The results of the phase-matching presented in ref. [72] reported that, within a small range of fiber taper size, matching of the propagation constants between a tapered fiber and a sphere can be seen over a wide range of sphere diameters. For a sphere resonator with a diameter smaller than 30 µm, a waist size of taper fiber $\rho \leq 1.4\mu m$ is chosen for this simulation. The total length of taper fiber is 100 µm, its waist size is ρ = 1 µm and waist

length is 70 µm. The signal is coupled into port 1 of sample and collected out at port 2, and the input wavelength ranges from 1530 nm to 1620 nm.

Fig. III. 25 shows the TM mode that is excited in taper and the optical field distribution obtained by simulation with CST Microwave Studio.

The frequency is expressed as:

$$f_{\min} = \frac{c_0}{\lambda_{\max}} \text{ and } f_{\max} = \frac{c_0}{\lambda_{\min}} \tag{3.17}$$

where $\lambda_{\min}$, $\lambda_{\max}$ are minimum and maximum input wavelengths, respectively and c_0 is the velocity of light.

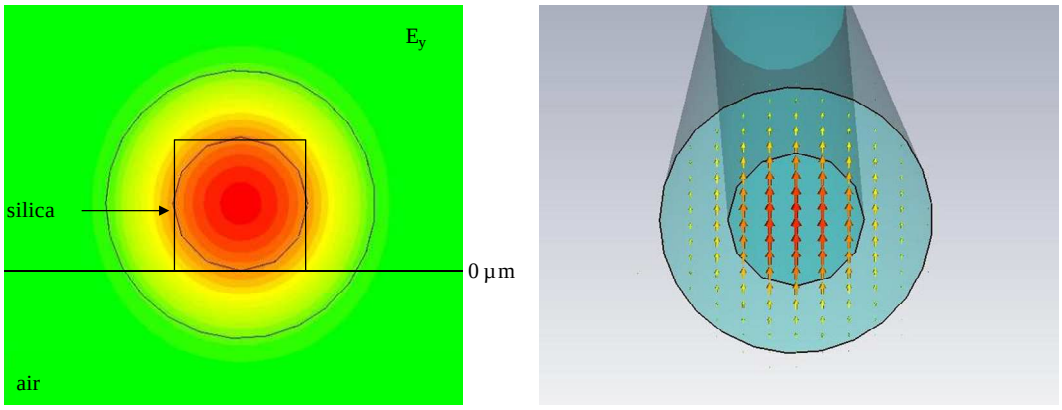

Figure III.25: TM mode in Taper fiber and its simulated optical field distribution by CST software.

The output plot showing the output transmission as a function of frequency is presented in figure III.9b. In this simulation, the transmission of signal by the taper depends on the input wavelength. For an input wavelength of 1540 nm (at 194.805 THz), the return loss equals to -41.694 dB. When the input wavelength increases, the return loss decreases, it reaches the minimum of -42.787 dB for a 1580 nm (189.873 THz) input wavelength. When compared to the experimental results of tapered fiber, it shows that the frequency dependence of the transmission spectrum roughly agrees with data of fig. III.9.

III.5.2 Taper-microsphere coupler

In simulations, the microsphere and taper fiber are created from silica material. Let us assume that a sphere with a diameter of 25 µm is coupled to the tapered optical fiber with a waist radius of 1 µm, its length being 70 µm. The coupling gap between fiber and the microsphere is changed for each simulation. The surrounding medium is assumed to be air. A continuous wave light is incident into the left end of the taper and light is collected at the right end. The wavelength of the incident light is tuned from 1530 nm to 1620 nm (corresponding to the 185 - 197 THz frequency range). The computational resolution of wavelength is 0.1 nm. The taper-microsphere coupler is shown in figure III.26.

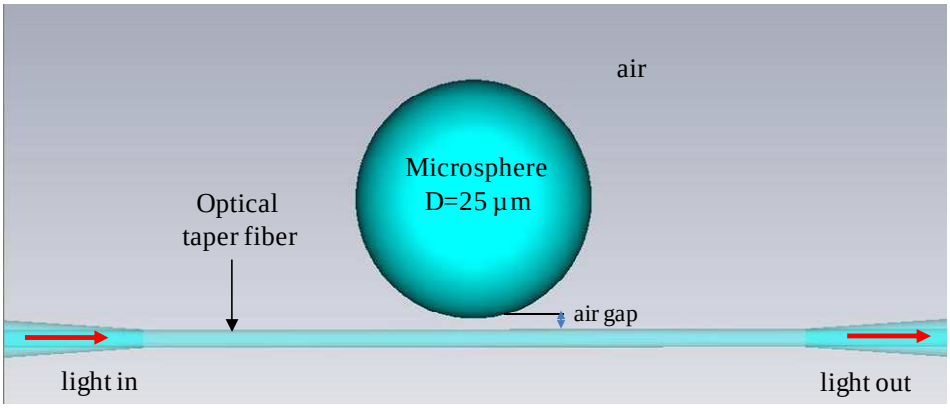

Figure III.26: The simulation model

First, the electromagnetic field and radiation energy field of the WGM resonator are calculated for excitation resonance frequencies ranging from 185 to 197 THz. For total multiple reflection, optical whispering gallery modes have small evanescent component that are located very close to the surface of the sphere. These modes correspond to the light trapped in circular orbits just below the surface of structure. Considering that the value of l (angular mode number) is close to the number of wavelengths that fit into the optical length of equator, the value $l-m+1$ is equal to the number of fields along the polar direction; the mode number n is equal to the number of field maxima in the direction along the radius of the sphere. The distribution of the electric field and the mode numbers are clearly visualized in figure III.27

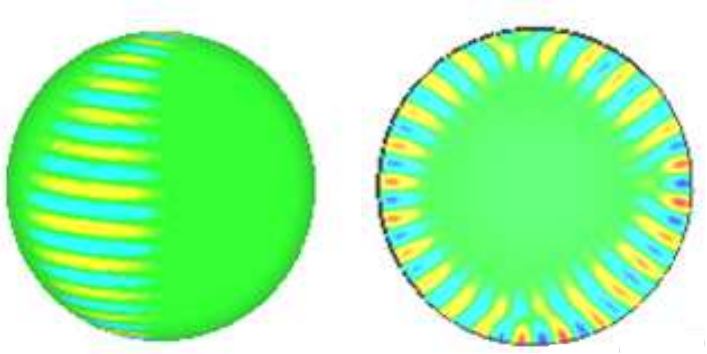

Figure III.27: Distribution of the electric field in microsphere with diameter of 10 µm, taper waist is 1 µm. TE-mode with mode number $n = 1$ and $m = l \approx 24$.

III.5.3 Transmission spectrum

After setting up a taper-resonator coupler, the transmission coefficients (S_{21} in term of *S* parameters) are calculated and measured. The first simulation result is presented in figure III.28. In this simulation, a microsphere with diameter of 25 µm has been used. It is coupled with a tapered fiber with a waist of 1 µm and a length of 70 µm, the air gap between taper and sphere being 0.4 µm.

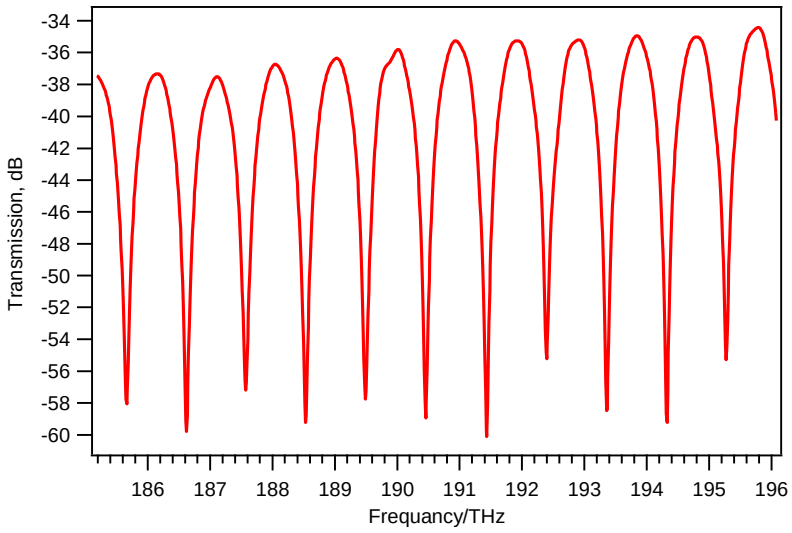

Figure III.28: Simulated transmission coefficient of a taper-resonator coupler calculated by CST software. The microsphere has a diameter of 25 µm, the waist of the taper is 1 µm and the coupling gap is 0.4 µm.

In general, total quality factor of taper-resonator coupler can be expressed by:

$$Q_T^{-1} = Q_{intrin}^{-1} + Q_c^{-1} \tag{3.18}$$

where Q_{intrin}. is the intrinsic quality factor of the resonator and Q_c is indentified as the external quality factor of cavity (losses caused by input and output coupling of the resonator) [80]. This external quality factor can be calculated from equation:

$$S_{21} = 20\log_{10}\left(\frac{Q_T}{Q_c}\right) \tag{3.19}$$

And the quality factor Q_T of the resonator can be determined as:

$$Q_T = \frac{f_{res}}{\Delta f_{res,\,3dB}} \tag{3.20}$$

where f_{res} is the resonant frequency and $\Delta f_{res,3dB}$ is the linewidth at -3 dB of resonance peak. From the simulated parameters of taper-resonator coupler in fig.III.28, the quality factor depending on resonant frequency of the resonator under simulated CST is inferred.

f_{res} (THz)	$\Delta f_{res,\,3dB}$ (GHz)	$Q_T = \frac{f_{res}}{\Delta f_{res,\,3dB}}$
186.623 ((λ_{res}=1607.52 nm)	4.6	4057
188.529 (λ_{res} =1591.26 nm)	4.7	4012
190.458 ((λ_{res}=1575.15)	4.3	4429
191.437 (λ_{res} =1567.09 nm)	4.6	4161
193.355 (λ_{res} = 1551.55 nm)	4.1	4751
194.324 (λ_{res} = 1543.81 nm)	4.1	4739

Table III.3: Total quality factor Q_T of the resonator with 25 µm diameter, g=0.4 µm at difference resonant frequencies.

III.5.4 Coupling gap and resonance parameter

Three major parameters can reflect the characteristics of an optical resonator: the energy storage capacity, quality factor value (considered as number of times that a trapped photon can be expected to cycle in the cavity), and various losses due to the cavity (scattering or other out-coupling). These phenomena can be determined by the broadening, the wavelength shift and the amplitude of the resonance line. In practice, optical coupling from a taper fiber into WGMs of a silica microsphere should be mentioned as a phenomenon which may affect the Q factor.

The coupling Q_c factor is defined by WGM losses related especially to leakage into the coupler. It can be approximately determined as a function of the coupling gap between taper and microsphere as [81]:

$$Q_c = 102\left(\frac{a}{\lambda}\right)^{5/2} \frac{N^3\left(N^2-1\right)}{4q-1}\exp(2\gamma g) \tag{3.21}$$

here a is the radius of microsphere,

g is the coupling gap between taper and sphere,

λ is the wavelength of input light,

q is denoted as the radial mode number (it is typically smaller than 10 for modes confined close to the sphere surface),

γ relates to the wave number and is expressed as: $\gamma \approx k\left(N^2-1\right)^{1/2}$ where N is the refractive index.

Equation (3.20) shows that the whispering gallery mode resonance line width is related to the total quality factor of cavity, which can be written as: $1/Q_T = 1/Q_c + 1/Q_{intrin}$, here Q_c is the external quality factor and Q_{intrin} accounts for cavity loss properties such as scattering and attenuation. Therefore, from equation (3.20) and (3.21), the coupling gap which affect the quality factor can be determined by:

$$\Delta f_{res}(g) = \frac{f_{res}}{Q_T} = \frac{f_{res}}{Q_{intrin}}\left(1 + \frac{Q_{intrin}}{Q_c}\right) \tag{3.22}$$

here Δf_{res} and f_{res} are respectively the linewidth and the resonance frequency position.

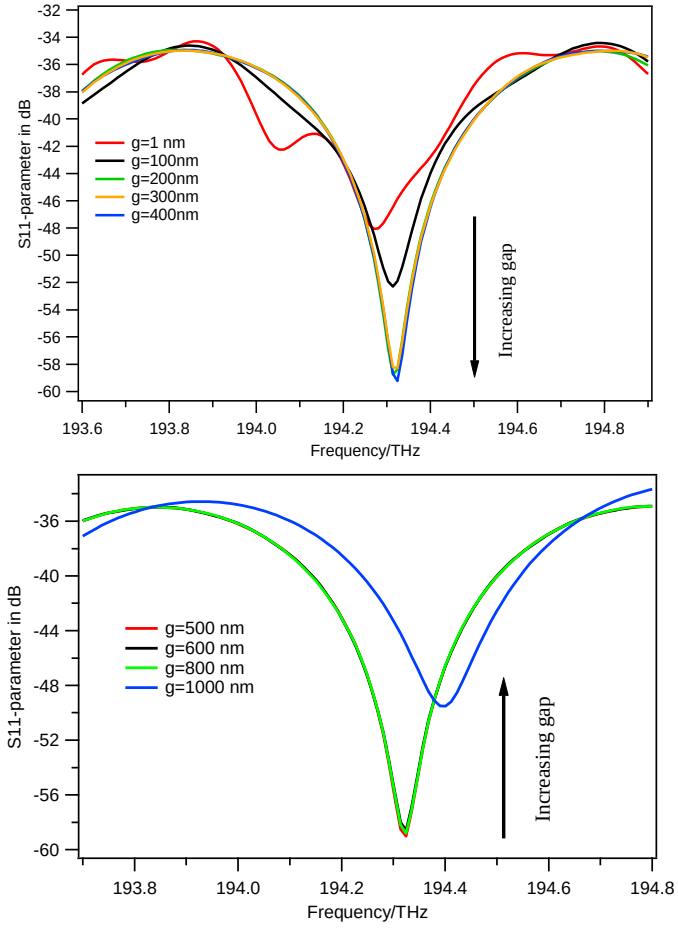

Figure III.29: Simulated parameter S_{11} of a taper-resonator-coupler calculated by CST. Microsphere diameter is 25 µm, the waist of taper is 1 µm, the coupling gap is tuned from 1 nm to 1000 nm, and operation wavelength is in 1543 nm region.

From the gap dependence of the microsphere resonance peaks occuring within the 1543 nm wavelength region as sketched in figure III.29, the total quality factor Q can be experimentally determined from the resonance linewidth. As the coupling gap varies from 1 nm to 500 nm, the quality factor first increases, reaches a maximum and then decreases for $g > 400$ nm when the coupling gap increases (see Figure III.30). This behavior is quite

expected, as for gap coming close to this value the amplitude of the evanescent wave becomes negligible.

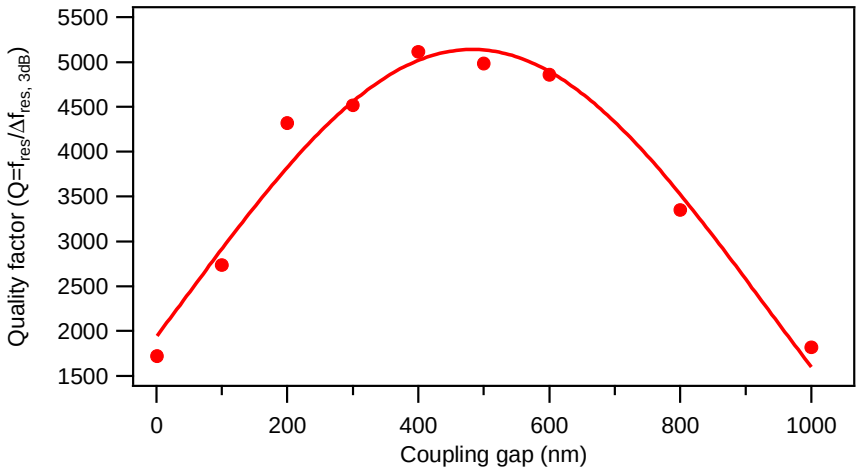

Figure III.30: Plot of the total quality factor Q_T as a function of the coupling gap. Q_T is calculated directly from resonance linewidth measurements figure III.29.

Another parameter that can be used to explore the role of the taper-microsphere separation is the fraction depth K of the resonance dip. The K factor can be expressed as a function of the coupling gap and intrinsic quality factor as [81]:

$$K = \frac{4Q_{intrin}Q_c\Gamma^2}{(Q_{intrin}+Q_c)^2} = \frac{4Q_T\Gamma^2}{Q_{intrin}+Q_c} \tag{3.23}$$

where Γ describes the mode matching between taper and microsphere. The case of $\Gamma = 1$ corresponds to ideal mode matching condition. In this case, input power is lost inside the resonator (the output power becomes zero). This regime is also called as critical coupling. In the case of critical coupling, $K = 1$. Critical coupling can be obtained until $\Gamma^2 > 1$ (partial matching), in this regime, it is considered as non-ideal matching. In this case, leakage into other modes can be considered as additional internal losses, and critical coupling is obtained with a lower quality factor Q_l. A comparative plot of the linewidth as a function of the coupling gap is shown in figure III.31. The linewidth presents a minimum value at the optical gap value of 400 nm corresponding to the highest quality factor Q of resonator.

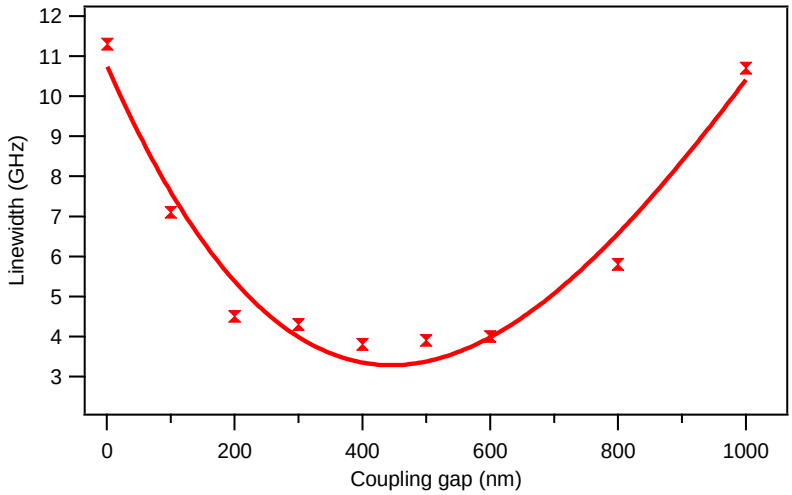

Figure III.31: Plot of the microsphere resonance linewidth, with a polynomial fit, as a function of taper-sphere coupler gap.

When the coupling gap changes, the transmission for various WGM in a 25 µm diameter silica microsphere is modified. The taper fiber diameter was chosen to optimize phase matching to the fundamental whispering gallery mode ($m = l$, $n = 1$). By adjusting the taper position to the sphere equator, the fundamental WGM is obtained, and figure III.32 shows resonant transmission versus coupling the position change.

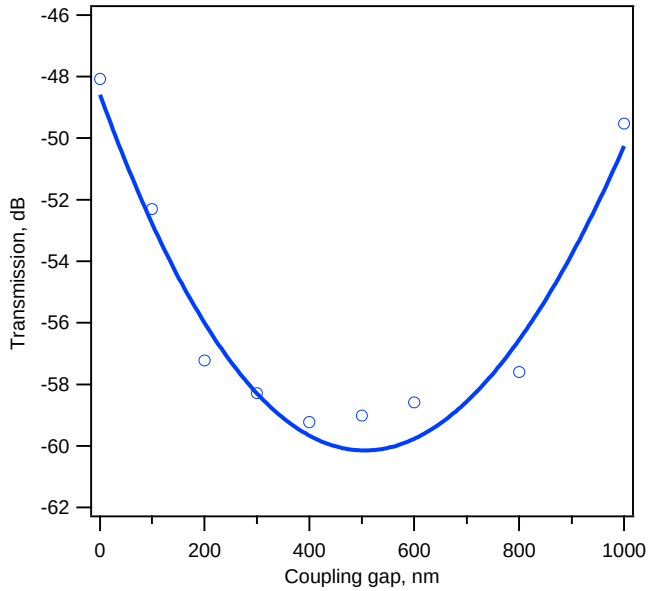

Figure III.32: Plot of the output intensity dip versus the taper-microsphere coupler distance (polynomial fit) for a low radial mode ($n = 1$) and fundamental WGM ($m = l$).

A clear minimum of intensity versus coupling position is apparent in this figure; we can consider that this distance corresponds to the critical point. The role of taper diameter is considered to result from phase matching mode selection. This result gives the ability to detect the critical point in a taper-sphere coupler.

In order to investigate the dependence of resonance on microsphere diameter changes, we have obtained transmission resonant dips for two different microsphere sizes with excitation frequencies ranging from 192 to 194 THz. Resonance property data such as resonance frequencies and their corresponding wavelengths, and quality factor are presented in table III.4.

Sphere diameter (µm)	Resonance frequency (f_{res}) (THz)	Excitation wavelength λ_{res} (nm)	Quality factor Q
25	192.564	1557.923	3156.78
	193.501	1550.379	3171.78
	194.437	1542.916	2700.51
30	193.353	1551.566	4394.38
	194.305	1543.964	4416.02
	195.261	1536.405	4339.13

Table III.4: Resonance data from figure III.29 for two microspheres with $D = 25\,\mu m$ and $D = 30\,\mu m$. The coupling gap is fixed at 0.4 µm, and the taper waist is 1 µm for both cases.

From figure III.33, it can be seen that three entire resonance frequencies appeared within the considered frequency range. The quality factors of these resonance modes vary between 2700 and 4416. The resonance frequency intervals for two spheres slightly vary between 0.94 and 0.96 THz. The increase of microsphere size increases the resonance frequency. The increase of microsphere size results in the increase of the effective traveling distance of light in the microsphere. Accordingly, light requires a longer wavelength to match the resonance condition under the same resonance mode. Therefore, the resonance frequency will decrease.

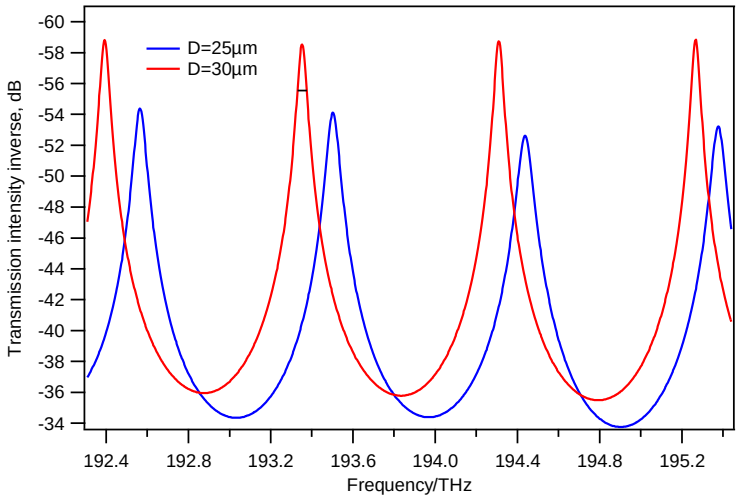

Figure III.33: Simulated transmission of taper-resonator coupler calculated by CST software. Microspheres diameters are 25 µm (blue curve) and 30 µm (red curve). The waist of the taper is 1 µm and the coupling gap is 0.4 µm. It shows WGM fundamentals with $n=1$, $l=73$, and $n=1$, $l=88$ respectively for 25 µm and 30 µm sphere diameters.

III.6 Conclusion

In this chapter, the fabrication and modal characteristics of silica microspheres were presented. For light coupling into microsphere, the tapered fibers with waist ranging from 1 µm to 4 µm were fabricated. The optical characteristics of microspheres were measured in order to understand their optical behavior. The quality factor of optical microsphere can reach up to 10^6 for a sphere size ranging from 90 µm to 150 µm at 1560 nm operating wavelength. The experimental quality factor *Q* and the free spectral range, for microsphere resonators are characterized after their fabrication process which takes several hours. Causes of quality factor decrease are water and dust absorption on the surface of microsphere. Based on the experimental resonance dips spectra of microsphere with various diameters; the dependence of free spectral range on the diameter of sphere has been investigated. To characterize the resonance by measuring light scattered from microsphere surface, a technique using a tip fiber to collect light is presented. The scattered light going out of the sphere is collected by a micron tip fiber (tip diameter of approximately 1 µm) which is placed close to sphere surface at its equator. The scattering spectra of microsphere are investigated. According to it, the polarization dependence of the

quality factor and FSR values are analyzed. From the dependence of FSR on sphere diameter, we have shown that a high FSR value can be achieved when the microsphere size increases. For a sphere with a diameter of 300 µm, FSR is 25 GHz. However, this FSR value of sphere is still far from the frequency needed for use in the OEO system developed in the laboratory (the oscillation frequency is 8 GHz). Another optical micro-resonator has been designed and fabricated in order to obtain a FSR corresponding to the desired oscillation frequency; it is based on waveguides, and has the shape of a micro racetrack. Its optical properties will be presented in the next chapter. In the last section of this chapter, we have presented some simulation results concerning the taper-silica microsphere coupler by using CST Microwave Studio software. The phase matching in coupling taper-sphere gives WGM resonance dips for low radial mode numbers. Based on the change of taper-microsphere coupling distance (coupling gap), the critical coupling condition between taper –sphere can be determined.

Chapter IV.

Add-Drop Ring Resonator

IV.1 Introduction

Optical microring resonators are used in many optical components such as sensors, optical switches, optical fibers, and wavelength division multiplexers [82, 85]. The shape of a microring resonator consists in general in an ordinary waveguide that channels light in a closed loop. The loop can take various shapes as disks, racetracks and ellipses. The first optical ring resonator waveguide was created by Weber and Ulrich in 1971 [86, 87]. This device consisted in a 5 mm diameter glass channel (N_g = 1.47) coated with Rhodamine-6G- doped polyurethane (N_{Rh}=1.55). Although this device demonstrated low-loss properties, the resonator circumference and the diameter of the guide were quite large. This resulted in a large background of non resonant light and in the convolution of resonances from multiple modes. In 2002 S. L. Rome et al from the University of Illinois developed a ring resonator with smaller circumference ($L = 247.2\mu m$) and a free spectral range slightly over 2 nm [88]. For filtering applications, both passively and electro-optically tuned, Ho's group recently reported a micro-ring resonator with a small radius of $20.1\mu m$ with a FSR greater than 30 nm [89]. In our work, for relevant applications in Opto-Electronic-Oscillator, we investigated racetrack add-drop resonators as potential small volume desire that could be used to replace a fiber loop in our OEO system in the same frequency regime.

IV.2 General properties

IV.2.1 Operation principle

Figure IV.1 shows a schematic diagram of a micro racetrack resonator. In this structure the laser light goes into input port and is coupled into the ring in the coupling

region. The optical wave in the ring is out coupled into the same straight waveguide and is sent in the through port.

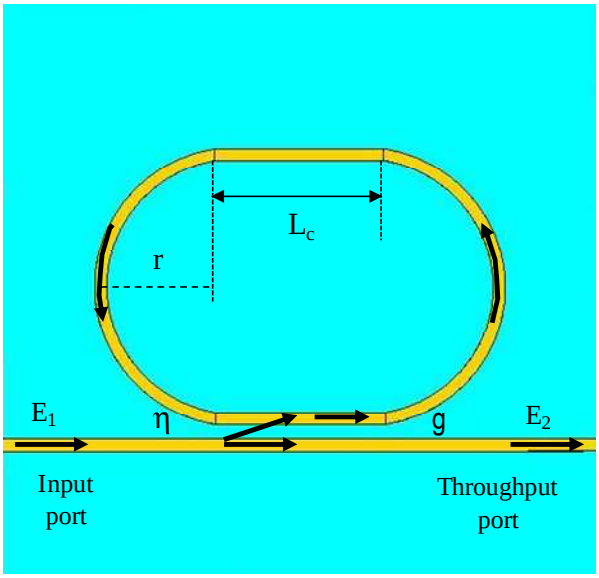

Figure IV.1: Schematic diagram of a single micro-racetrack add-drop resonator coupled waveguide. The gap between the racetrack and the waveguide is g, L_c is the coupling length and η is the coupling coefficient.

We consider E_1 as the input continuous wave (CW) probe beam, η_a being the between the racetrack and waveguide, t is the transmission coefficient and τ is the attenuation. The light extracted at the throughput waveguide is analyzed as the transfer function of the device given as [90]:

$$|T_{21}|^2 = \left|\frac{E_2}{E_1}\right|^2 = \frac{t^2 - 2t\tau\cos\phi + \tau^2}{1 - 2t\tau\cos\phi + (t\tau)^2} \tag{4.1}$$

where $\phi = 2\pi\left(N_{eff}\,L/\lambda\right)$ is the phase shift per round trip around the resonator,

N_{eff} is the effective refractive index of the waveguide,

$L = 2(\pi r + L_c)$ is the circumference of the ring resonator,

and λ is the input wavelength.

On another hand, the round-trip phase shift can be labeled as:

$$\phi = \beta L \tag{4.2}$$

where $\beta = \frac{2\pi N_{eff}}{\lambda}$.

For the add-drop micro-racetrack, an asymmetrical coupling of the single waveguide to the micro-ring is used (figure IV.2). This structure leads to a crosstalk reduction between the drop and add signals at the output of the guide.

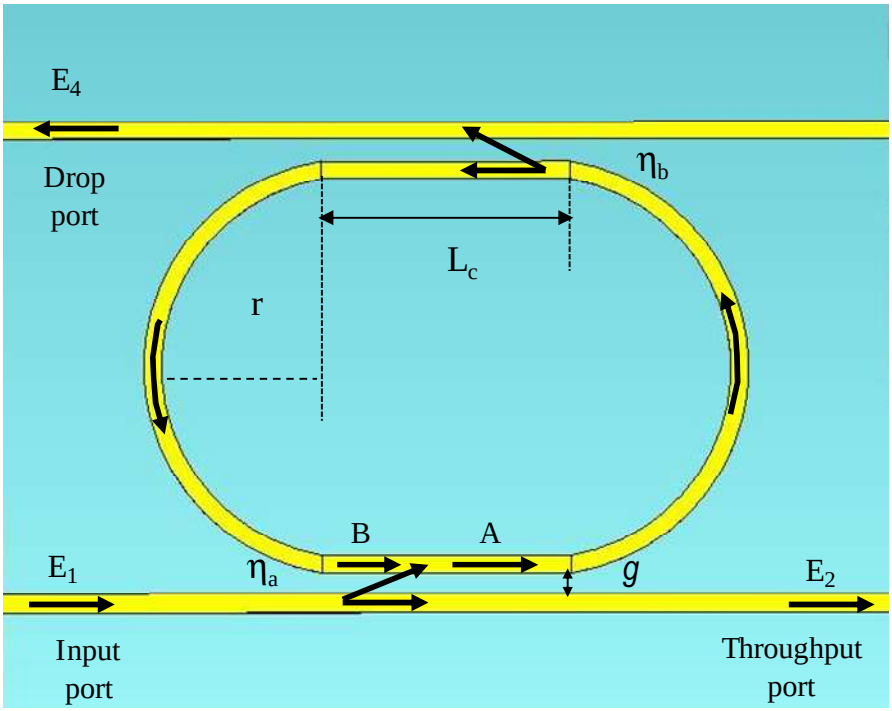

Figure IV.2: Schematic diagram of a single micro-racetrack add-drop resonator coupled waveguide.

In the case of an asymmetrically coupler resonator, the amplitude and phase of the field inside and at the output port of resonator can be expressed [91] as:

$$A = t_a B + j\eta_a E_1 \tag{4.3}$$

$$B = t_b A \tau \exp(j\phi) \tag{4.4}$$

$$E_2 = t_a E_1 + j\eta_a B \tag{4.5}$$

$$E_4 = j\eta_b A\sqrt{\tau}\exp\left(\frac{j\phi}{2}\right) \tag{4.6}$$

A is the optical power injected by coupling in the micro-ring, *B* is the optical power coming back after one round trip in the micro-ring. η_a and η_b are the coupling coefficients between the racetrack and the two asymmetric rib waveguides, t_a and t_b are the transmission coefficients given by $t_{a,b} = \sqrt{1-\eta_{a,b}^2}$. The equations from (4.3) to (4.6) give the transfer function between input port and throughput ports (through attenuation), and the intensity at the output of the waveguide is proportional to:

$$|T_{21}|^2 = \left|\frac{E_2}{E_1}\right|^2 = \frac{t_a^2 + t_b^2\tau^2 - 2t_a t_b \tau\cos\phi}{1 + t_a^2 k_b^2 \tau^2 - 2t_a t_b \tau\cos\phi} \tag{4.7}$$

$$|T_{41}|^2 = \left|\frac{E_4}{E_1}\right|^2 = \frac{\eta_a^2\eta_b^2\tau}{1 + t_a^2 t_b^2 \tau^2 - 2t_a t_b \tau\cos\phi} \tag{4.8}$$

In a racetrack structure (fig.IV.1), a resonance occurs if

$$m\lambda_m = N_{eff} L \tag{4.9}$$

where λ_m is the resonance wavelength and m is the mode number.

Consider multiple wavelengths (λ_1, λ_2, … λ_i, λ_n) going into the input port and coupled into the ring. The optical wave in the ring will be partially coupled into the straight waveguide, the output signal at the drop port will show resonance wavelengths satisfying the resonant condition (4.9). So we can say that the coupling of the wave at resonant wavelengths λ_i will be enhanced and all others will be suppressed. As a result only λ_i will be removed from the drop port, while the other wavelengths are transmitted to the output port.

The point corresponding to $|T_{21}|^2 = 0$ is called the critical coupling (or situation of zero crosstalk). The light stays in the micro-ring, $|T_{41}|^2$ should be maximum at this point, but the signal transfer (output signal at drop port) is not complete and $|T_{41}|^2 < 1$.

IV.2.2 Free spectral range

The spectral separation of successive resonances is determined by the free spectral range (FSR). At resonance, $\omega t = m.2\pi$ where *t* is round trip time and *m* is an integer. The FSR of two successive resonances $\nu_2 - \nu_1$ is expressed in [92] as:

$$FSR = \nu_2 - \nu_1 = \frac{2\pi}{\tau} = \frac{2\pi c_0}{LN_{eff}} \tag{4.10}$$

Translating to wavelength, it is defined as:

$$FSR = \frac{\lambda_i^2}{N_{eff} L} = \frac{\lambda_i^2}{N_{eff}(2\pi r + 2L_c)} \tag{4.11}$$

here r is the ring radius and L_c is the coupling length.

Because the FSR is inversely proportional to the size of the ring resonator, the ring must be small in order to achieve a high FSR.

IV.2.3 Finesse

The finesse $\mathcal{F}$ is a convenient measure of the sharpness of resonance relative to FSR. It is defined as the ratio of the FSR and the resonance width. According to [93], $\mathcal{F}$ can be determined by:

$$\mathcal{F} = \frac{FSR}{\Delta\lambda_{FWHM}} = \frac{\pi}{2\sin^{-1}\left(\frac{1-R}{2\sqrt{R}}\right)} \tag{4.12}$$

here R is the reflection coefficient given by $R = e^{-\alpha}(1-K)$, α is the total amplitude attenuation coefficient for each round trip and K is the normalized coupling coefficient.

Equation (4.12) shows that $\mathcal{F}$ depends on the internal and coupling losses (external losses) of the resonator. Therefore, the higher total losses the lower resonator's finesse.

It is always an advantage to reduce both external and internal losses in order to obtain a higher finesse. However, for the resonator can operate as an optical filter, some external losses due to the coupling are necessary and cannot be too small. If it is smaller than the internal loss then no power can be coupled out. Another source of external losses is the curvature of the resonator waveguide, which increases the amplitude of the evanescent wave and reduces the confinement. Therefore the resonator should not be small in order to minimize curvature losses. Because of this constraints, the typically ring resonator uses a strongly guiding waveguide to minimize the bending loss for a curved waveguide with a small radius.

IV.2.4 Q factor

For the proper design and optimization of a high quality resonator, several parameters have to be considered. Besides the FSR, finesse, sharp resonance values, and low loss a high *Q* factor must be maximized. *Q* factor of micro-ring resonator coupled to a single waveguide is given by [91]:

$$Q = \frac{2\pi N_{eff}}{\lambda} \frac{L}{2\arccos\left(\frac{1+t_a^2 t_b^2 \tau^2 - 4t_a t_b \tau}{-2t_a t_b \tau}\right)} = \frac{\lambda}{\Delta\lambda_{3dB}} \tag{4.13}$$

$\Delta\lambda_{3dB}$ is the line width of resonance peak at 3dB, λ is the resonance wavelength, N_{eff} is the effective refractive index of the mode propagating in the microring, L is the length of the ring, t_a, t_b are the field transmission coefficients at the waveguide-resonator coupling, and $\tau = \exp\left(-\frac{\alpha L}{2}\right)$ is defined as the attenuation of the field per round trip with an attenuation constant α [91]. From equation 4.13, it is clear that the Q factor of a cavity device depends on the propagation losses in the ring and on the chosen geometry, which is determined by parameters such as: k, L and N_{eff}. For $t_a t_b \tau$ close to 1, equation 4.13 can be expressed by:

$$Q = \frac{2\pi N_{eff}}{\lambda} \frac{L}{-2\ln t_a t_b \tau} \tag{4.14}$$

Eq.(4.13) depends on propagation and coupling losses $t_a t_b \tau$, so the maximum Q factor can be achieved if the propagation loss $\alpha = -2\left(\ln \tau / L\right)$ inside cavity is controlled. If neglecting the coupling loss to external waveguides, the Q factor can be determined from equation (4.14) as:

$$Q_{\lim} = \frac{2\pi N_{eff}}{\lambda} \frac{1}{\alpha} \tag{4.15}$$

In case of a SOI based waveguide technology, low propagation losses can be achieved with ultra-smooth waveguide surfaces and this condition requires specific optimized process steps. The condition for critical coupling is achieved when $t_a t_b \tau = 1$ in eq.(4.13) [91], at this point $|T_{21}|^2 = 0$. At the critical coupling condition, the throughput attenuation at resonance is compensated by an increased coupling into the micro-ring.

IV.3 Add-Drop micro racetrack resonator

The add/drop racetrack resonators which are used in our work were fabricated at "Institut d'Electronique Fondamentale" (IEF, CNRS, Paris 11 University) [94-97]. Based on the SOI substrates provided by SOITEC [94], a rib waveguide is 1000 nm wide and 260 nm high with a 30 nm thick slab layer was fabricated. The racetrack radium have been realized with a bend radius of the racetrack semi-circle required to 1600 µm, the straight section of the racetrack, L_c, is 1400 µm and the spacing gap (gap distance between the coupling straight waveguides and the racetrack waveguide) is 2.25 µm (figure IV.3). The fabrication process can be briefly described as follow. The device was fabricated on the silicon-on-insulator (SOI) wafer using a standard silicon nanofabrication process line. Rib waveguides were fabricated by using 193 nm deep-UV lithography and reactive-ion etching (RIE) process. A self-aligned 248 nm deep UV lithography step followed by a RIE is then realized to define the etched structure. The main advantages of the SOI substrate technique are strong light confinement in rib waveguides, a large difference between

refractive indices of silicon and silicon oxide ($\Delta N = N_{sub} - N_{rib} \approx 2$). That method allows a significant miniaturization of an optical device.

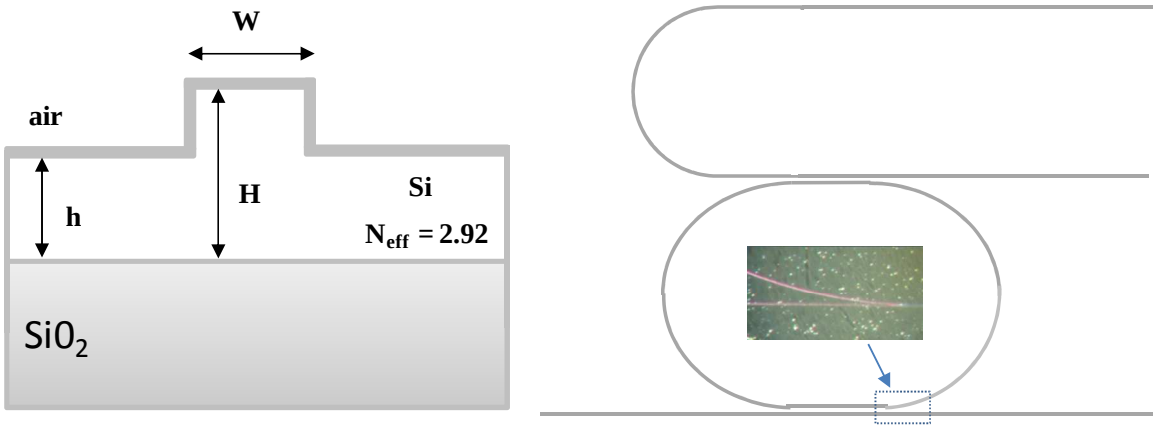

Figure IV.3: (a) Cross section schematic view of a rib waveguide. The dimensions used in fabrication are H=260 nm, W=1000 nm and h=230 nm; (b) schematic view of racetrack resonator structure and photograph of its coupling region (inset zoom).

The rib width is fixed to 1 µm, this allows a strong light confinement in spite of the small etched depth (in this case it is 30nm). This rib width is chosen to provide a condition that the light to be injected into the waveguide in mono mode and TE mode polarization [95]. The overall length L of the racetrack stadium is given by $L = 2(\pi r + L_c)$. With the $\Delta\nu_{FSR}$ value and the refractive index of waveguide are defined, the length L of stadium can be calculated by:

$$L = 2(\pi r + L_c) = \frac{c}{N_{eff}\Delta\nu_{FSR}} \tag{4.16}$$

The coupling between the waveguide and the ring is an important factor which determines the quality factor of rings. In most of laterally coupled micro-ring resonators, the gap distance between the bus waveguide and the ring must not exceed a magnitude of 1 micron to ensure sufficient coupling. For the micro racetrack which is investigated in this work, the dependence of the quality factor Q of the resonator with respect to the gap size between bus waveguide and rings is presented in [97] in details. For optical losses around

0.1 cm^{-1} and a gap value of approximately 2.4 µm, the quality factor is $Q \approx 10^6$. In practice, as the air-gap width decreases, the interaction between the access waveguide and ring increases, leading to the reduction of the self-coupling coefficient.

IV.4 Optical characterization of an add-drop racetrack resonator

IV.4.1 Introduction

To evaluate the propagation characteristics and the optical properties of micro rings (SOI-waveguide devices), it is important to use adequate coupling techniques to excite the waveguide mode. For light coupling into and out of ring resonator structure, several coupling techniques are employed such as prism couplers [98], grating couplers [88, 89] and edge coupling or end-butt coupler [101, 102]. In the prism coupling technique, the laser beam can be coupled into a waveguide using a high-index prism. The prism is pressed onto the surface of the waveguide at a very small air gap (the order of a half wavelength) as shown in figure IV.4.

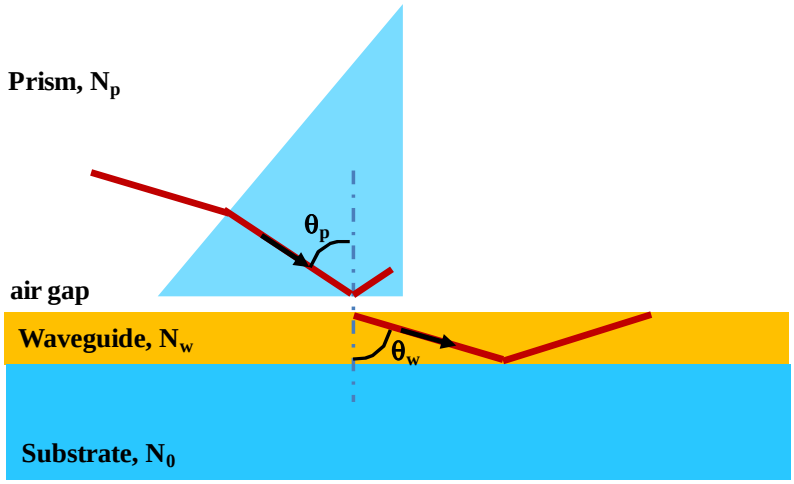

Figure IV.4: Schematic of laser beam coupled into a waveguide by prism technique.

A laser beam is then coupled into the prism so that total reflection occurs inside the prism, at the prism - air interface close to the waveguide. In the vicinity of the waveguide the overlapping incident and reflected beams generate a standing wave. The evanescent

field of the standing wave penetrates into the waveguide. Under a certain angle and if the phase matching conditions are fulfilled, the evanescent field stimulates a mode that is guided by the waveguide.

In the grating coupler system, the optical component (SOI-waveguide) is coupled with two adiabatic tapers to couple light into and out of SOI. At the end of the two tapers, the grating is etched into the top silicon layer. A single mode fiber is coupled at both grating ends for light in and out coupling. These fibers are tilted (angle about 10 degrees) to avoid unwanted back reflections.

Other coupling techniques such as edge coupling or parallel end-butt coupler are also used. In butt coupling method, the front face of a laser diode is placed close to the polished waveguide edge. The laser diode is mounted on a 3D translating stage and a 2D rotation set-up. Using these positional tools the emitting region of the laser diode is adjusted to the waveguide layer, the distance between laser and waveguide being kept at a minimum [102].

In order to investigate optical properties of the studied add-drop racetrack resonator, we used parallel end-butt coupling techniques. But instead of coupling directly the laser beam into the waveguide layer, we used micro-lenses which are fabricated on the top of a single mode optical fiber. The micro-lenses fabrication method and coupling results will be presented in detail in the following sections.

IV.4.2 Tapered micro-lens

IV.4.2.1 Fabrication

Micro-lenses located at the end of single mode fibers have been fabricated using several methods such as attachment of pre-existing lenses at the end of a fiber, photolithography, etching techniques, by melting a drop silica rod to the fiber end or by laser shaping the fiber end [103-107]. In this work, the micro lenses have been fabricated by melting the fiber while pulling it to form a molten taper micro-lens at the end of the single mode fiber via the electric-arc technique. The fabrication process of a micro-lens can be described as follows. In the first step, the coating at the end of single mode fiber is

cleaved and cleaned. Then this cleaned fiber is placed between two electrodes of an electric arc source. The fiber melts at high temperature (up to 1600°C) between these electrodes, and is pulled to form a tapered micro-lens. This technique provides a mean to control the lens radius over a wide range.

IV.4.2.2 Result and discussion

A fiber micro-lens fabricated via electric arc technique together with a schematic sketch of the fabrication of a fiber lens are shown in figure IV.5

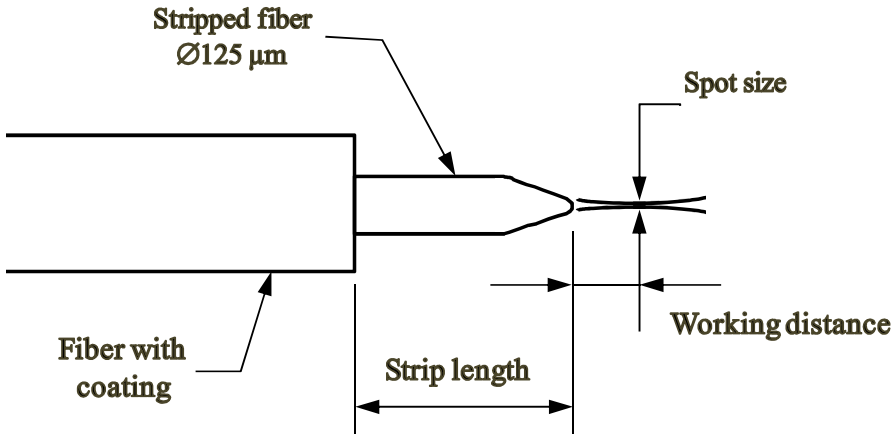

(a)

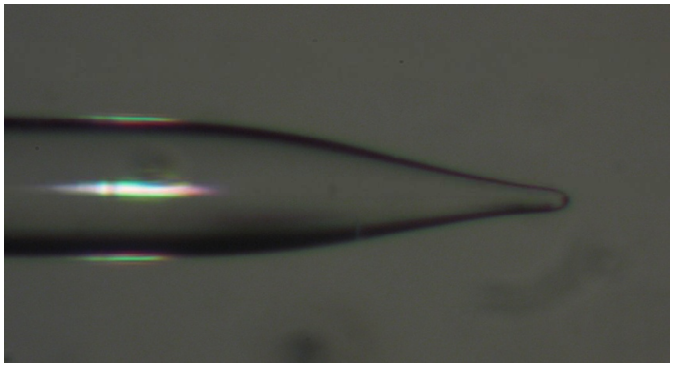

(b)

Figure IV.5: (a) schematic representation of the elaboration method of a fiber micro-lens and (b) a photograph of a fabricated fiber micro-lens.

The characteristics of a fiber taper depend greatly upon its capability to couple out Gaussian beams. For waveguide coupling applications, the focused spot characteristics must match the waveguide characteristics as closely as possible to ensure good coupling. A Gaussian approximation is typically used to predict the focusing effect of a fiber micro-

lens. A laser Gaussian beam goes through the fiber of refractive index *N*, and is focused by a micro-lens with radius *r* to a spot size in air (spot radium W_L) is expressed [108] as:

$$W_f^2 = \frac{W_L^2}{1+\left[\frac{\pi W (N-1)_L^2}{f\lambda}\right]} \tag{4.17}$$

where $f = \frac{r}{(N-1)}$ is the focal length of the tapered micro-lens, λ is the free space wavelength and the parameter W_L is the Gaussian Beam Radius at the lens (also called waist spot size).

For a step index optical fiber, the spot diameter defined as the radial distance at which the field amplitude is $1/e^2$ of its maximum [109] is given by:

$$W_L = a\left(0.65 + \frac{1.619}{v^{3/2}} + \frac{2.879}{v^6}\right) \tag{4.18}$$

Here a is the fiber core radius and the term *V* is determined as:

$$V = \frac{2\pi a}{\lambda}\left(N_{core}^2 - N_{clad}^2\right)^{1/2} \tag{4.19}$$

where N_{core}^2, N_{clad}^2 are , respectively the core and cladding refractive indices. For a step-index fiber with $a = 5\ \mu m$, $N_{core} = 1.457$ and $N_{clad} = 1.453$ we find from equation (4.18) the value of $V = 2.25$ and $W_L = 5.75$ at 1.5 µm wavelength operation.

A good quality micro-lens can transform the fiber mode into another Gaussian beam that propagates in the free space. The surface quality and the asymmetry of the lens cannot be accurately determined by optical microscopy. In practice, the quality of fiber micro-lenses can be identified by a fiber far-field profile measurement. In the present work, both fiber micro-lenses which are used to couple light into and out of the racetrack are tested via a far-field scanning technique to define their qualities. Their far-field intensity distributions are presented in figure IV.6.

The straight and axially symmetry of these fiber micro-lenses show that they may been a well Gaussian profile of the propagation wave. This indicates that the mode transmitted and coupled by the laser is symmetric similar in shape to fundamental fiber mode.

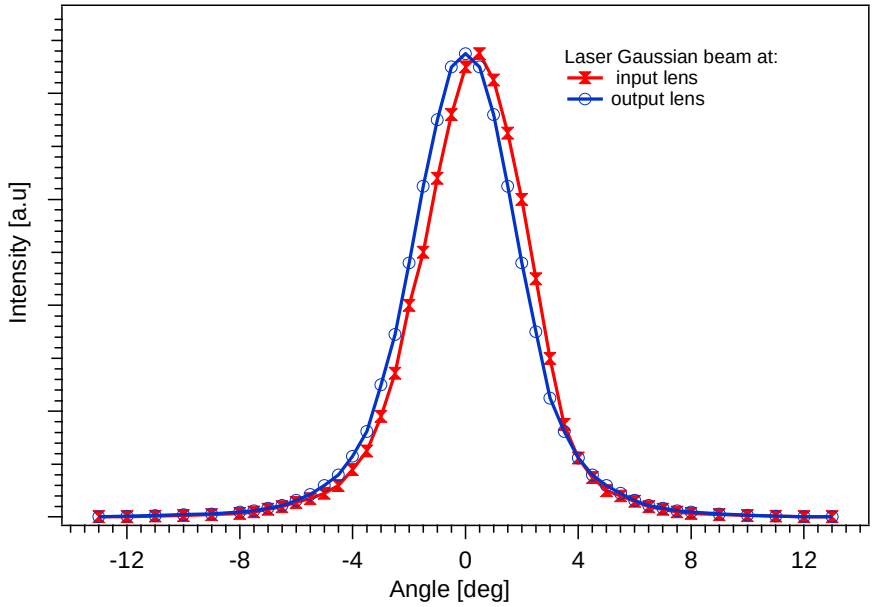

Figure IV.6: Far-field intensity distribution of two micro-lenses. An input lens is used to couple laser beam into the input port, and an output lens is used to collect light from the output port of a micro racetrack resonator. r_{in} (radius of input lens) and r_{out} (radius of output lens) are approximately 4 µm.

IV.5 Light in and out coupling from a racetrack by fiber micro-lenses

IV.5.1 Experimental setup

In this setup, we use the same laser source that was used to characterize the optical properties of micro-resonator. Its specifications are listed in table 3.1 (section III.3.2.1). Two polarization controllers are used in this experimental set up. One is placed at the output of the laser source to matching the polarization of the laser light with the polarization of the resonator mode. The other one is placed at the end of the output fiber to control the polarization light before it goes to the detector. Because the output power at the

drop port of resonator is a weak (it is reduced by both external and internal coupling loss), the output signal is collected by a power sensor (Agilent 81636B Power sensor module), which can detect the power intensity down to -80 dBm. Its specifications are presented in the following table (Table IV.1).

Photodiode material	InGaAs
Wavelength range	1250nm-1640nm
Power receive range	+10 dBm to -80 dBm
Application fiber type	SMF and MMF, core size maximum 62.5µm, NA ≤ 0.24
Noise (peak to peak)	< 20 pW

Table IV.1: Specification of power sensor module Agilent 81636B

To control accurately the coupling zone between the racetrack and the micro-lens, the SOI waveguide micro-ring device is fixed on steady stages, then the pigtail fiber bearing the fiber micro-lens is coupled to the laser source via a polarization controller, and it is mounted on 3D translation stages (Newport Ultra-Align metric). The micro-lens at the end of this pigtail fiber is adjusted to focus in the coupling zone of the racetrack. At the output ports of the resonator (both through and drop ports), another pigtail fiber with a micro-lens is fixed on another translation stage system to collect the output light. The coupling setup uses tapered fiber micro-lenses which have diameter less than 10 µm. The coupling distance between the fiber micro-lenses and the waveguide can be controlled by a fine tuning of the translation stage systems. This coupling method opens the possibilities to package a micro-ring device (micro-ring resonator module) via adequate coupling to optical fiber at both input and output. This module gives the convenience for connecting the micro-ring resonator to other optical component in the developed systems.

The setup for injecting light into the add-drop micro-racetrack resonator is schown in Figure IV.7a. A tunable laser diode, used as pump source is coupled into rib waveguide via a fiber micro-lens. The light travels in rib and is coupled into stadium at coupling zone and goes to through and drop port. The generated modes are coupled out to fiber optical via other fiber micro-lens and they are collected by power sensor. A photograph of the

coupling zone between micro-lenses and rib waveguide (input port of racetrack) is shown in Figure IV.7b. The light at output ports is collected by fiber micro-lens that has approximately the same quality as the fiber lens for input coupling.

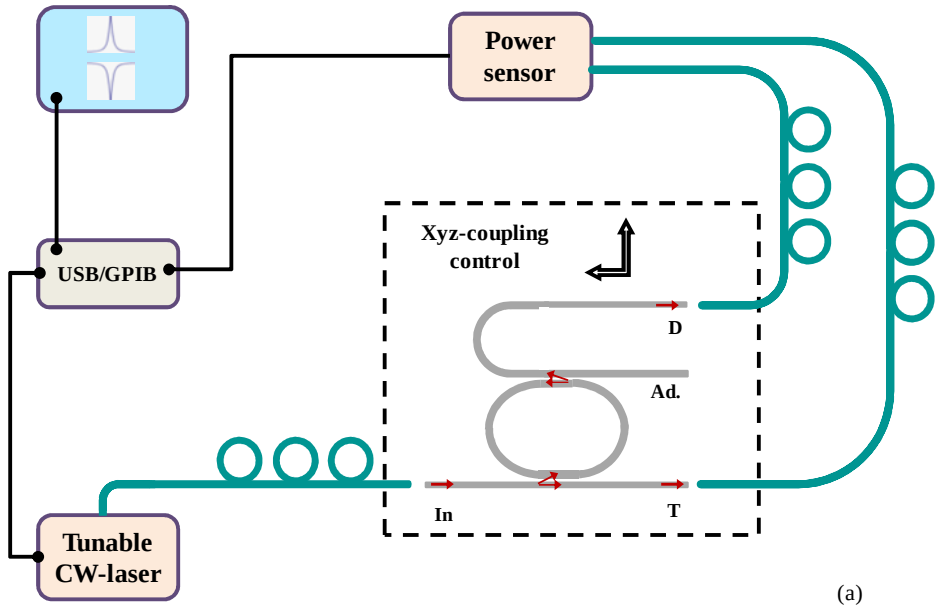

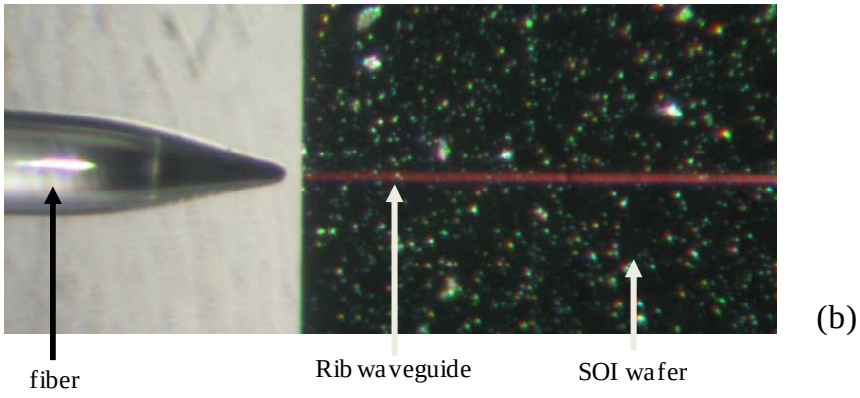

Figure IV.7: (a) Schematic of experimental set-up for measuring the optical injection in add-drop micro racetrack resonator. (b) Photograph of the coupling zone between fiber micro-lens and rib waveguide.

IV.5.2 Experimental wavelength spectra of add-drop racetrack resonator

IV.5.2.1 Wavelength spectra at through port

This racetrack resonator has zone coupling length $L_C = 1400\,\mu m$, $r = 1600\,\mu m$ and gap coupling is $g = 2.25\,\mu m$. The SOI wafer consist of 260 nm thick silicon layer that is etched down to 30 nm ($P = 30\,nm$) with the rib width of 1000nm. When a laser beam couples into the optical fiber and focuses into rib waveguide via fiber micro-lens, it propagates in ring geometry and converges into the output lens at through put. While the laser diode is tuned for a wavelength ranging from 1586 nm to 1587 nm, the resonance dips appear in output wavelength spectra as shown in figure IV.8.

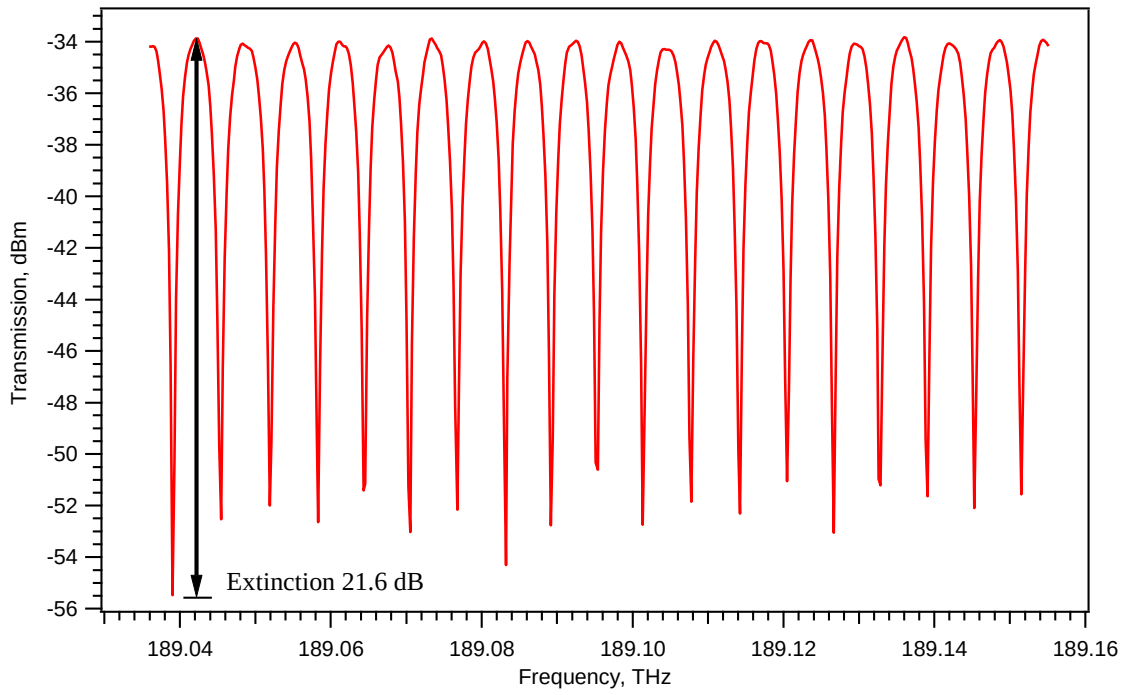

Figure IV.8. Transmission spectrum of add-drop racetrack with $r = 1600\,\mu m$, $L_C = 1400\,\mu m$ and $g = 2.25\,\mu m$ for a wavelength ranging from 1586 nm to 1587 nm. The radius of fiber micro-lens for light in and out coupling is approximately 4 µm.

The transmission spectrum of the fabricated device have been measured based on the experimental set-up as described in section IV.5.1. Two micro lens fibers fabricated at the

end of two pigtail SM fibers are used to couple light from the laser into and out of device. The best distance of gap coupling is obtained via a 3D alignment system with a spatial resolution smaller than 1 µm. Figure IV.8 shows a measured transmission spectrum in case of TE polarization. The racetrack resonator has a free spectral range (FSR) of 6GHz (0.05 nm) and a maximum extinction ratio of 21.6 dB in near 1586.6 nm. In this work, the laser power is 4 mW (corresponding to 6.02 dBm). So the losses determined from this transmission spectrum are about 40dB. These losses include the external losses (losses by coupling between fiber micro lenses and rib waveguide, by coupling loss between rib waveguide and ring), and the intrinsic losses (material loss). A high extinction ratio indicates that the resonator works near the critical coupling regime. Assuming that the micro racetrack resonator with a gap $g = 2.25\,\mu m$ has a FSR of 6 GHz at steady state, with an effective refractive index $N_{eff} = 2.92$, then from equation (4.16), the stadium length L of racetrack is calculated $L = 17123.28\,\mu m$.

Quality factor *Q* and Free spectral range (FSR)

The quality factor is given by the ratio of the frequency at a spectral line to the width at half-maximum or -3 dB. From Figure IV.8 a zoom can be made at some points of the abscise, as shown in Figure IV.9.

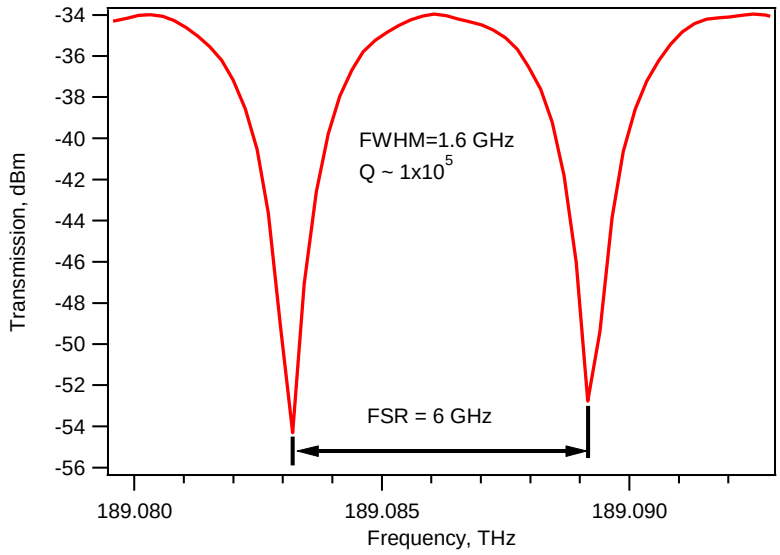

Figure IV.9: Transmission spectrum of the two resonance modes at 189.086 THz and 189.038 THz.

From this figure, the line width of the resonance mode at 189.083 THz is $\Delta\nu_{FWHM} = 1.6\,\text{GHz}$ corresponding to a quality factor $Q = \frac{\nu_{res}}{\Delta\nu_{-3dBm}} \approx 1\times10^5$. The free spectral range value (FSR) in frequency is determined from this transmission spectrum. Its FSR is 50 pm in term of wavelength or 6 GHz in term of frequency.

In order to investigate the micro-racetrack resonator that can be used in our OEO system, two racetracks with the same geometrical parameters except for the gap width have been characterized. Their parameters such as *Q* factor, *FSR* are determined and presented in table IV.2.

g (μm)	λ_{res} (nm)	$\Delta\lambda_{FHWM}$ (nm)	Q factor	$\Delta\lambda$ (nm)	$\Delta\nu$ (GHz)
2.2	1544.583	0.025	61783	0.051	5.9
	1554.378	0.025	62178	0.048	6.25
2.25	1544.378	0.013	$\simeq 1$ x 10^5	0.05	6
	1554.448	0.014	$\simeq 1$ x 10^5	0.05	6

Table IV.2. Comparison of two micro racetrack resonators with $r = 1600\,\mu\text{m}$, $L_c = 1400\,\mu\text{m}$ and $\Delta g = 0.05\,\mu\text{m}$.

We note that the small difference of air gap width ($\Delta g = 0.05\,\mu\text{m}$) has no influence on the free spectral range of both racetracks but the resonator with the smaller gap presents a smaller value of the Q factor. The optical characteristics of these racetracks resonators are presented in Table IV.3.

Characterizing the optical properties of these racetracks for a wide range of operating wavelengths, from 1540 nm to 1610 nm, we found that the racetrack with an air-gap of 2.25 μm has a higher Q factor, its FSR value is more stable and its internal losses are lower.

λ_{res} (nm)	*FSR* (nm)	$\Delta\lambda_{FHWM}$ (nm)	Q factor	Extinction ratio (dBm)
1534.162	0.049	0.01	1.5 x 10^5	8.8
1544.378	0.05	0.013	1.2 x 10^5	8.1
1554.448	0.05	0.014	1.1 x 10^5	7.5
1558.102	0.05	0.01	1.5 x 10^5	8.8
1564.304	0.052	0.011	1.4 x 10^5	8.6
1580.162	0.052	0.013	1.2 x 10^5	7.3
1586.603	0.05	0.002	7.9 x 10^5	20.1
1594.479	0.049	0.005	3.1 x 10^5	14.3
1606.384	0.052	0.007	2.2 x 10^5	10.5
1610.252	0.054	0.006	2.6 x 10^5	9.8

Table IV.3 Performances of the micro racetrack resonator with $r = 1600\ \mu m$, $L_c = 1400\ \mu m$ and $g = 2.25\ \mu m$.

From the FSR values of this table, the free spectral range of the add-drop racetrack resonator is plotted as a function of the wavelength in figure IV.10. When the laser is tuned from 1534 nm to 1610 nm (a span of 76 nm), the FSR of this resonator is approximately constant at 0.050 nm ±0.004 nm (corresponding to 6 GHz in frequency). This is an interesting point for an integrated stadium resonator. This micro racetrack resonator with high Q factor and FSR at high frequency gives a promising device that can be used for integration into the OEO system.

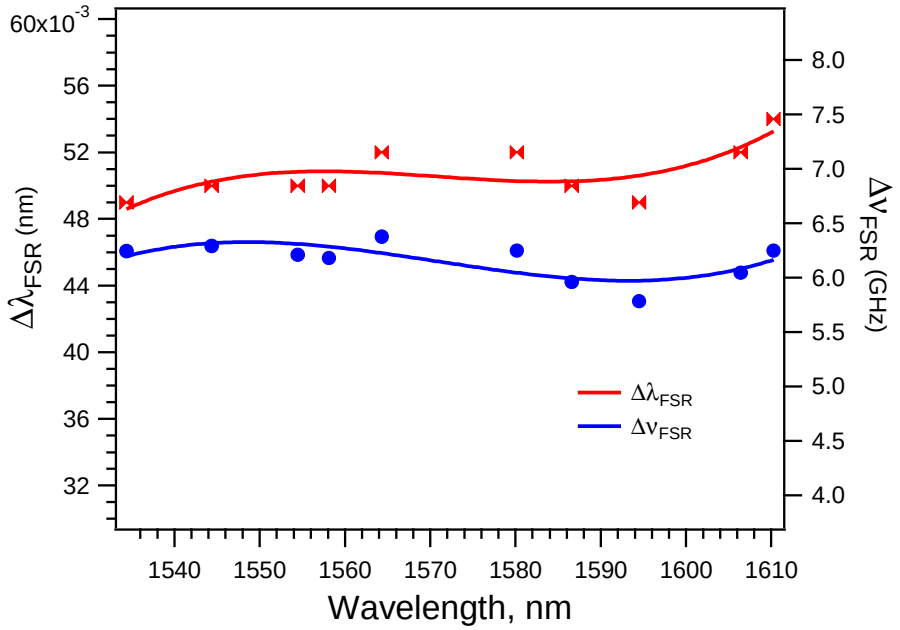

Figure IV.10. Dependence of FSR on the wavelengths of add-drop racetrack resonator with $r = 1600\,\mu m$, $L_c = 1400\,\mu m$ and $g = 2.25\,\mu m$. FSR = (50 ± 4) pm for a 70 nm wavelength range.

IV.5.2.2 Wavelength spectral at drop port

For characterizing the output signal at the drop port of this resonator, another micro lens fiber is used to couple the out-coming light. This lens is fabricated at the end of a pigtailed single mode fiber with a radius of 4 µm. The gap coupling is controlled via a 3D alignment system. When the light travels in the coupling region between the stadium and the rib waveguide 2, a part of light is coupled into this rib waveguide and goes out at the drop port. The light at this port is focused into the optical fiber via fiber micro-lens and then is collected by the power sensor. The resonance response at the drop port of the resonator around 1586 nm is measured and presented in figure IV.11. The transmission spectrum at the drop port has a line width $\Delta\lambda_{FWHM} = 0.018\,nm$, corresponding to a quality factor $Q = \frac{\lambda_{res}}{\Delta\lambda_{FWHM}} = 88127$. The free spectral range (FSR) is 0.05 ± 0.003 nm for a wavelength ranging from 1586 nm to 1587 nm or in frequency ranging from 189.03 to 189.16 THz.

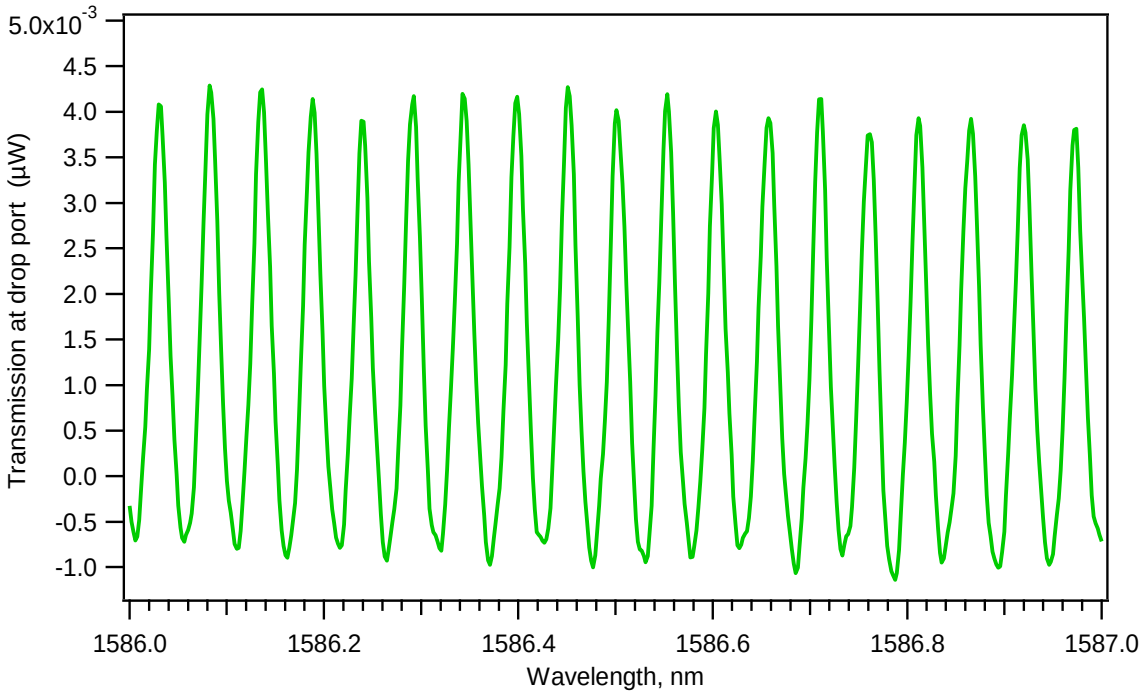

Figure IV.11: Transmission spectrum at the drop port of the micro-racetrack resonator. The radius of micro-lens for out light coupling is 4µm.

IV.5.3 Add-drop racetrack resonator for OEO system

The OEO system in figure I.1 uses RF filter for filtering the RF signal and up-converting it to optical frequencies by an electro-optic modulator. The RF signal is carried on the optical signal by a long optical fiber which acts as a delay line. This signal is reconverted into the electrical domain by a detector and fed back at input signal after pass the RF filter. Therefore, only one frequency should be selected by RF filter as the oscillation frequency. The quality factor of the delay line is expressed as: $Q = 2\pi f_{osc}\tau_d$, where f_{osc} is the RF oscillation frequency and τ_d is delay time of signal introduced by delay line, it can be defined as: $\tau_d = \frac{LN_{fib}}{c_0}$ where L is the length of the fiber and N_{fib} is the refractive index of the optical fiber line and c_0 is the velocity of light. For the delay line of 2 km corresponding to a delay $\tau_d = 9.66\,\mu s$, $f_{osc} = 8\,GHz$, then a Q factor of 4.8×10^5 is calculated.

For miniaturizing the OEO, investigations have been focused on the replacement of the long fiber delay by an optical resonator, either a whispering gallery mode based high-Q resonator [110] or a fiber ring resonator [13] with optical quality factors Q_{opt} up to 10^8 for resonance mode around $1.55\,\mu m$. With these resonators the optical free spectral range determines the oscillation frequency of the OEO.

Assuming the use of an add/drop racetrack resonator in the optoelectronic oscillator a new structure has been designed as shown in the Fig.IV.12. The resonator has its transmission spectra at throughput and drop port presented in Fig. IV.13. A continuous wave light generated by a laser source was tuned exactly to the resonance wavelength of racetrack resonator. The optical quality factor of employed racetrack is determined by transmission spectrum (fig.IV.13). At 1615.92 nm, corresponding to optical frequency 185.653 THz, the width of resonant mode is 0.2 GHz. With these measurements, we can determine an optical quality factor for this resonator Q equal to 9.4×10^5.

The filter is theoretically not required but can be useful in order to reduce the electronic noise injected in the electro-optic modulator. Obviously the FR filter must be centered on the same frequency as the frequency FSR of the resonator.

Unfortunately the new OEO system presented in the Figure IV.12 did not lead to a positive result: the optoelectronic oscillator has not been working in this configuration. Many reasons can be found to explain this situation.

The first one concerns the important losses in the resonator and around it: they can be estimated to more than 60 dB, the amplifiers available in the laboratory were not enough powerful for compensating such losses.

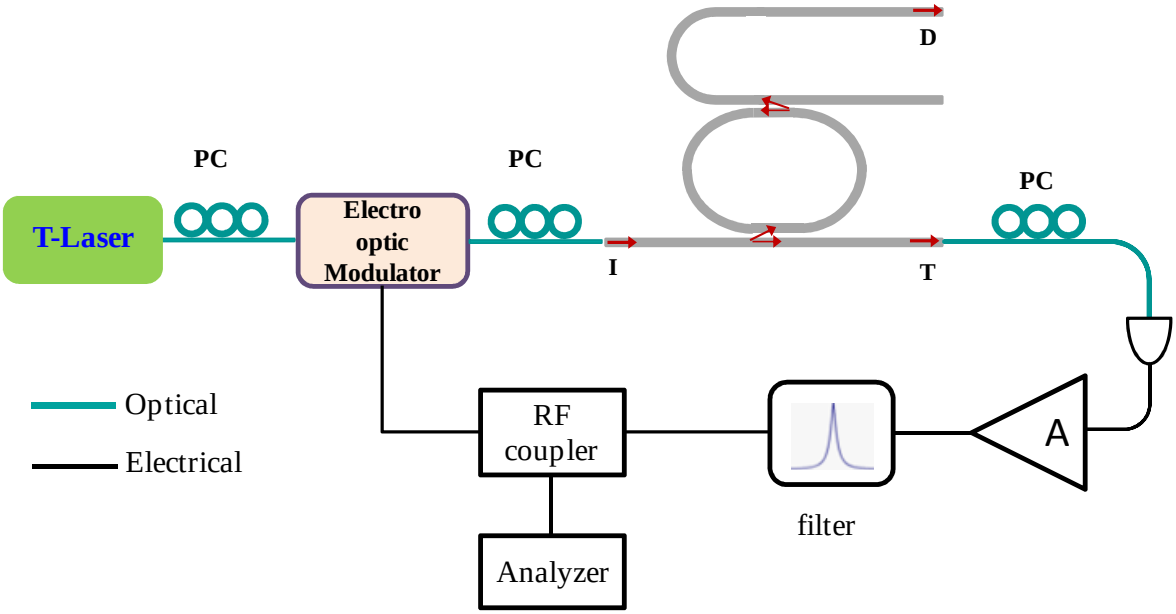

Figure IV.12: (a) Proposed add/drop racetrack resonator in optical wave signal generator, PC: polarization controller; T-Laser: tunable laser; I: input port; T: throughput port and D: drop port.

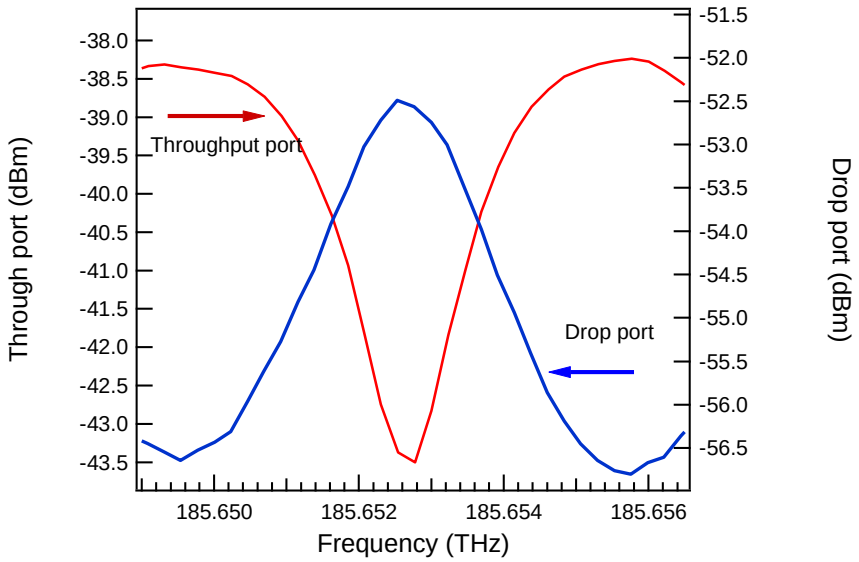

Figure IV.13: Transmission spectrum of the add–drop resonator racetrack measured at the through port.

The second reason concerns the phase shift in the complete loop which has not been adjusted: a RF phase shifter must be introduced in the loop.

The third reason concerns the conception of the system itself: there is no reason that the laser wavelength really fit in a stable way the resonant spectral line of the resonators. Another fundamental development has so to be done in order to control the wavelength of the laser according to the variations of the resonance spectral lines of the resonator which highly depend on the external characteristics such as the temperature. Another solution could also be a tuning of the resonator temperature in order for the spectral lines to be locked on the wavelength of the laser.

Concerning the resonator itself future works consist in a reduction of the global losses, and mainly of the coupling losses, rejoining the first reason indicated above. Of course an improvement of the quality factor in order to increase the spectral purity of the oscillator is also important but absolutely not required before the oscillator really works.

Conclusion

The purpose of this works is to investigate the suitability of tapered fiber-resonator coupler which can be promising as a future integrated optical device used in an Opto-Electronic Oscillator system. This section summarizes the works presented in this thesis and gives a brief outlook to future research which related to the application of optical resonator in OEO system. The following list gives an overview of the main works that have been presented in the previous chapter.

We started the works with optical microsphere resonator. Commercial single mode optical fibers are used as material to fabricate silica microspheres. All studied silica microsphere are fabricated by using electric arc. By this method, microspheres with a diameter ranging from 20 µm to 400 µm are produced. In order to characterize the optical properties of these microsphere resonators, the modal fiber taper–microsphere couplers have been discussed and used. A simple kind of coupler is introduced to understand the condition required for optical coupling both into and out from the microsphere resonator. We have chosen optical tapered fiber to probe the WGM of microsphere, so the fiber taper has been fabricated to this purpose. Based on the electric arc source, the single mode optical fiber is tapered down to micrometer in diameter, the used tapered fibers have waist diameter (ρ) ranging from 1 µm to 3 µm.

In second step, an experimental set-up to couple fabricated tapered fiber and fabricated silica microsphere is build. Experimental results indicated that the quality factor Q of microspheres which are measured several hours after fabrication is approximately equal to 10^5. The FSR value is changed according to the sphere diameter. The results have shown that not only fundamental modes ($l = m$, $n = 1$) are coupled out of sphere but also higher-order mode appears in fiber transmission. In order to examine the excited WGM on the surface of the microsphere, we fabricated tip-fibers with diameters in a range from 0.5µm to 1µm. This method allows mapping the electromagnetic-field distribution directly on the

surface of the microsphere. The optical properties (Q factor, FSR, polarization dependence) of the sphere can be determined by mapping scattering spectra. To optimize the coupling between a taper and a microsphere resonator some studies have been conducted by using CST microwave studio software. The simulation gives the result in WGM resonance at fundamental mode. The critical gap coupling between taper-microsphere is determined by changing the coupling distance.

The system used for microsphere fabrication is limited, and should be improved in order to realize spheres with large diameters. To increase high quality factor *Q* of silica sphere, the taper fiber - microsphere coupler need to be improved to avoid the water and dust absorption on the surface of the sphere. High *Q* factors of microsphere resonator are another attracting point for achieving high sensitivity devices used as sensors: that could be another application of these microspheres.

Continuing to investigate resonator devices which are suitable for insertion in OEO system, an add/drop micro racetrack resonator structure has been fabricated and characterized. A resonator in shape of a racetrack has been design and fabricated. It is based on a waveguide, with a width of 1000 nm wide and a rib of 260 nm of rib, the racetrack semi-circle has a radius *R* of 1600µm and straight section of the racetrack (L_c) is 1400 µm. It was designed according to its theoretical FSR be used in the OEO system developed in the laboratory. It was necessary to find the solution for problems such as: how to couple the light into and from racetrack and how to connect this device with other optical components in the OEO system. Thus in this works, we proposed a method using the fiber micro lens to light coupling into and out of racetrack. By electric-arc source, the micro lenses are fabricated at the end of the pigtail single mode optical fibers. The adequate fiber-micro lenses for light coupling have diameter in range from 4 to 10µm. Experimental behavior of micro racetrack is characterized via fiber micro-lens coupling. The transmission spectra at through port are measured, they appear as the resonance dips with average quality factor of 10^5 for a scanned wavelength range from 1534 nm to 1610 nm. From the experimental transmission spectra, the FSR of this device is determined, it is equal to 0.050 ± 0.003 nm (corresponding to 6GHz). With high quality factor *Q* and small FSR value (high in frequency), this device promises a suitability for

being used in high frequency OEO system as optical filter and energy storage component. Otherwise, using fiber micro-lens to light coupling into and from of racetrack promises a method for the packaging of an optical resonator device which should be easily connected to other optical components in the application system.

Unfortunately the OEO based on the microracetrack could not operate as expected. Different problems have to be solved such as the high level of losses due to this component, but also phase-shift and mainly the control of the spectral lines position according to the laser wavelength.

The most promising feature of the micro-racetrack resonator is its high *Q* factor, high frequency free spectral range, which give it the high suitability for being used in OEO systems.

Addendum

Program for spectral analysis

As presented in thesis, the experimental results on transmission spectral of optical microsphere and micro racetrack resonator are measured and analyzed by computer. Here we used Visual Programming Environments (Agilent VEE) to extract the data from power sensor follows input wavelength when laser scans pass optical devices. Program to extract the data to analyze the output transmission spectral of optical resonator is shown in following figure A.

This program uses an Agilent 8163B device which includes a tunable laser (84940A) and Power sensor (81636B). It is connected to computer via a USB/GPIB Interface (82357A). Before start measurement, the required parameters are chosen. For example, we can chose the operate wavelength range for tunable laser, the operate power of laser, and the measurement step or measure point in this wavelength range. The measure process state at the minimum wavelength and stop at maximum wavelength. The number of output data depends on the input measure point. The measurement process can be summary in major steps following:

Step 1: Press “start” in Panel driver, the GPIB address of Agilent 8463B instrument is defined

Step 2: The wavelength value with input power is sent to optical coupler system and received by power sensor

Step 3: Program define the wavelength and power values. Here wavelength value is confined by actual wavelength + n x step, n is point number, it is increased 1 after one repeat and step is resolution

Step 4: The dependence of power on wavelength is plotted in monitor of computer. After one repeat of program, two point values on wavelength and power are added on this curve

Step 4: The wavelength value and correspond power are saved in a file data. The data are saved in file type ‘file.txt’, which allows analyzing these data with a software such as MATLAB, Igor or Origin.

Step 5: After a time delay, the program return to step 2

Step 6: Program stops when the output wavelength reach the input maximum wavelength.

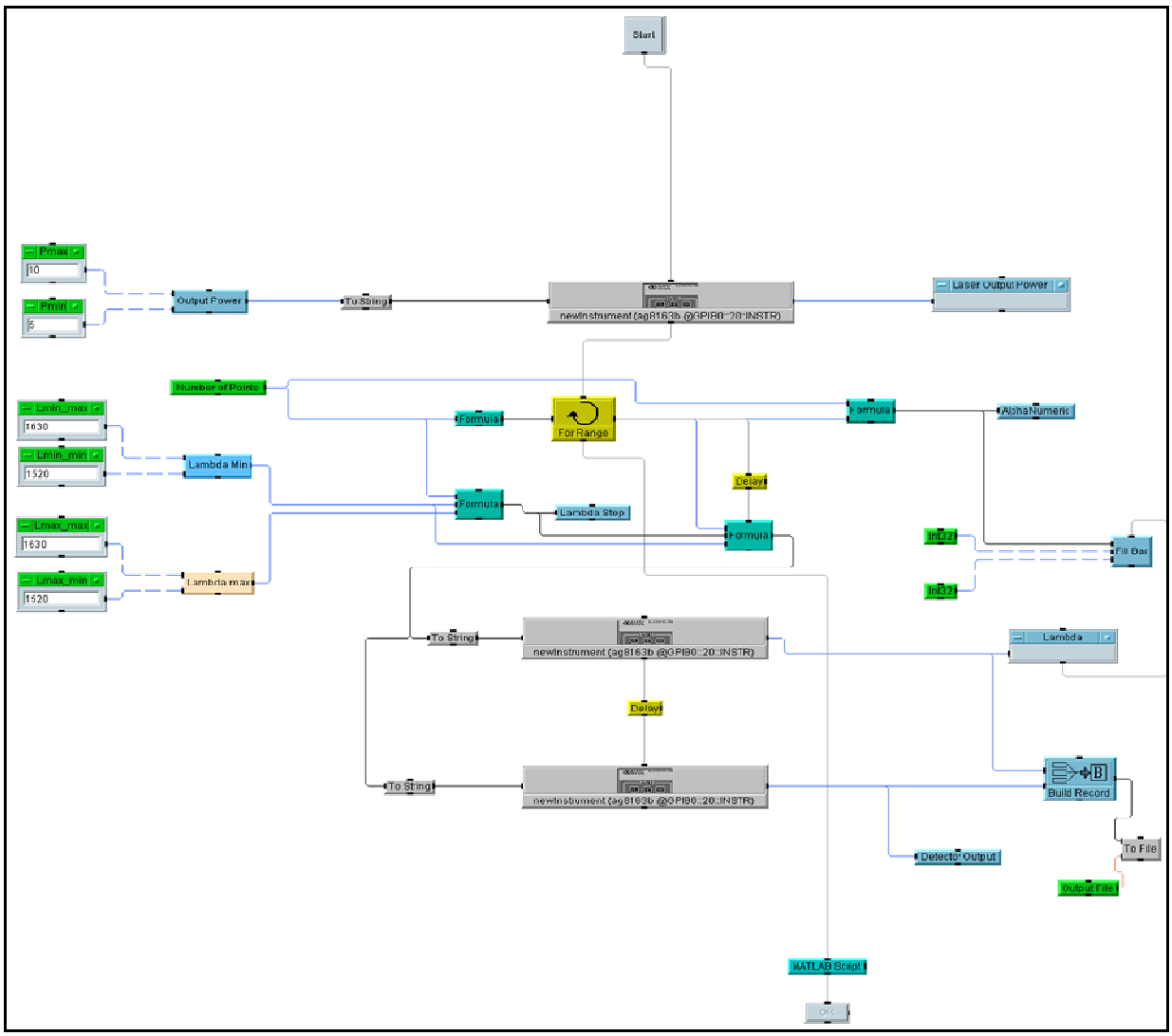

Figure A: Program to analyze the output optical spectral of micro resonator

References

[1]: A. Neyer and E. Voger, "High frequency electro optic oscillator using an integrated interferometer", *Appl. Phys. Lett*., vol. 40(1), pp. 6-8 (1982).

[2]: X.S. Yao and L. Maleki "High frequency optical subcarrier generator", *Electronic letters*, Vol. 30(18), pp. 1525-1523 (1994).

[3]: X.S. Yao and L. Maleki "Optoelectronic microwave oscillator", *J. Opt. Soc. Am. B*, vol. 13(8), pp. 1725-1735 (1996).

[4]: D. Eliyahu, K. Sariri, J. Taylor and L. Maleki "Opto-electronic oscillator with improved phase noise and frequency stability", *Proceedings of Photonic Integrated Systems Conference*, San Jose, CA, USA, Vol. 4998, pp. 139-147, (2003).

[5]: X.S. Yao and L. Maleki, "A Light-Induced Microwave Oscillator", *TDA Progress Report* 42-123, pp. 47-68 (1995).

[6]: X.S. Yao and L. Maleki, "Multiloop Optoelectronic Oscillator", *IEEE Journal of Quantum Electronics*, Vol. 36 (1), pp. 79-84 (2000).

[7]: D. Eliyahu and L. Maleki, "Low phase noise and spurious level in multiloop optoelectronic oscillator", in *Proc. IEEE Int. Frequency Control Symp.*, p. 405 (2003).

[8]: W. Zhou and G. Blasche, "Injection-locked dual opto-electronic oscillator with ultra-low phase noise and ultra-low spurious level", *IEEE Transactions on Microwave Theory and Techniques*, Vol. 53 (3), pp. 929-933 (2005).

[9]: Dmitry Strekalov, David Aveline, Nan Yu, Robert Thompson, Andrey B. Matsko, and Lute Maleki, "Stabilizing an optoelectronic microwave oscillator with photonic filters". *Journal of Lightwave Tech*., vol. 21(12), pp. 3052-3061 (2003).

[10]: X.S. Yao, L. Maleki, and V. Ilchenko, "Opto-Electronic Oscillators having optical resonators". *United States Patent*, US patent No. 6, 567, 436 B1 (2003).

[11]: P. H. Merre, H. Brahimi, and O. Llopis, "Optical techniques for microwave frequency stabilization: resonant versus delay line approaches and related modelling problems". *IEEE Topical Meeting on Microwave Photonics*, Australia (2008).

[12]: A. B. Matsko, A. A. Savchenkov, D. Strekalov, V. S. Ilchenko, and L. Maleki, "Review of applications of whispering-gallery mode resonators in photonics and nonlinear optics". *IPN Progress Report*, pp. 42-162 (2005).

[13]: P. Salzenstein, H. Tavernier, K. Volyanskiy, N.N.T. Kim, L. Larger and E. Rubiola, "Optical Mini-Disk Resonator Integrated into a Compact Optoelectronic Oscillator". *Acta Physica Polonica*, Vol. A(116), pp. 661- 663 (2009).

[14]: P.-H. Merrer, A. Bouchier, H. Brahimi, O. Llopis, “High-Q Optical Resonators for Stabilization of High Spectral Purity Microwave Oscillators”. *EFTF-IFCS, Besançon* (2009).

[15]: Anatoliy A. Savchenkov, Enrico Rubiola, Andrey B. Matsko, Vladimir S. Ilchenko1, and Lute Maleki, “Phase noise of whispering gallery photonic hyper-parametric microwave oscillators”. *Opt. Exp*., vol.16 (6), pp. 4137 (2008).

[16]:B.E.A. Saleh and M.C. Teich, “*Fundamentals of Photonics*”, Ch. 9: Resonator Optics

[17]: Richard K. Chang and Anthony J. Campillo, “*Optical Processes in Microcavities*”. World Scientific (1996).

[18]: Stratton J., “*Electromagnetic Theory*”, IEEE Press Series on Electromagnetic Wave Theory (2007).

[19]: Jackson J., “*Classical Electrodynamics*”. John Wiley & Sons (1975).

[20]: C.C. Lam, P. T. Leung, and K. Young**, “**Explicit asymptotic formulas for the positions, widths, and strengths of resonances in Mie scattering”. *J. Opt. Soc. Am. B*, vol. 9(9), pp.1585-1592 (1992).

[21]: M. Abramowitz and I. Stegun, “*Handbook of mathematical functions*”. Dover publications, 1970.

[22]: F.-M. Treussart, “Étude expérimentale de l’effet Laser dans des microsphères de silice dopées avec des ions néodyme”. Ph.D. thesis, Université Pierre et Marie Curie – Paris VI (1997).

[23] : H. Nussenzveig, “*Diffraction Effects in Semiclassical Scattering*”. Cambridge University Press, 1992.

[24]: B. E. Little, J. S. Foresi, G. Steinmeyer, E. R. Thoen, S. T. Chu, H. A. Haus, E. P.Ippen, L. C. Kimerling, and W. Greene, “Ultra-compact Si-$Si0_2$ microring resonator optical channel dropping filters”. *Photon. Tech. Lett*. *IEEE*, vol. 10(4), pp. 549-551 (1998).

[25]: S. L. McCall, A. F. J. Levi, R. E. Slusher, S. J. Pearton, and R. A. Logan, “Whispering-

gallery mode microdisk lasers”. *Appl. Phys. Lett*., vol. 60, pp. 289-291(1992).

[26]: Jacob T. Robinson, Christina Manolatou, Long Chen, and Michal Lipson, “Ultrasmall Mode Volumes in Dielectric Optical Microcavities”. *Phys. Rev. Lett*. Vol. 95, pp. 143901 (2005).

[27]: Kartik Srinivasan, Matthew Borselli, and Oskar Painter Andreas Stintz and Sanjay Krishna, “Cavity *Q*, mode volume, and lasing threshold in small diameter AlGaAs microdisks with embedded quantum dots’’, *Opt. Exp.* Vol. 14(3), pp. 1094-1105 (2006).

[28]: V. B. Braginsky *et al.,* “Quality-factor and nonlinear properties of optical whispering-gallery modes”. *Phys. Lett*. A, vol. **137,** pp. 393-396 (1989).

[29]: B. E. Little, J. P.Laine, D. R. Lim, H. A. Haus, L. C. Kimerling, and S. T. Chu, "Pedestal Antiresonant Reflecting Waveguides for Robust Coupling to microsphere Resonators and for Microphotonic Circuits". *Opt. Lett*., vol. 25**,** pp. 73-75 (2000)

[30]: G. Rempe, R. J. Thompson, and H. J. Kimble, "Measurement of ultralow losses in an optical interferometer". *Opt. Lett*., vol. 17(5), pp. 363-365 (1992)

[31]: M. L. Gorodetsky, A. A. Savchenkov, and V. S. Ilchenko, "ultimate Q of optical microsphere resonators". *Opt. Lett*., vol. 21(7), pp 453-455 (1996)

[32]: D. S. Weiss, V. Sandoghdar, J. Hare, V. Lefevre-Seguin, J.-M. Raimond, and S. Haroche,"Splitting of high-*Q* Mie modes induced by light backscattering in silica microspheres". *Opt. Lett*., vol. 20(18), pp. 1835-1837 (1995)

[33]: Ivan S. Grudinin, Vladimir S. Ilchenko, and Lute Maleki, "Ultrahigh optical Q factors of crystalline resonators in the linear regime". *Phys. Review A*, vol.74, 063806 (2006).

DOI: 10.1103/PhysRevA.74.063806

[34]: M. L. Gorodetsky, A. D. Pryamikov, and V. S. Ilchenko, "Rayleigh scattering in high-Q microspheres". *J. Opt. Soc. Am. B*, vol. 17(6), pp.1051-1057 (2000)

[35]: D.W. Vernooy, V.S. Ilchenko, H. Mabuchi, E.W.Streed, and H.J. Kimble, "High-Q measurements of fused-silica microspheres in the near infrared". *Opt. Lett*., Vol. 23(4), pp. 247-249 (1998)

[36]: Gorodetsky *et al.,* "Rayleigh scattering in high-*Q* microspheres", *J. Opt. Soc. Am. B,* vol. 17(6), pp. 1051-1057 (2000)

[37]: M.L. Gorodetsky, A.A. Savchenkov, and V.S. Ilchenko,"UltimateQ of optical microsphere resonators". *Opt. Lett.,* vol. 21(7), pp. 453-455 (1996)

[38]: Ilchenko, V.S. Matsko, "Optical resonators with whispering-gallery modes-part II: applications". *IEEE Journal of selected topics in Quantum Electronics*, vol. 12(1), pp. 15-32 (2006)

[39] : D. G. Rabus, M. Hamacher, U. Troppenz, and H. Heidrich, "High- Channel-Dropping Filters Using Ring Resonators With Integrated SOAs". IEEE Photon. Tech. Lett., vol. 14(10), 10, pp. 1442-1444 (2002)

[40]: D. Strekalov, D. Aveline, N. Yu, R. Thompson, A. B. Matsko, and L. Maleki, "Stabilizing an Optoelectronic Microwave Oscillator with Photonic Filters," *J. Lightwave Technol*., vol. 21, pp. 3052–3061, 2003.

[41]: A. Melloni, F. Morichetti, and M. Martinelli, "Linear and nonlinear pulse propagation in coupled resonator slow-wave optical structures". *Opt. Quantum. Electron*., vol. 35, pp-365-379 (2003)

[42]: John E. Heebner, Robert W. Boyd and Q-Han Park, "Slow light, induced dispersion, enhanced nonlinearity, and optical solitons in a resonator-array waveguide", *Phys. Rev. E*, vol 65, pp. 036619 (2002)

[43]: Dmitry Strekalov, David Aveline, Nan Yu, Robert Thompson, Andrey B. Matsko, and Lute Maleki, "Stabilizing an Optoelectronic Microwave Oscillator With Photonic Filters", *J. Lightw. Technol*., vol. 21(12), pp. 3052-3061 (2003)

[44]: S. Arnold, M. Khoshsima, and I. Teraoka, S. Holler, F. Vollmer, "Shift of whispering-gallery modes in microspheres by protein adsorption". *Opt. Lett*. vol. 28(4), pp. 272-274 (2003)

[45]: A. L. Huston and J. D. Eversole, "Strain-sensitive elastic scattering from cylinders", *Opt. Lett*. vol. 18(13), pp. 1104-1106 (1993)

[46]: G. Annino, M. Cassettari, M. Fittipaldi, L. Lenci, I. Longo, M. Martinelli, C. A. Massa, and L. A. Pardi, "Whispering Gallery Mode Dielectric Resonators in EMR Spectroscopy above 150 GHz: Problems and Perspectives". *Appl. Magn. Reson*. vol.19, pp. 495-506 (2000)

[47]: S. Fan, "Sharp asymmetric line shapes in side-coupled waveguide-cavity systems". *Appl. Phys. Lett.*vol.80, pp. 908-910 (2002)

[48]: Chung-Yen Chao and L. Jay Guo, "Biochemical sensors based on polymer microrings with sharp asymmetrical resonance". *Appl. Phys. Lett*. vol. 83(8), pp. 1527-1529 (2003)

[49]: HerbertWalther, BenjaminTHVarcoe, Berthold-Georg Englert and Thomas Becker, "Cavity quantum electrodynamics". *Rep. Prog. Phys*., vol. 69, pp.1325–1382 (2006)

[50]: H. Walther, "Experiments on cavity quantum electrodynamics". *Physics Reports*, vol. 219 (3–6), pp. 263–281 (1992)

[51]: D. W. Vernooy, A. Furusawa, N. Ph. Georgiades, V. S. Ilchenko, and H. J. Kimble, "Cavity QED with high-*Q* whispering gallery modes". *Phys. Rev. A*, vol. 57(4), pp. R2293-R2296 (1998)

[52]: S. Gotzinger, O. Benson, and v. Sandoghdar, "Towards controlled coupling between a high-Q whispering-gallery mode and a single nanoparticle". *Appl. Phys. B*, vol. 73, pp. 825–828 (2001)

[53]: H. J. Kimble, "Strong Interactions of Single Atoms and Photons in Cavity QED". *Physica Scripta*. vol. T76, pp. 127-137 (1998)

[54]: E. Lidorikis, M. M. Sigalas, E. N. Economou and C. M. Soukoulis, "Tight-Binding Parameterization for Photonic Band Gap Materials". *Phys. Rev. lett*., vol. 81, pp. 1405-1408 (1998)

[55]: S. Arnold, C. T. Liu, W. B. Whitten and J. M. Ramsey, "Room-temperature microparticle-based persistent spectral hole burning memory". *Opt. Lett., vol*. 16 (6), pp. 420-422 (1991)

[56]: Arnold *et al.*, "Room-temperature microparticle-based persistent hole-burning spectroscopy". *J. Opt. Soc. Am. B*, vol. 9(5), pp. 819-824 (1992)

[57]: L. Collot, V. Lefvre-Seguin, M. Brune, J. M. Raimond and S. Haroche, “Very High-Q Whispering-Gallery Mode Resonances Observed on Fused Silica Microspheres”. *Europhys. Lett*., vol. 23 (5), pp. 327-334 (1993)

[58]: V. Sandoghdar, F. Treussart, J. Hare, V. Lefevre-Seguin, J.-M. Raimond, and S. Haroche, “Very low threshold whispering-gallery-mode microsphere laser”. *Phys. Rev. A,* vol. 54(3), pp. R1777-R178 (1996)

[59]: M.L.Gorodetsky, V.S.Ilchenko, “High-Q optical whispering-gallery microresonators: precession approach for spherical mode analysis and emission patterns with prism couplers”. *Optics Communications*, Vol. 113(1-3), pp. 133-143 (1994)

[60]: M. L. Gorodetsky and V. S. Ilchenko, “Optical microsphere resonators: optimal coupling to high-Q whispering-gallery modes”. *J. Opt. Soc. Am. B*, vol. 16(1), pp. 147-154 (1999)

[61]: N. Dubreuil, J.C. Knight, D.K. Leventhal, V. Sandoghdar, J. Hare, and V. Lefevre “Erodedmonomode opticalfiber forwhispering-gallery mode excitation infused-silica microspheres”. *Opt. Lett*. Vol. 20(8), pp. 813-815 (1995)

[62]: Giora Griffel, Stephen Arnold, Dogan Taskent, and Ali Serpenguzel, “Morphology-dependent resonances of a microsphere–optical fiber system”. *Opt. Lett*. vol. 21(10), pp. 695-697 (1996)

[63]: Vladimir S. Ilchenko, X. Steve Yao, and Lute Maleki, “Pigtailing the high-Q microsphere cavity: a simple fiber coupler for optical whispering-gallery modes”. *Opt. Lett*., vol. 24(11), pp. 723-725 (1999)

[64]: J.-P. Laine, B. E. Little, D. R. Lim, H.C. Tapalian, L.C. Kimerling, and H.A. Haus, “Planar integrated wavelength-drop device based on pedestal anti-resonant reflecting waveguides and high-Q silica microspheres”. *Opt. Lett*., vol. 25(22), pp. 1636-1638 (2000)

[65]: Paul E. Barclay, Kartik Srinivasan, and Oskar Painter, “Nonlinear response of silicon photonic crystal microresonators excited via an integrated waveguide and fiber taper”. *Optics Express*, vol. 13(3), pp. 801-820 (2005)

[66]: Kartik Srinivasan, Matthew Borselli, Oskar Painter, Andreas Stintz, and Sanjay Krishna, “Cavity Q, mode volume, and lasing threshold in small diameter AlGaAs microdisks with embedded quantum dots”. *Optics Express*, vol. 14(3), pp. 1094-1105 (2006)

[67]: Frangois Gonthier, Suzanne Lacroix, Xavier Oaxhelet, Richard J. Black, and Jacques Bures, “Broadband all-fiber filters for wavelength division multiplexing application”. *Appl. Phys. Lett.,* vol. 54 (14)**,** pp. 1290-1292 (1989)

[68]: P. N. Moar, S. T. Huntington, J. Katsifolis, L. W. Cahill, A. Roberts, and K. A. Nugent, “Fabrication, modeling, and direct evanescent field measurement of tapered optical fiber sensors”. *J. Appl. Phys*., vol. 85(7)**,** pp. 3395-3398 (1999)

[69]: A.J.C. Tubb, F.P. Payne, R.B. Millington, C.R. Lowe, “Single-mode optical fibre surface plasma wave chemical sensor”. *Sensors and Actuators B.* vol. 41, pp. 71-79 (1997)

[70]: G. J. Pendock, H. S. MacKenzie, and F. P. Payne, “Dye lasers using tapered optical fibers”. *Appl. Opt.*, vol. 32(27), pp. 5236-5242 (1993)

[71]: Fabien Bayle and Jean-Pierre Meunier, “ Efficient fabrication of fused-fiber biconical taper structures by a scanned CO2 laser beam technique”. *Appl. Opt*., vol. 44(30), pp. 6402-6411 (2005)

[72]: J.C. Knight, G.Cheung, F.Jacques, and T.A. Birks,“Phase-matched excitation of whispering-gallery-mode resonances by a fiber taper”. *Opt. Lett*., vol. 22(15), pp. 1129-1131 (1997)

[73]: Fedja Orucevic, Valerie Lefevre Seguin, Jean Hare, “Transmittance and near-field characterization of sub-wavelength tapered optical fibers”. *Opt. Exp*., vol. 15(21), pp. 13624-13629 (2007)

[74]: Birks, T.A.; Li, Y.W., “The shape of fiber tapers”, *Journal of Lightwave Technology*, *v*ol. 10 (4), pp. 432 -438 (1992)

[75]: A. W. Snyder and J. D. Love, “*Optical Waveguide Theory*”. New York: Chapman and Hall, (1983.)

[76]: H. A. Haus, “*Waves and Fields in Optoelectronics*”. Prentice-Hall, Englewood Cliffs, NJ, 1984

[77]: S. M. Spillane, T. J. Kippenberg, O. J. Painter, and K. J. Vahala, “Ideality in a Fiber-Taper-Coupled Microresonator System for Application to Cavity Quantum Electrodynamics”. *Phys. Rev. Lett*., vol. 91(4), pp. 043902-1 (2003).

[78]: J.C. Knight, G.Cheung, F.Jacques, and T.A. Birks,“Phase-matched excitation of whispering-gallery-mode resonances by a fiber taper”. *Opt. Lett*., vol. 22(15), pp. 1129-1131 (1997)

[79]: Hill, S.C. and Benner, H.J, “Optical Effects Associated with Small Practicles”. Ed. by P.W. Baraber and R.K. Chang, pp. 4-29. *World Scientific*, *Singapore* (1988)

[80]: John Papapolymerou, Jui-Ching Cheng, Jack East, and Linda P. B. Katehi, “A Micromachined High- X-Band Resonator”. *IEEE Microwave and Guided wave letters*, vol. 7(6), pp. 168-190 (1997)

[81]: M. L. Gorodetsky and V. S. Ilchenko, “Optical microsphere resonators: optimal coupling to high-Q whispering-gallery modes”. *J. Opt. Soc. Am. B*, vol. 16(1), pp. 147-154 (1999)

[82]: A.M. Armani, R.P. Kulkarni, S.E. Fraser, R.C. Flagan, and K.J. Vahala, “Label-Free, Single-Molecule Detection with Optical Microcavities”. *Science Express*, vol. 317, pp. 783–787 (2007).

[83]: E.Little, H.A. Haus, J.S. Foresi, L.C .Kimerling, E.P.Ippen, and R.J. Ripin,“Wavelength switching and routing using absorption and resonance”. *IEEE Photon. Technol. Lett*., vol.10, pp. 816–818 (1998).

[84]: B. E. Little, J. S. Foresi, G. Steinmeyer, E. R. Thoen, S. T. Chu, H. A. Haus, E. P. Ippen, L. C. Kimerling, and W. Greene, "Vertically coupled glass microring resonator channel dropping filters". *IEEE Photon. Technol. Lett*., vol.11, 215–217 (1999)

[85]: S. T. Chu, B. E. Little, W. Pan,T. Kaneko, and S. Y. K. Greene, "Second-order filter response from parallel coupled glass microring resonators". *IEEE Photon. Technol. Lett*. 11, 1426–1428 (1999).

[86]: H. P. Weber and R. Ulrich, "A Thin-Film Ring Laser". *Appl. Phys. Lett*., vol. 19(2), pp. 38-40 (1971)

[87]: R. Ulrich and H.P. Weber, "Unidirectional Thin-Film Ring Laser". *Appl. Phys. Lett*., vol. 20(1), pp. 38-39 (1972)

[88]: Sean L. Rommel, Jae-Hyung Jang, Wu Lu, Gabriel Cueva, Ling Zhou, Ilesanmi Adesida, Gary Pajer, Ralph Whaley, Allen Lepore, Zane Schellanbarger, and Joseph H. Abeles, "Effect of H_2 on the etch profile of InP/InGaAsP alloys in $Cl_2/Ar/H_2$ inductively coupled plasma reactive ion etching chemistries for photonic device fabrication ". *J. Vac. Sci. Technol. B*, vol. 20, pp. 1327-1330 (2002).

[89]: R. Grover, T.A. Ibrahim, T.N. Ding, Y. Leng, L.-C. Kuo, S. Kanakaraju, K. Amarnath, L.C. Calhoun, P.T. Ho, "Laterally coupled InP-based single-mode microracetrack notch filter". *IEEE Photon. Technol. Lett*, vol. 15(8), pp. 1082-1084 (2003)

[90]: Jan Niehusmann, Andreas Vörckel, Peter Haring Bolivar, Thorsten Wahlbrink, Wolfgang Henschel, and Heinrich Kurz, "Ultrahigh-quality-factor silicon-on-insulator microring resonator". *Optics Letters*, vol. 29(24), pp. 2861-2863 (2004)

[91]: A. Vörckel, M. Mönster, W. Henschel, P. Haring Bolivar, and H. Kurz, "Asymmetrically coupled silicon-on-insulator microring resonators for compact add-drop multiplexers". *IEEE Photon. Technol. Lett*., vol. 15, pp. 921-923 (2003).

[92]: John Heebner, Rohit Grover and Tarek Ibrahim, "*Optical microresonators Theory, Fabrication, and Applications*". Springer Series in Optical Science. 138

[93]: T Kominato, Y Ohmori, N Takato, H Okazaki, M Yasu, "Ring resonators composed of GeO/sub 2/-doped silica waveguides". *J. Lightwave Technol*., vol. 10(12), pp. 1781-1788 (1992)

[94]: S. Lardenois, D. Pascal, L. Vivien, E. Cassan, S. Laval, R. Orobtchouk, M. Heitzmann, N. Bouzaida, L. Mollard, "Low-loss submicrometer silicon-on-insulator rib waveguides and corner mirrors". *Optics Letters vol*. 28, pp. 1150-1152 (2003)

[95]: L. Vivien, S. Lardenois, D. Pascal, S. Laval, E. Cassan, J.L. Cercus, A. Koster, J.M. Fédéli, M. Heitzmann, "Experimental demonstration of a low-loss optical H-tree distribution using SOI microwaveguides". *Applied Physics Letters*, vol. 85, pp. 701-703 (2004)

[96]: Gilles Rasigade, Xavier Le Roux, Delphine Marris-Morini, Eric Cassan, Laurent Vivien. Rasigade G., Le Roux X., Marris-Morini D., Cassan E., Vivien L., « Compact wavelength-insensitive fabrication-tolerant silicon-on-insulator beam splitter ». *Optics Letters*, vol. 3(21), pp. 3700-3702 (2010)

[97]: Yu-Mei Wu, Laurent Vivien, Eric Cassan, Vu Hai Nam Luong, Lam Duy Nguyen, and Bernard Journet, " Optical microresonator for application to an opto-electronic oscillator". Proc. SPIE, vol. 7598, pp. 75980F-75980F-8 (2010).

[98]: P. K. Tien and R. Ulrich, "Theory of Prism-Film Coupler and Thin-Film Light Guides". *Jour. Opt. Soc. Am.*, vol. 60(10), pp. 1325-1337 (1970).

[99]: G. Roelkens, D. Vermeulen, D. Van Thourhout, R. Baets, S. Brision, P. Lyan, P. Gautier, and J.-M. Fédéli, "High efficiency diffractive grating couplers for interfacing single mode optical fiber with a nanophotonic silicon-on-insulator waveguide circuit". *Appl. Phys. Lett*. vol. (92), pp. 131101-1(3) (2008).

[100]: D. Taillaert, W. Bogaerts and R. Baets, "Efficient coupling between submicron SOI-waveguides and single-mode fibers". *Proc. Sym. IEEE/LEOS Benelux Chapter, Enschede*, pp.289-303 (2003).

[101] R. G. Hunsperger, A. Yariv, and A. Lee, "Parallel end-butt coupling for optical integrated circuits". *Appl. Opt*., vol. 16(4), pp. 1026-1032, (1977).

[102]: D. G. Hall, J. D. Spear-Zino, H. G. Koenig, R. R. Rice, J. K. Powers, G. H. Burkhart, and P. D. Bear, "Edge coupling of a GaAlAs DH laser diode to a planar Ti:LiNbO3 waveguide". *Appl. Opt.*, vol. 19(11), pp. 1847-1853(1980).

[103]: L. G. Cohen and M. V. Schneider, "Microlenses for Coupling Junction Lasers to Optical Fibers". *Appl. Opt*., vol. 13(1), pp. 89-94 (1974).

[104]: A. KOTSAS, H. GHAFOURI-SHIRAZ, T. S. M. MACLEAN, "Microlens fabrication on single-mode fibres for efficient coupling from laser diodes". *Opt. Quant. Electron.*, vol. 23, pp. 367-378 (1991).

[105]: H. Sakaguchi, N. Seki, and S. Yamamoto, "Power coupling from laser diodes into single-mode fibres with quadrangular pyramid-shaped hemiellipsoidal ends". *Electron. Lett*., vol. 17(12), pp. 425-426 (1981).

[106]: Y. Murakami, J.I. Yamada, J.I. Sakai, T. Kimura, "Microlens tipped on a single-mode fibre end for InGaAsP laser coupling improvement". *Electron. Lett*., vol. 16, pp. 321- 322 (1980).

[107]: U. C. Paek and A. L. Weaver, "Formation of a Spherical Lens at Optical Fiber Ends with a CO2 Laser". *Appl. Opt*., vol. 14(2), pp. 294-298 (1975).

[108]: C. W. Barnard and J. W. Y. Lit, "Single-mode fiber microlens with controllable spot size". *Appl. Opt*., vol. 30, pp. 1958-1962 (1991).

[109]: D. Marcuse, "Loss Analysis of Single-Mode Fiber Splices". *Bell Syst. Tech. J*., vol. 56, pp. 703-718 (1977).

[110]: Kirill Volyanskiy, Patrice Salzenstein, Herve Tavernier, Maxim Pogurmirskiy, Yanne K. Chembo, and Laurent Larger, "Compact optoelectronic microwave oscillators using ultra-high Q whispering gallery mode disk-resonators and phase modulation". *Opt. Exp.*, vol. 18(21), pp. 22358-22363 (2010).

Studying optical micro-resonators coupling for future insertion in an optoelectronic oscillator

Abstract - The classical structure of an Opto-Electronic Oscillator (OEO) is based on a long fiber loop acting as a delay line and leading to the high spectral purity, or very low phase noise, of the oscillator. Such an OEO has been developed in SATIE/LPQM laboratory at ENS Cachan, operating at 8 GHz frequency. However, this system has some main disadvantages such as a bulky size, the difficulty to control temperature and a wide range of peaks among which it is difficult to select only one mode. In order to eliminate these disadvantages, high quality factor optical resonator can be used instead of the optical fiber loop.

In this thesis, two resonator structures are produced and investigated. Microspheres are fabricated based on optical single mode fiber. Whispering gallery modes of these resonators are characterized by tapered fiber – resonator coupling. The experimental results show that the quality factor of the microsphere is up to 10^6 and FSR depends on the diameter of the resonator. A microsphere with a diameter of 300 µm, presents a FSR of 0.2 nm corresponding to a frequency of 25 GHz. However, for an OEO system which should work at 8 GHz, microsphere with a smaller FSR or with diameter of some millimeters should be fabricated; that is really difficult to obtain.

Another add/drop racetrack resonator is designed and investigated. Optical experimental behavior of racetrack is characterized via fiber micro-lens coupling. The transmission spectrum shows resonance dips with average quality factor of 10^5 and a small FSR of 0.050 ± 0.003 nm (actually corresponding to 6 GHz) for a scanning wavelength range from 1534 nm to 1610 nm. The most promising features of the racetrack resonator are its high quality factor, and its free spectral range, which give it the high suitability for being used in the OEO system. Nevertheless the coupling with fiber lens leads to high losses and it is not possible to fulfill the oscillation conditions. Future work should be conducted for improving the coupling and for controlling the resonance dips position in agreement with the wavelength of the laser used in the OEO.

Résumé - La structure traditionnelle d'un oscillateur optoélectronique (OEO) s'appuie sur une boucle de fibre optique très longue, servant de ligne à retard et lui conférant la grande pureté spectrale, ou le très faible bruit de phase de l'oscillateur. Un tel oscillateur fonctionnant à la fréquence de 8 GHz a été mis en œuvre aux laboratoires SATIE/LPQM de l'ENS Cachan. Néanmoins un tel système présente des inconvénients comme les dimensions un peu grandes, la difficulté de contrôler la température et un large peigne de fréquences parmi lequel il est difficile d'extraire un seule mode. Il est en fait possible d'éliminer ses inconvénients en remplaçant la boucle de fibre par un micro-résonateur optique de grand facteur de qualité.

Dans cette thèse deux types résonateurs ont été fabriqués et étudiés. Des microsphères ont été fabriquées à partir de fibres optiques de fibres optiques monomodes. Les modes de galeries de ces résonateurs sont caractérisés grâce à couplage avec une fibre effilée. L'étude expérimentale met en évidence un facteur de qualité pouvant atteindre une valeur de 10^6 et un intervalle spectral libre (FSR) dépendant du diamètre de la sphère. Ainsi pour un diamètre de 300 µm on obtient un FSR de 0,2 nm soit 25 GHz en fréquence. Mais pour un OEO fonctionnant à la fréquence de 8 GHz il faudrait un FSR plus petit et donc une sphère dont le diamètre serait de taille millimétrique, donc très difficile à fabriquer.

Un autre type de résonateur, en forme d'hippodrome, a été conçu et étudié. L'étude expérimentale a été conduite par un couplage avec de fibres lentillées. Le spectre en transmission présente des pics de résonances avec un facteur de qualité moyen de $0,050 \pm 0.003$ nm (correspondant en fait à 6 GHz) sur une plage de longueurs d'onde allant de 1534 nm à 1610 nm. Les caractéristiques les plus intéressantes de ce résonateur en forme d'hippodrome sont un facteur de qualité élevé et un intervalle spectral libre tout à fait en accord avec les besoins de l'OEO étudié. Néanmoins le couplage avec les fibres lentillées induit des pertes optiques trop importantes pour satisfaire aux conditions d'oscillations. Les travaux futurs devront porter sur l'amélioration du couplage ainsi que sur l'asservissement des pics de résonnance du micro-résonateur sur la longueur d'onde du laser employé dans l'OEO.